

Ethane Recovery from Residue Gas Using Pressure Swing Adsorption

by

LIBARDO ESTUPINAN PEREZ

A thesis submitted in partial fulfillment of the requirements for the degree of

Master of Science

in

CHEMICAL ENGINEERING

Department of Chemical and Materials Engineering

University of Alberta

© LIBARDO ESTUPINAN PEREZ, 2015

Abstract

Separation of ethane and heavier hydrocarbons from natural gas stream is a major topic in petrochemical industry due to the increase in Natural gas reserves in North America. Natural gas liquids are frequently separated using a cryogenic distillation process, which is able to separate all the C₃+ hydrocarbons and is able to recover 90-97% of C₂. Usually, the trace composition of ethane in the residue gas was not recover but with the increasing demand for ethane as chemical feedstock for the ethylene production, the recovery of this dilute fraction has become important in industry and academia. In this context, pressure swing adsorption is an attractive separation process to achieve the target.

The aim of this thesis is the design of a PSA process for the separation of ethane from residue gas. To achieve this, experimental measurements, modeling and optimization tools are developed to characterize the adsorbents, define the cycle configuration, and find the optimal operating conditions for the process. Adsorbents from two different classes were chosen, namely, titanosilicates and activated carbons. Experimental isotherm data was obtained in-house for all of them. Subsequently, the experimental data was fitted to an isotherm model and further, heat of adsorption was determined to complete the adsorbent characterization.

A rigorous one-dimensional model that takes into account mass, momentum, and heat balances and several constitutive equations such as pressure drop, adsorption isotherms, and equation of state for the gas phase is developed to simulate adsorption the adsorption process. Three different cycle configurations are proposed to achieve the separation. To compare their performance, C₂ purity and recovery are used as performance metrics. Using standard operating conditions, cycle configurations are compared and through a parametric study, the effect of feed temperature and heat effects are completely described.

A multi-objective optimization, based on an evolutionary algorithm, using C₂ purity and recovery as objective function is developed to obtain three important insights for the process developments: the adsorbent with the best performance, the most suitable cycle configuration,

and the optimal operating conditions. The results from the optimization are analyzed using Pareto fronts in terms of the objective function and a full description of the process is obtained.

To my parents

Acknowledgements

First, I would like to thank to my supervisors Prof. Arvind Rajendran and Prof. Steven Kuznicki for the opportunity to work in their research groups. I deeply appreciate your guidance and support through the development of my project. Professor Arvind Rajendran always gave me the right advice and the insights during the difficult moments and throughout my research; thank you Arvind for your unconditional support and for teaching me that excellence and perfection should be pursued even in the simplest tasks. In addition, I really enjoyed our intense individual and group meetings for both the invaluable knowledge and experience I gained. Further, our weekly group lunch was always a nice moment where we shared our political, cultural, and social views about the world.

I am grateful to Jim Sawada for the experimental measurements of the adsorption isotherms for all the adsorbents and temperatures I required for the development of my research. In addition, I would like to thank Adolfo Avila for his insights and opinions. Although we rarely agreed in technical aspects, he was always ready to help and share his knowledge with me.

My group mates and friends Ali, Ashwin, Johan, Behnam, and Parinaz made my days at the University of Alberta enjoyable. I appreciate their support, patience, and collaboration when it was needed. Our afternoon coffee was a magnificent moment where I learned a lot about different cultures and where we tried to solve academic and worlds problems. Special thanks to my friend and colleague Ashwin, he was a big support not only in academic but also in personal issues. I will miss our Thursday beer with nachos after the group meetings and our endless discussions about both meaningful and meaningless topics. Thank you Aswhin.

I am also grateful to my closest friends in Edmonton, Lina, Luis Carlos, and Andres. They showed patience, sympathy, and goodness to me and knew the precise moment to take me out of the routine to have a joyful time. Despite the distance, Rosa has been a big support during these years. She was always ready to listen to all my issues and after that comforted me with a wise advice and a word of wisdom that made my difficult days bearable.

I acknowledge gratefully the funding from the Natural Sciences and Engineering Research Council of Canada (NSERC). I also want to thank the industrial partner, Nova Chemicals Inc. for the useful discussion we had throughout the project, which made me analyze the project under two perspectives, academic and industrial.

Finally, I would like to thank my parents for their constant support at every moment in my life. None of this would have been possible without their love, kindness, and sacrifice to make my studies possible. They convey me the value of humbleness and constant search for knowledge. My brothers, grandparents, and uncles always gave me support and confidence to accomplish my goals.

Libardo Estupinan

Contents

1	Introduction	1
1.1	General introduction	1
1.2	Separation of ethane from natural gas	3
1.3	Pressure swing adsorption	5
1.4	Adsorbents	7
1.5	Trace component separation through adsorption	8
1.6	Optimization of pressure swing adsorption processes	10
1.7	Objectives and outline of the thesis	12
2	Experimental measurement of adsorption isotherms	15
2.1	Introduction	15
2.2	Experimental	16
2.2.1	Materials	16
2.2.2	Setup and experimental procedure	16
2.3	Modeling experimental adsorption equilibrium data	18
2.3.1	Single component isotherm	18
2.3.2	Description of competitive isotherms	19
2.3.3	Pure component adsorption isotherms	21
2.3.4	Heat of adsorption	23
2.4	Conclusion	25
3	Modeling and simulation	27
3.1	Introduction	27
3.2	Model equations	27
3.3	Solution technique	28
3.4	The 4-step PVSA process	30
3.4.1	Adsorption	31
3.4.2	Forward blowdown	31
3.4.3	Reverse evacuation	32
3.4.4	Pressurization	32
3.5	Model validation	33

3.6	Conclusion	37
4	Ethane recovery from residue gas	39
4.1	Introduction	39
4.2	Process design and configuration	39
4.2.1	4-step cycle with light product pressurization (LPP)	42
4.2.2	5-step cycle with light product pressurization and heavy reflux (LPP+HR)	43
4.3	Column dynamics of the PVSA cycles	44
4.3.1	Effect of light product pressurization and heavy reflux (LPP+HR) on process performance	46
4.3.2	Effect of isothermal assumption in the simulation	47
4.3.3	Effect of temperature on process performance	49
4.4	Conclusion	53
5	Material selection through optimization	55
5.1	Introduction	55
5.2	Issues with current methods to select materials	55
5.3	Formulation of the optimization problem	56
5.3.1	Optimization of the 4-step cycle with LPP	57
5.3.2	Optimization of the 5-step cycle with LPP and heavy reflux	61
5.4	Conclusion	67
6	Concluding remarks	69
6.1	Conclusions	69
6.2	Outlook	70
	Bibliography	73
A	Decision variables for the 4-step cycle with LPP	77
B	Decision variables for the 5-step cycle with LPP+HR	83

List of Figures

1.1	Natural Gas Production in the United States by Source, 1990 to 2040 (trillion cubic feet per year). Source: U.S. Energy Information Administration [1].	1
1.2	A simplified ethylene supply chain from ethane feed stock through petrochemical [2].	3
1.3	Schematic of the Natural Gas (NG) process.	4
1.4	Pressure Swing Adsorption (PSA) description.	5
1.5	Skarstrom PSA Cycle.	7
1.6	Basic cycle for the purification and recovery of the heavy component.	9
1.7	Enriching cycle for the purification and recovery of heavy component (Raffinate).	10
2.1	Schematic of the volumetric apparatus.	17
2.2	Procedure to obtain dual-site Langmuir parameters.	19
2.3	Adsorption Isotherms. Symbols and lines represent experimental and fitted values, respectively.	22
2.4	C1 heat of adsorption.	24
2.5	C2 heat of adsorption.	25
3.1	Schematic of a column discretized in finite volume.	29
3.2	Basic 4-step PVSA process and corresponding pressure profile.	31
3.3	Decrease of the mass balance error with the number of cycles.	36
3.4	Transient profiles for each step of the PVSA cycle. Starting from the first cycle, profiles for every fifth cycle are shown	37
4.1	Cycle configuration and process conditions. a) Basic 4-step; b) Basic 4-step with light product pressurization (LPP); c) 5-step with LPP and heavy reflux (LPP+HR).	41
4.2	C2 gas and solid phase column profiles for the cycles chosen using Na-ETS-10.	45
4.3	Comparison of Basic, LPP and LPP+HR cycles at 298.15K. Operating conditions shown in Figure 4.1.	47
4.4	Comparison between isothermal and nonisothermal simulations. Note that for the case of La-ETS-10 and Sr-ETS-10, only isothermal simulations were performed due to lack of experimental data at multiple temperatures.	48

4.5	Temperature profiles in the 0.5 non-dimensional length of the column for the basic 4-step cycle using two different feed temperatures. Operating conditions depicted in Figure 4.1.	49
4.6	Adsorption isotherms of C1 and C2 on all the adsorbent at different temperatures.	50
4.7	LPP+HR Cycle at different temperatures.	51
4.8	C2 gas and solid phase column profiles for 5-step cycle with LPP+HR at different feed temperatures using Na-ETS-10.	52
5.1	Pareto fronts for the LPP process.	58
5.2	The decision variables corresponding to the Pareto front of the 4-step PVSA cycle with LPP. The lower and upper bound of the x axis refer to the bounds used for the optimization.	60
5.3	Gas and solid phase profiles for C2 on Na-ETS-10 using optimized conditions from Table 5.2.	61
5.4	Pareto fronts for the 5-step cycle with LPP and HR.	63
5.5	The decision variables corresponding to the Pareto front of the 5-step PVSA cycle with LPP+HR.	64
5.6	C1/C2 isotherms, gas and solid column profiles for C1 using Micro carbon and A. Carbon 1 and the optimal conditions from Table 5.4	66
A.1	The decision variables corresponding to the Pareto front for BPL carbon.	77
A.2	The decision variables corresponding to the Pareto front for Micro carbon.	78
A.3	The decision variables corresponding to the Pareto front for Macro carbon.	79
A.4	The decision variables corresponding to the Pareto front for A. carbon 2.	80
A.5	The decision variables corresponding to the Pareto front for A. carbon 1.	81
B.1	The decision variables corresponding to the Pareto front for A. carbon 2.	83
B.2	The decision variables corresponding to the Pareto front for Micro carbon.	84

List of Tables

1.1	Compounds and uses of Natural gas liquids (NGL).	2
2.1	Adsorbent Features.	16
2.2	Dual-site Langmuir parameters for adsorbents considered in this study. Henry selectivity was calculated at 303.15K	21
3.1	Model equations for modeling adsorption column dynamics.	28
3.2	Boundary conditions for a 4-step PVSA process.	33
3.3	Parameters used in the process simulation.	34
3.4	Process conditions for the 4-step PVSA process.	35
5.1	Optimization bounds for the 4-step LPP process.	57
5.2	Optimized conditions for LPP process using Na-ETS-10.	59
5.3	Optimization bounds for the 5-step LPP+HR process.	62
5.4	Process conditions at same recovery from the Pareto fronts for Na-ETS-10, A. Carbon 2, and Micro Carbon.	65

Chapter 1

Introduction

1.1 General introduction

Natural gas (NG) is one of the most abundant fossil fuels on earth. Its low production cost and high energetic value make it a widely used fossil fuel. The recent technologies to extract shale and tight gas have increased the proven reserves of natural gas [1, 2]. In 2014, the U.S. Energy Information Agency (EIA) estimated the proven shale gas reserves of the world as nearly 2.7 trillion cubic metres (tcm), and the unproved resources are greater than 200 tcm [3]. According to the U.S. Energy Information Administration, shale gas will account for almost 50% of national domestic gas production by 2030 as shown in Figure 1.1.

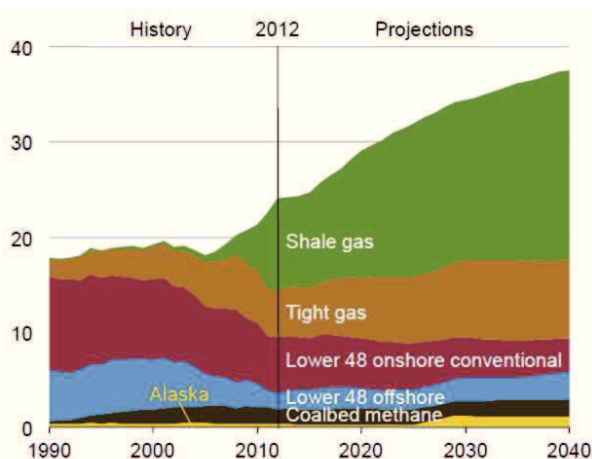


Figure 1.1: Natural Gas Production in the United States by Source, 1990 to 2040 (trillion cubic feet per year). Source: U.S. Energy Information Administration [1].

Nowadays, United States and Canada contribute to around 25% of the global production of Natural gas [3]. With respect to Canada, the proven reserves of conventional natural gas are estimated at 1.7 tcm. Additionally, Canada also has large deposits of shale gas in Alberta, British

Columbia, Manitoba, Ontario, Quebec, New Brunswick, and Nova Scotia. The estimates about the shale gas reserves is around 16.2 tcm. These reserves place Canada in the top five of the countries with technically recoverable shale gas resources in the world [3].

The increase of the natural gas reserves has caused a major impact on the chemical industry due to the cheaper prices of both natural gas and natural gas liquids (NGLs), i.e., ethane and heavier hydrocarbons. These compounds have a variety of applications that are summarized in Table 1.1. Due to the extensive uses and as raw material to manufacture ethylene, ethane (C₂) is one the most important compounds of the NGLs. Ethylene is an organic compound with different applications in the chemical industry that are described in Figure 1.2 [2]. It can be manufactured from either ethane or oil-based naphtha. The reduced prices in natural gas (\$2-\$3 per million BTU) makes it competitive for North American based companies to manufacture ethylene from NG.

Natural Gas Liquid	Chemical Formula	Applications	End Use Products	Primary sectors
Ethane	C ₂ H ₆	Ethylene for plastics production; Petrochemical feedstock	Plastic bags; plastics; anti-freeze; detergent	Industrial
Propane	C ₃ H ₈	Heating; Cooking fuel; Petrochemical feedstock	home heating; small stoves and BBQs; LPG	Industrial Residential Commercial
Butane	C ₄ H ₁₀	Petrochemical feedstock; Blending with propane or gasoline	Synthetic rubber for tires; LPG; lighter fuel	Industrial Transportation
Isobutane	C ₄ H ₁₀	Refinery feedstock; Petrochemical feedstock	Alkylate for gasoline aerosols; refrigerant	Industrial
Pentane	C ₅ H ₁₂	Natural gasoline; Blowing agent for polystyrene foam	Gasoline; polystyrene; solvent	Transportation
Pentanes+	Mix of C ₅ H ₁₂ and heavier	Blending with vehicle fuel; Bitumen production in oil sands	Gasoline; ethanol; blends; oil sands production	Transportation

Table 1.1: Compounds and uses of Natural gas liquids (NGL).

The cheap price of natural gas and the increase of its proven reserves has promoted the expansion and construction of chemical facilities to boost the production of ethylene and its derivatives. In 2012, Dow Chemical Company agreed to invest US\$4 billion to expand their facilities in Texas and construct an ethylene cracker and a new propylene production facility [2]. In Canada, Nova Chemicals Inc. will put into operation by 2016 a third world-scale reactor to produce more linear low-density polyethylene. Based on the facts mentioned above, it is clear that C₂ recovery from NG has acquired high relevance both in the academic and industrial fields because

more economically and technically efficient separations methods are needed to satisfy the global market while reducing energy consumption and associated carbon emissions.

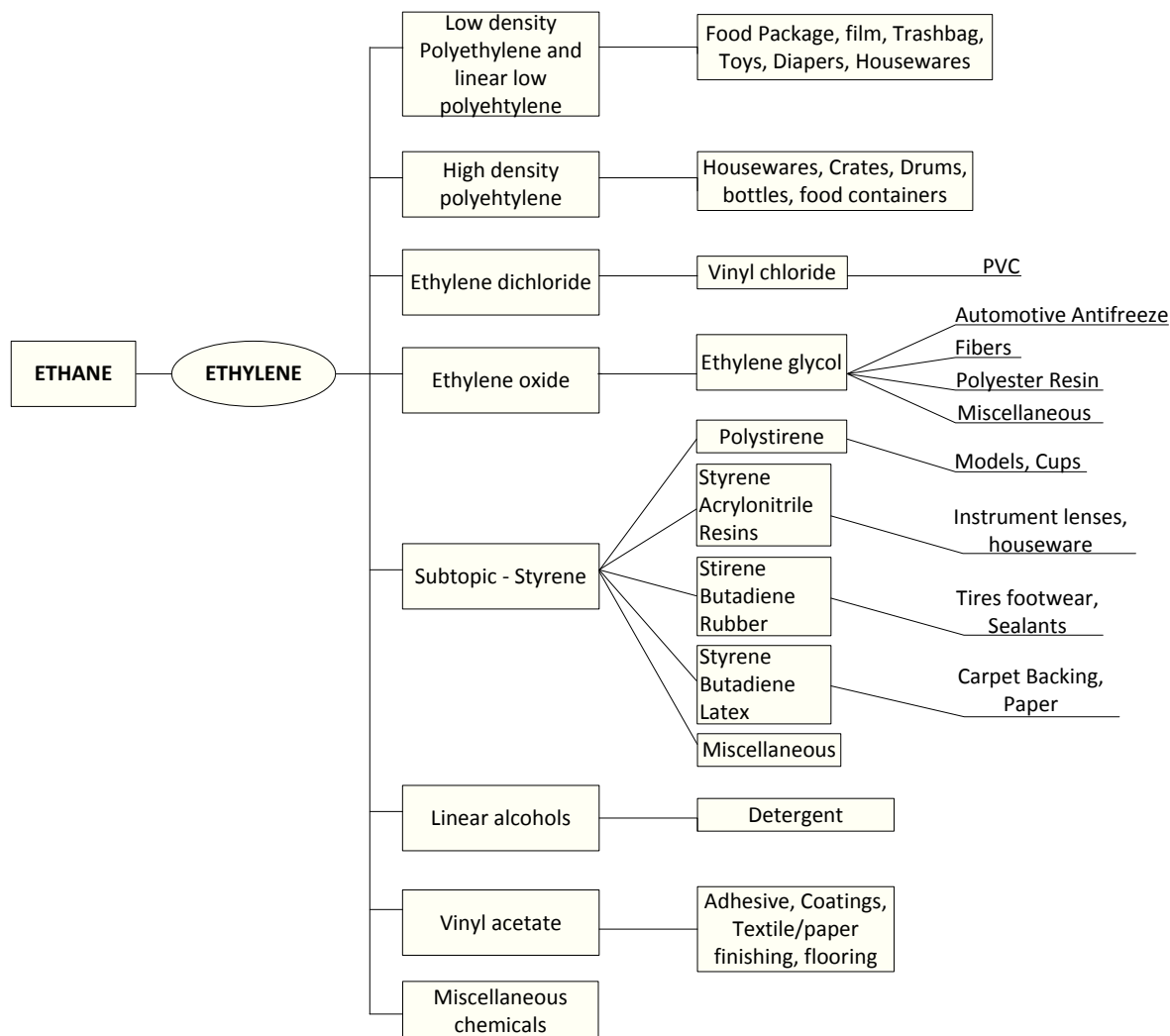


Figure 1.2: A simplified ethylene supply chain from ethane feed stock through petrochemical [2].

1.2 Separation of ethane from natural gas

Natural gas (NG) is a mixture of hydrocarbons and other impurities. While mainly methane (C1), the other hydrocarbons include ethane (C2), propane, and butane. Water, oil, sulphur, carbon dioxide, and nitrogen are typically found as impurities when extracted from the ground. These impurities are removed before the separation of NGLs from natural gas. Conventionally NGLs are separated from NG stream using a cryogenic distillation process, also known as turboexpander process [4]. In this process, shown in Figure 1.3, external refrigerants are used to cool the natural gas stream. Then, an expansion turbine is used to rapidly expand the chilled

gases, which causes the temperature to drop significantly. This temperature drop condenses ethane and other hydrocarbons in the gas stream, while maintaining methane in gaseous form. This process allows for the recovery of about 90 to 95 percent of the ethane originally in the gas stream. In addition, the expansion turbine is able to convert some of the energy released when the natural gas stream is expanded into recompressing the gaseous methane effluent, thus saving energy costs associated with extracting ethane. The extraction of NGLs from the natural gas stream produces both cleaner and purer natural gas, as well as the valuable hydrocarbons that are collectively referred to as NGL. The stream reach in methane is usually called residue gas and its (C1) composition is around 97-98%. A small fraction of ethane, which accounts for 2-3%, is also present in the residue gas stream. With the increasing demand of ethane, it is worth developing separation technologies capable of recovering and concentrating C2 from the residue gas.

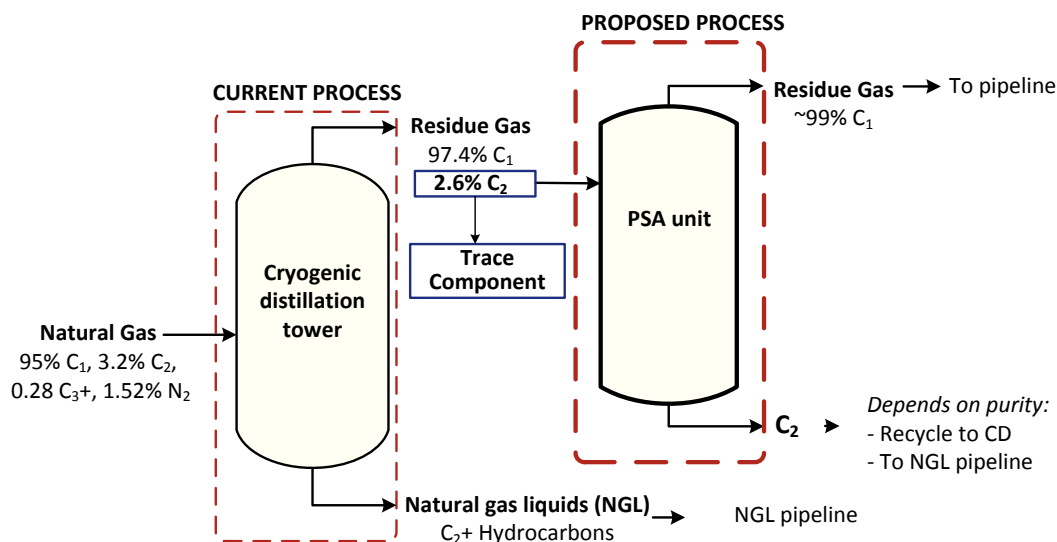


Figure 1.3: Schematic of the Natural Gas (NG) process.

Nova Chemicals Inc. was interested to recover ethane from residue gas and a research collaboration between them and the University of Alberta was established to develop an adsorption process for this purpose. The schematic of the process is shown in Figure 1.3. At the first stage of the project, both technical details and technical feasibility should be evaluated. In short this implies the search, and the subsequent experimental and theoretical characterization, for adsorbents which provide the best performance in terms of C₂ purity and recovery. Further, modeling and simulation of the possible adsorption process configurations and a multi-objective optimization of this processes are to be explored.

1.3 Pressure swing adsorption

Pressure Swing Adsorption (PSA) and Pressure Vacuum Swing Adsorption (PVSA) are widely used industrial gas separation technologies based on the principles of adsorption. Prior to the use of adsorption to CO₂ capture and NG separation, the main industrial applications of PSA processes were air separation, air drying, and hydrogen purification [5]. With the development of new adsorbent material, the possibility of using adsorption processes for different separation systems has increased. In an adsorption process, less strongly adsorbed component is called raffinate and more strongly adsorbed component is called extract. The first one is also called light product while the second one is also called heavy product.

Basically an adsorption process involves two steps: adsorption and desorption. As depicted in Figure 1.4, during the adsorption step, the most strongly adsorbed component is retained in the solid material. This process is carried out at high pressures because at this condition the capacity of the material to adsorb gas is higher. The less strongly adsorbed component passes through the column or is excluded from the material (size-selective sieving). During regeneration or desorption step the adsorbed components are released from the solid by lowering their gas phase partial pressures inside the column. After this operation, the adsorbent is ready to be employed in a further cycle. The gaseous mixture obtained from regeneration (the extract) is enriched in the more strongly adsorbed component of the feed. Thus, the pressure dependency of an adsorption process is exploited [6]. In Figure 1.4, Δq represents the difference in the solid phase loadings between the high pressure feed step and the low pressure desorption for a single component, also known as working capacity. Effecting a desorption by lowering pressure results in the process called pressure swing adsorption (PSA). The same effect can also be implemented by increasing the temperature, in which case the process will be called temperature swing adsorption (TSA).

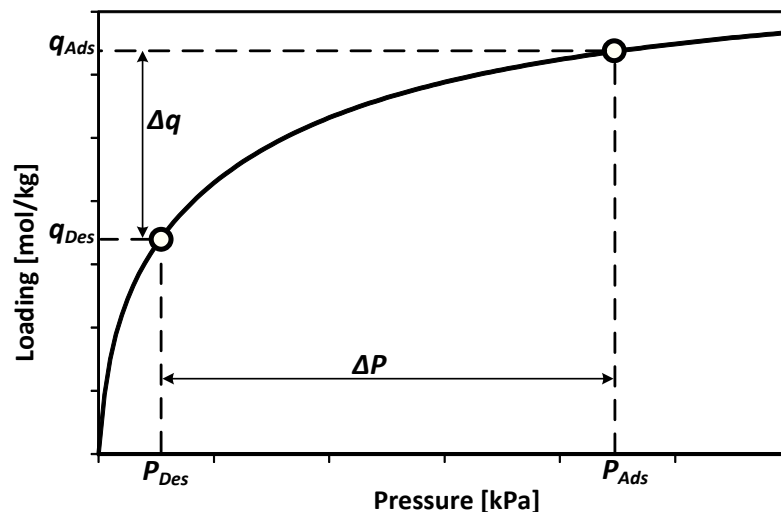


Figure 1.4: Pressure Swing Adsorption (PSA) description.

As a mass transfer operation, adsorption is based on attraction forces among the solid phase and the species constituting the gas phase. Adsorption forces can be categorized into two main groups: first, van der Waals forces, directly correlated to the polarizability of the adsorbate molecule, and second electrostatic forces such as polarization forces, surface field-molecular dipole interactions and surface field gradient-molecular quadrupole interactions [7]. Furthermore, adsorbent selectivity may depend on difference in adsorption at equilibrium (equilibrium selectivity or thermodynamic selectivity) or on the difference in adsorption rates (kinetic selectivity). Kinetic selectivity is possible when there exist a significant difference between adsorption/desorption rates of different components exists. In the first case, the process is controlled by thermodynamics whereas in the second case the process is kinetically controlled.

The original design of a PSA process was developed by Skarstrom, was designed to produce a light product at a very high purity [8]. The schematic of the basic Skarstrom cycle for the pressure swing adsorption process is shown in Figure 1.5. The cycle consists of two adsorption columns packed with adsorbent particles and has four steps, namely, pressurization, adsorption, blowdown and purge. In the first step, column 2 is pressurized up to the high pressure and column 1 is blown down to the low pressure. During the second step, high-pressure adsorption occurs in column 2 whereas column 1 is purged at the low pressure with part of the raffinate product from column 2 undergoing high-pressure adsorption. In the subsequent two steps, the roles of the two beds are interchanged. In the third, after the high-pressure adsorption step, column 2 is blown down to the low pressure. Simultaneously, the high pressure feed stream is switched to column 1 to repressurize it. In fourth step, high-pressure adsorption takes place in column 1 and column 2 is purged at the low pressure using part of the product from the other column. The cyclic operation on each column continues and after a while the columns reach cyclic steady state (CSS) condition. CSS is accomplished when both columns produce same quality product in every cycle. Product purity, product recovery and adsorbent productivity are used to evaluate the performance of a PSA cycle.

The pressure swing adsorption process present a key advantage with respect to another adsorption processes such as temperature swing adsorption (TSA). The advantage resides in the rapid change of pressure that can be performed in practice, which results in shorter cycle times and higher throughput per unit of adsorbent volume. On the other hand, PSA process faces disadvantages when the heavy component is too strongly adsorbed since low vacuum pressures would be needed to regenerate the adsorbent and hence, the process may be economically unfeasible [5].

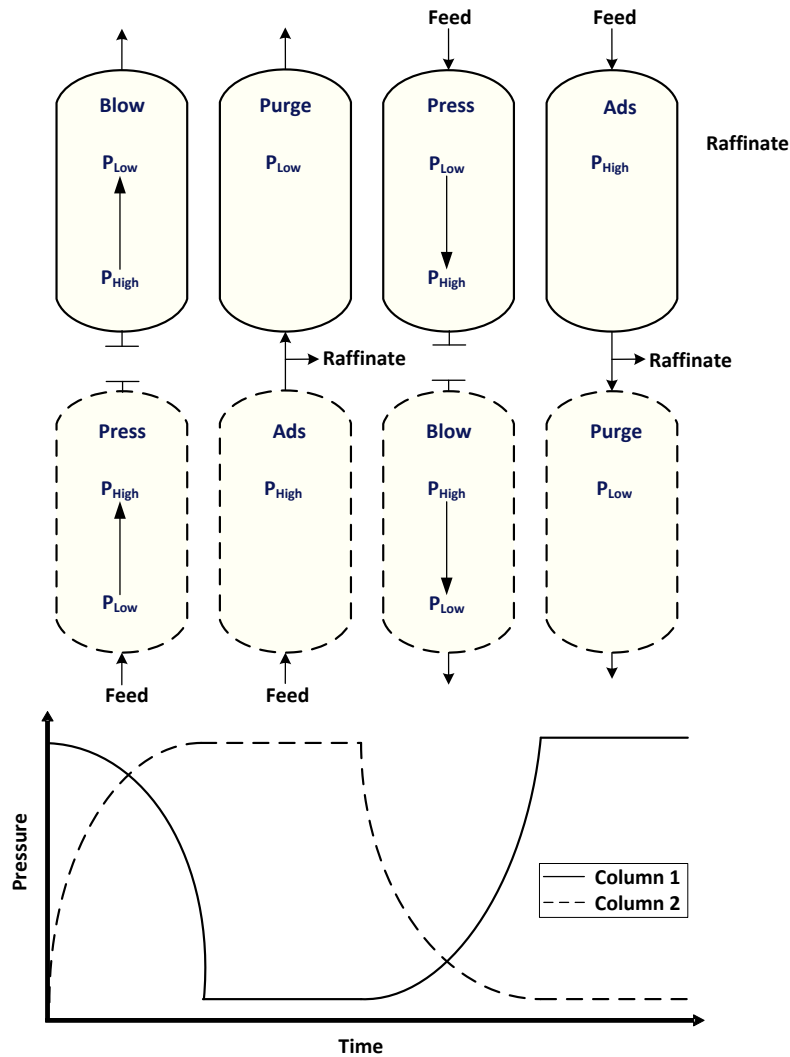


Figure 1.5: Skarstrom PSA Cycle.

1.4 Adsorbents

Adsorbents are essential part for the design of a separation process using adsorption. Depends on the process, e.g., PSA/PVSA or TSA, the adsorbent should have some specific features that make the process efficient. For instance, for the separation of the heavy component using PSA/PVSA separations, it has been shown that the ideal adsorbent is that which adsorption capacity and heat of adsorption for the light component is very low when compared to the heavy component [9]. Furthermore, Adsorbents suitable to PSA processes have to satisfy requirements such as selectivity, regenerability by pressure reduction, specific capacity, low cost per unit volume and reasonable packing density to avoid oversized vessels [7]. For the separation of ethane from residue gas, adsorbents such as zeolites, titanosilicates, activated carbons, and

metal-organic frameworks were found in the literature.

As for the use of zeolites for the recovery of C2 from residue gas by PSA/PVSA, several processes have been reported in literature where adsorbents such as zeolites A, X, silicalite, mordenite or 5A are employed [7, 10]. On the other hand, ETS-10 is a member of the mixed coordination molecular sieves or titanosilicates (ETS) family. Its structure consists of an interconnected octahedral-tetrahedral framework of SiO_4 and TiO_6 linked through bridging oxygen atoms. Further, its pore system contains 12-membered rings that can be tuned by exchanging cations from sodium to strontium or lanthanum and by dehydration using a controlled thermal treatment [11]. Studies about the use of Na-ETS-10 for the recovery of C2 showed that the material has the potential to perform efficiently the separation [12–15].

Carbon adsorbents are widely employed because of their singular properties: a) they are able to perform separation and purification without requiring prior stringent moisture removal (in contrast to most zeolites); b) they adsorb more non-polar and weakly polar organic molecules than other adsorbents do; c) they exhibit low heat of adsorption, resulting in low energy intensive regeneration operations [7]. For PSA/PVSA applications, different types of activated carbons have been investigated [16–18]. Metal organic frameworks (MOFs) are emerging adsorbents that are gathering great attention because of their outstanding pore volumes [7]. MOF materials are being intensely investigated for capture applications; however, for the separation of C2 from residue gas more studies are required to scale-up the process to industrial applications. In this thesis, mixed coordination molecular sieves (ETS-10) and activated carbons are considered as the materials for the recovery of C2 from residue gas. As was mentioned above, both materials have shown potential to perform the separation by PSA/PVSA processes.

1.5 Trace component separation through adsorption

Depending on the application and the industrial requirements, the key component to purify and recover can be either the light or the heavy component. The Skarstrom cycle explained above and depicted in Figure 1.5 was designed for the purification of the raffinate or light component. For the separation of CO_2 from N_2 or natural gas separation, the interest is focused on the strongly adsorbed component or extract. To achieve the separation, the cycle configuration of the Skarstrom was changed and the blowdown step is performed in the cocurrent direction. Additionally, the purge step can be replaced either by a vacuum step or by a purge step using the heavy component. The process for the purification of the heavy component using a vacuum or evacuation step is depicted in Figure 1.6. In summary, the cycle has 4 steps: adsorption, cocurrent blowdown, countercurrent evacuation, and pressurization. This cycle has been studied in literature for CO_2 capture applications [19].

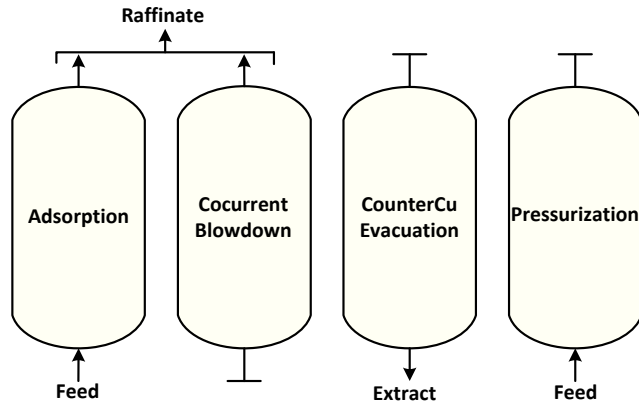


Figure 1.6: Basic cycle for the purification and recovery of the heavy component.

Another cycle configuration called rectifying or enriching PSA cycle has also been reported in the literature [20, 21]. This cycle is used to concentrate the heavy component present in trace quantities. Rectifying cycle uses a large fraction of the heavy component product as purge, which means that the process utilizes an enriching reflux stream to remove the light component from the heavy product end of the column. There is no limitation on the purity of the strongly adsorbed component. Nevertheless, the purity of the light component will be limited by the thermodynamics [22]. The rectifying cycle transposes the feed and purge steps of the Skarstrom cycle, and thereby the feed gas is fed into the column at low pressure whereas purge step is carried out at high pressure. As shown in Figure 1.7, the cycle consists of two adsorption columns similar to the Skarstrom cycle with the same four steps, namely, pressurization, adsorption, blowdown and purge but using different scheduling and changing the pressure conditions for purge and adsorption step. Also, pressurization step does not use feed stream to increase the pressure; instead, the product stream from the blowdown step is used for this purpose.

A dual-reflux pressure swing adsorption cycle with intermediate feed inlet position was also proposed to concentrate and recover the heavy component either in bulk or in trace compositions [20, 23–25]. Since the dual-reflux cycle results from the combination of the Skarstrom cycle with the enriching cycle, it is possible to separate and concentrate both heavy and light components. Locating the feed inlet in an intermediate position of the columns removes the thermodynamic constraint with respect to the the maximum enrichment ratio that can be reached in a conventional cycle. Ritter and coworkers showed that the enrichment ratio is equal to the pressure ratio [22].

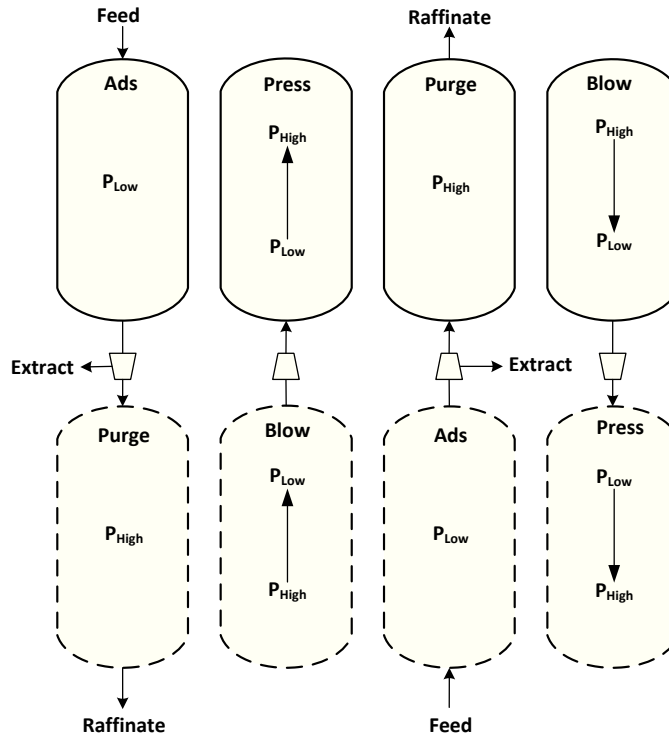


Figure 1.7: Enriching cycle for the purification and recovery of heavy component (Raffinate).

1.6 Optimization of pressure swing adsorption processes

The optimization of adsorption processes using pressure swing adsorption (PSA), temperature swing adsorption (TSA) or pressure vacuum swing adsorption (PVSA) started gaining attention 25 years ago with evolution of computational power and optimization techniques. Intrinsicly, adsorption processes are complex because they are multi-step, multicomponent, and dynamic system where the process has to overcome a transient state before reaching cycle state (CSS) condition. To model an adsorption process, a system of partial differential equations, usually discretized on space and integrated on time, have to be solved simultaneously. The system of equations describes mass, energy, and momentum transport phenomena within the adsorption column. Depending on the complexity of the system, CSS condition can be reached in less than hundred cycles for less complex systems and can be hundreds of cycles for complex systems and configurations.

Different approaches, in terms of the solution of the PDEs, optimization strategy, and objective functions, have been proposed for the optimization of PSA processes. Westerberg and coworkers used a mixed-integer nonlinear program (MINLP) to optimize the design of PSA processes based on the minimization of the capital and operating costs and using the number of beds, scheduling of the operation, and operating conditions as decision variables [26]. Additionally, they used a simple time integrated balances to describe concentration and energy profiles.

The mathematical model of the 5-step PSA process with pressure equalization considered by Nilchan and Pantelides involves a system of partial differential and algebraic equations (PDAEs) in time and two spatial dimensions [27] where heat effects were not taken into account. A third order orthogonal collocation method on finite elements was used for the discretization of both the axial and the radial domains. The resulting model leads to a nonlinear programming problem (NLP) with a large number of variables and constraints. The objective function proposed for the optimization problem was the minimization of the power requirement using as the duration of step times, feed pressure, and bed length as the decision variables.

The use of adsorption for CO₂ capture and sequestration increased the attention for the optimization of PSA and PVSA processes in the last 15 years. Biegler and coworkers used a discretization of the spatial domain and integration in time to solve the system of PDEs [28]. The method of centered finite differences is adopted for the discretization of the spatial domains, and a reduced space SQP method was used for the optimization of a PSA and PVSA processes using zeolite 13X as adsorbent. The optimization was carried out in a commercial software with the objective to maximize the purities of CO₂ and N₂ by changing seven operating conditions which were the decision variables. Subsequently, the same authors presented an evolution of the previous methodology, which allows obtaining optimization results with better convergence and faster computation times [29].

A superstructure-based approach was also developed by Biegler research group to simultaneously determine optimal cycle configurations and design parameters for PSA units for both pre-combustion and post-combustion CO₂ capture [30, 31]. They considered a rigorous set of partial differential algebraic model (PDAE) which was completely discretized in both spatial and time domains, and the resulting large-scale nonlinear programming problem (NLP) was solved using an interior point NLP solver. Maximization of recovery and minimization of power consumption were defined as objective functions.

Floudas and coworkers also used a super-structure representation of the PVSA process to model, simulate, and optimized the process configuration [32]. They made use of the Kriging-based surrogate model to optimize the set of PDEs, which describes the process. The objective function defined for the optimization problem was the minimization of the total annualized cost of the PSA and VSA process.

Multiobjective evolutionary algorithms may be a useful methodology for multiobjective optimization problems and provide the well-known Pareto-optimal solution. An advantage of these algorithms is their capability to calculate multiple Pareto optimal solutions in one simulation run. Unfortunately, these methods have not been considered widely to optimize adsorption processes due to their computational complexity and nondominated sorting which leads to the calculation of many generations making the method computationally expensive if the problem involves a large population size. These kind of algorithms have presented significant improvements as the evolution of the nondominated sorting genetic algorithm called NSGA-II [33]. This

method includes introduction of elitism to enhance the convergence properties of the original algorithm and hence, reducing the computational complexity.

The NSGA-II algorithm has been implemented with success in two recent papers for the multi-objective optimization of PVSA processes for CO₂ capture [19, 34]. Purity and recovery were considered as the objective functions. In those papers, the algorithm was capable to search in the entire range of the decision variables in order to obtain the Pareto-optimal solution using no more than 60 generations and with a population equal to ten times the number of decision variables. Moreover, a multi-objective constrained optimization was also implemented used this algorithm. The objective functions were defined in terms of energy and productivity of the process whereas a constraint in purity and recovery was assigned [19, 34]. The NSGA-II algorithm was also adopted in this work and its implementation and results will be detailed in Chapter 5.

1.7 Objectives and outline of the thesis

The principal objective of this thesis is to study the separation of ethane from residue gas using pressure swing adsorption (PSA). The project encompasses from the material characterization to the model-based process design and multi-objective optimization using the measured adsorption parameters as input data. To reach the main objective, a series of steps were followed and are described below:

- The experimental measurement of single-component adsorption isotherms at different temperatures for the adsorbents selected in this study and its subsequent modeling using a theoretical or empirical model.
- The implementation of a rigorous and efficient model to simulate a complete pressure swing adsorption cycle.
- Different PVSA configurations found in literature for CO₂ capture were simulated using the rigorous model. Furthermore, an identification of the process variables that most affect the process performance was carried out.
- A multi-objective optimization study was conducted to determine the optimal process conditions that maximize C₂ purity and recovery. The multi-objective optimization study also provided a clear answer about the adsorbent selection.

Chapter 2 presents the characterization of six different materials. The single component experimental adsorption isotherms are measured at different temperatures and the experimental data is fitted to an isotherm model. Competitive isotherms are predicted from the single component data using an extended version of the isotherm model. To complete the characterization, experimental heat of adsorption is compared with that obtained from the isotherm equation. To compare with previous studies, two adsorbents from literature were included in the thesis.

Chapter 3 deals with the mathematical modeling and design of a PSA cycle for the separation and concentration of C₂ from residue gas. The model is implemented to simulate the basic 4-step cycle and a validation was carried out.

Chapter 4 presents two additional PSA configurations, namely, the 4-step cycle with light product pressurization (LPP) and the 5-step cycle with light product pressurization and heavy reflux (LPP+HR). A determination of key operating variables in the process performance is carried out through the simulation of the different cycle configurations using different operating conditions.

Chapter 5 deals with the multi-objective optimization problem for the PSA configurations proposed in Chapter 4. The optimization problem was posed in terms of purity and recovery as objective function. For the 4-step cycle with LPP and the 5-step cycle with LPP+HR, seven and eight operating conditions were included as decision variables, respectively. Pareto curves in terms of the objective functions were obtained for all the adsorbents. Therefore, the optimization not only provides the optimal operating conditions for the given processes but also the information about the best adsorbent for the separation problem.

In chapter 6 the conclusions from the experimental studies, modeling and simulation, and multi-objective optimization are presented. The recommendations for further study are also presented in the same chapter.

Chapter 2

Experimental measurement of adsorption isotherms

2.1 Introduction

Two different types of adsorbents were characterized in this study, titanosilicates and carbons. Mixed coordination molecular sieves or titanosilicates (ETS) are micro-porous crystalline solids consisting mainly of an assemblage of titanium oxide (TiO_2) and silicate (SiO_2) [11,35]. The pore size in ETS-10 is uniform ($\sim 8\text{\AA}$) and similar in dimension to large-pore classical zeolites. It is also known to have high thermal stability. ETS-10 has been used in previous studies to separate ethane from natural gas using pressure swing adsorption (PSA) [12,15]. Three different cation exchanged titanosilicates were synthesized in Kuznicki laboratory: Na-ETS-10, La-ETS-10, and Sr-ETS-10. Additionally, three commercial activated carbons were utilized: BPL, Macroporous, and Microporous carbons.

On all 6 materials equilibrium adsorption isotherms of pure methane (C1) and ethane (C2) were measured over a wide pressure range (up to 40 bar for methane and up to 10 bar for ethane). For the case of Na-ETS-10, 6 different temperatures were investigated, namely, 303.15K, 323.15K, 343.15K, 373.15, 403.15K, and 423.15K. For the case of carbons, the first three temperatures above mentioned were investigated. Isotherms on La-ETS-10, and Sr-ETS-10, were not measured as a part of this study, but were available at one temperature from a previous investigation. This chapter provides the description of the experimental method used, the measurements and their description.

2.2 Experimental¹

2.2.1 Materials

The adsorbent characteristics such as particle density and average pore size are summarized in Table 2.1. Titanosilicates (ETS) synthesis and subsequent cation exchange was carried out in Kuznicki laboratory. The detailed preparation procedure is reported in the literature [35]. The samples were pelletized before being tested. Pure C1 and C2 with a purity of 99.9% purchased from Praxair was used to perform the experiments.

Adsorbent	Particle Density [kg/m ³]	Average Pore size [\sim Å]
La-ETS-10	1184	8
Sr-ETS-10	1156	8
Na-ETS-10	1000	8
Micro Carbon	833	6
Macro Carbon	625	20
BPL Carbon	766	13.9

Table 2.1: Adsorbent Features.

2.2.2 Setup and experimental procedure

The adsorption isotherms were measured using a high pressure adsorption analyzer (HPVA-100) from VTI scientific instruments. A schematic of the volumetric apparatus used to perform the equilibrium adsorption experiments is shown in Figure 2.1.

The volumetric apparatus consists of a reservoir and a sample cell with a known volume, V_{dose} and V_{sample} , respectively. The device is equipped with temperature and pressure sensors. Dead volume (V_{dead}) due to the piping in between the reservoir, and the sample cell were taken into account. Bulk gas phase density was calculated from the experimental measurements of temperature and pressure in each section of the apparatus, with ρ_{sample} , ρ_{dose} , and ρ_{dead} being the densities for sample, reservoir, and dead volume sections, respectively. In order to get a more accurate value of density, the ideal gas law with the compressibility factor correction using the NIST Chemistry WebBook data was used [36].

¹Experimental data was obtained by Jim Sawada and the author performed the analysis

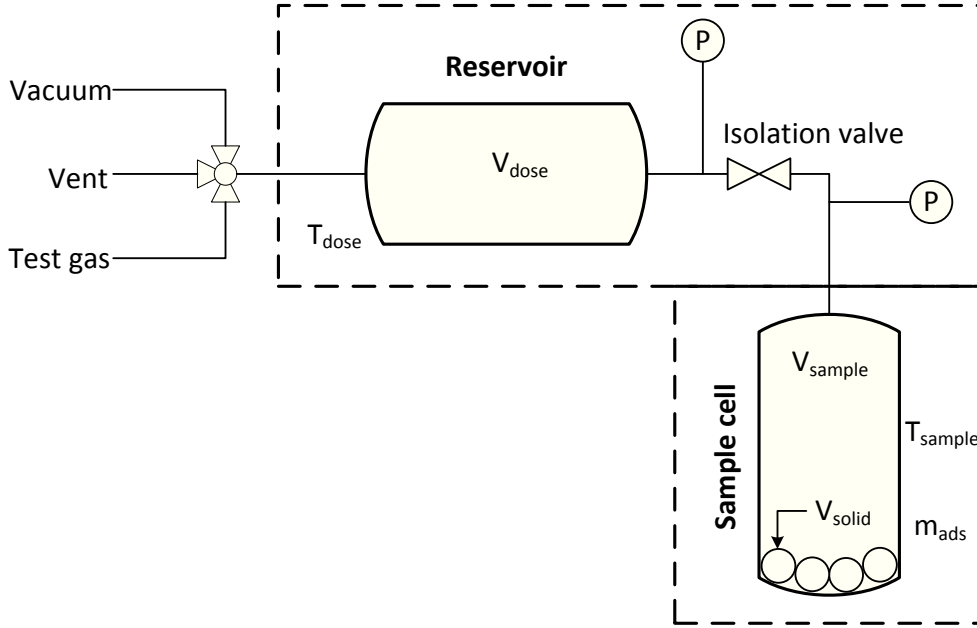


Figure 2.1: Schematic of the volumetric apparatus.

At the beginning of an experiment an adsorbent sample of mass m_{ads} is loaded on the sample cell. Then, the sample cell is closed and evacuated while the dosing cell is filled with the sorbate. The isolation valve is opened and the gas flows into the sample cell where part of the gas will adsorb, while the rest will remain in the gas phase. In a volumetric system the pressure on both the dosing and sample cell is monitored using transducers. The experimental measurement obtained from this experiment is the excess adsorption that can be calculated from the mass balance for the volumetric apparatus using the expression:

$$\begin{aligned}
 \overbrace{(\rho_{dose,a} - \rho_{dose,b})V_{dose}}^{\text{moles dosed}} &= \overbrace{(\rho_{sample,a} - \rho_{sample,b})(V_{sample} - V_{solid})}^{\text{moles in sample cell}} + \overbrace{(\rho_{dead,a} - \rho_{dead,b})V_{dead}}^{\text{moles in dead volume}} \\
 &\quad + \overbrace{(n_{ads,a} - n_{ads,b})m_{ads}}^{\text{moles adsorbed}} \tag{2.1}
 \end{aligned}$$

In the above equation, subscripts a and b refer to the states at the beginning and the end of a particular experiment. Further, the only unknown in the previous equation is n_{ads} , which can be calculated by rearranging Equation 2.1.

$$n_{ads,i} = \frac{(\rho_{dose,a} - \rho_{dose,b})V_{dose}}{m_{ads}} - \frac{(\rho_{sample,a} - \rho_{sample,b})(V_{sample} - V_{solid})}{m_{ads}} - \frac{(\rho_{dead,a} - \rho_{dead,b})V_{dead}}{m_{ads}} \quad (2.2)$$

Subsequently, the data is analyzed and the excess adsorption is calculated from equation 2.2 for each experimental pressure since the experimental conditions were far from the critical conditions of the gases, the excess isotherms were considered to be equal to absolute values.

2.3 Modeling experimental adsorption equilibrium data

2.3.1 Single component isotherm

Mathematical description of single component adsorption isotherms constitute a key step in modeling, simulation, and knowledge about the adsorption process. Empirical and theoretical expressions have been formulated and explained in literature [37]. The Langmuir isotherm is one of the most commonly used and simplest description of adsorption equilibria. It assumes that adsorption is monolayer and energetically homogeneous; only one gas molecule can be adsorbed on each site of the adsorbent; and adsorbate-adsorbate interaction is negligible. The Langmuir isotherm has the following form:

$$q_i^* = \frac{q_{sb,i}b_i c_i}{1 + b_i c_i} \quad (2.3)$$

where $q_{sb,i}$ and b_i are respectively the saturation capacity and affinity parameter, and c_i is the fluid phase concentration of component i . Although the Langmuir model is simple, it fails to describe accurately the equilibria in many practical cases; especially adsorbents that are structurally/energetically heterogeneous. An extension of the single-site Langmuir isotherm is the dual-site Langmuir (DSL) equation which is described as:

$$q_i^* = \frac{q_{sb,i}b_i c_i}{1 + b_i c_i} + \frac{q_{sd,i}d_i c_i}{1 + d_i c_i} \quad (2.4)$$

where $q_{sd,i}$ and d_i are respectively the saturation capacity and affinity parameter for the second site. In both the single-site and dual-site models, the temperature dependence is described by the following relationships:

$$b_i = b_{0,i}e^{-\Delta U_{b,i}/RT} \quad (2.5)$$

$$d_i = d_{0,i}e^{-\Delta U_{d,i}/RT} \quad (2.6)$$

where $b_{0,i}$ and $d_{0,i}$ are the pre-exponential factors while $\Delta U_{b,i}$ and $\Delta U_{d,i}$ are the internal energy of adsorption. Dual-Site Langmuir (DSL) isotherm model has 6 parameters, $b_{0,i}$, $d_{0,i}$, $\Delta U_{b,i}$, $\Delta U_{d,i}$, $q_{sd,i}$, and $q_{sb,i}$, that should be fitted in order to describe accurately the experimental data. In this work, parameters were obtained by simultaneous nonlinear regression of experimental isotherm data measured at different temperatures following a two stage process depicted in Figure 2.2 where first, initial guesses are obtained for each parameter. After that, an error minimization, between the experimental and calculated values, is carried out in order to measure how accurate is the fit and to guarantee a reliable fitting with physically meaningful values for each parameter. It is worth noting that in order for consisted thermodynamics representation of binary data it is important that $q_{sb,1} = q_{sb,2}$ and $q_{sd,1} = q_{sd,2}$. This condition was enforced in the fitting process. The fitting process was repeated for all the six adsorbents tested in-house.

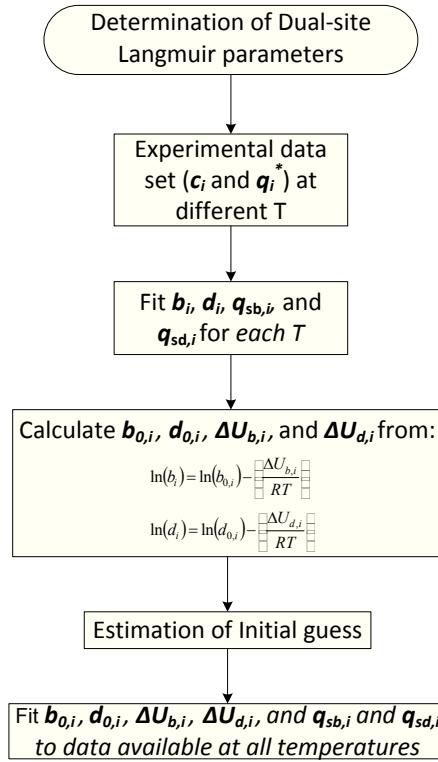


Figure 2.2: Procedure to obtain dual-site Langmuir parameters.

2.3.2 Description of competitive isotherms

The description of competitive isotherms is a rather complex subject. How adsorbates compete for sites on the adsorbent continues to be a challenging topic. From the practical perspective, two approaches are used. First, the use of simple extensions of single component isotherms. For

instance, the competitive version of the single and dual-site Langmuir isotherm are given by,

$$q_i^* = \frac{q_{s,i} b_i c_i}{1 + \sum_{i=1}^{n_{comp}} b_i c_i} \quad (2.7)$$

$$q_i^* = \frac{q_{sb,i} b_i c_i}{1 + \sum_{i=1}^{n_{comp}} b_i c_i} + \frac{q_{sd,i} d_i c_i}{1 + \sum_{i=1}^{n_{comp}} d_i c_i} \quad (2.8)$$

The second approach is to consider single component isotherms as given by Equations 2.3 and 2.4 or any suitable description and estimate the competitive adsorption through the use of the ideal adsorbed solution theory (IAST) [38]. In this approach the adsorbed phase is considered as ideal and the loading of the various components are calculated. Many systems show deviations from the IAST model. The main advantage of using an extended model compared to the IAST is its simplicity of calculation. While the extended model is straightforward to calculate, the IAST requires the solution of simultaneous-non linear equations, which is cumbersome, especially when it has to be incorporated in a simulation code where such calculations have to be repeated for thousands of times.

The choice between which approach is to be used is made based on the verification of model calculations with experimentally measured mixture isotherms. This is, again, a very cumbersome process that is avoided in the early stage development. In the current study, no mixture experiments were performed and the extended models were used to describe the mixture equilibria. Needless to say that the model predictions rely heavily on the choice of the model and when a real process needs to be design a detailed experimental campaign to measured isotherms needs to be incorporated.

Using dual-site Langmuir model for binary systems raises an issue related with the appropriate combination of the affinity parameters (b_i and d_i) for the summation posed in the denominator of equation 2.8. Each component has two affinity parameters that should be combined with the affinity parameters of second component in a certain way that it predicts well the binary adsorption. Therefore, four possible combinations are obtained and an adequate choice is necessary. Ritter and coworkers showed, with experimental and predicted data, that for mixtures with similar properties, i.e., molecular size and adsorbent capacities such as methane-ethane a perfect positive (PP) correlation can be described with accuracy the binary adsorption [39]. A PP correlation implies that the sites are chosen in such a way that the higher and lower values of the affinity coefficient are matched between the two components. This methodology was adopted in this work for all the adsorbents.

2.3.3 Pure component adsorption isotherms

The DSL parameters obtained for each adsorbent are shown in Table 2.2. Two additional adsorbents, namely, activated carbons 1 and 2, denoted as A. Carbon 1 and A. Carbon 2, respectively, were considered and their isotherm isotherm parameters from the literature are listed [17, 39]. Also, parameters for Sr-ETS-10 and La-ETS-10 were fitted at only one temperature (303.15K) because of the absence of experimental adsorption equilibrium data at more than one temperature.

Adsorbent	Comp.	q_{s_a} [mol/kg]	q_{s_b} [mol/kg]	b_{0a} [m ³ /mol]	b_{0b} [m ³ /mol]	$-\Delta U_a$ [kJ/mol]	$-\Delta U_b$ [kJ/mol]	Henry Selectivity
Sr-ETS-10	C1	1.122	1.559	2.049×10^{-2}	2.107×10^{-3}			43.918
	C2	1.106	0.771	1.017×10^0	3.933×10^{-2}			
La-ETS-10	C1	1.084	0.818	2.951×10^{-3}	1.625×10^{-2}			38.748
	C2	0.689	1.032	1.330×10^{-2}	6.099×10^{-1}			
Na-ETS-10	C1	0.630	1.981	1.010×10^{-9}	5.857×10^{-6}	35.061	21.132	58.588
	C2	0.602	1.584	2.234×10^{-8}	3.256×10^{-6}	35.508	33.252	
Macro Carbon	C1	0.670	8.059	5.077×10^{-3}	4.878×10^{-6}	4.124	15.283	13.771
	C2	2.386	6.974	3.414×10^{-4}	7.900×10^{-7}	15.551	24.273	
Micro Carbon	C1	1.015	4.459	5.271×10^{-4}	1.614×10^{-6}	10.074	19.790	28.762
	C2	1.578	3.420	4.036×10^{-4}	7.590×10^{-7}	19.025	27.813	
BPL Carbon	C1	1.188	5.715	6.358×10^{-5}	4.080×10^{-6}	14.096	15.378	27.977
	C2	1.462	5.429	1.125×10^{-6}	2.090×10^{-6}	32.923	22.454	
A. Carbon 1 [17]	C1	5.824		1.918×10^{-6}		16.633		7.916
	C2	5.474		5.611×10^{-7}		25.102		
A. Carbon 2 [39]	C1	5.300	3.910	2.413×10^{-6}	7.730×10^{-6}	11.331	15.484	12.731
	C2	3.330	4.460	3.331×10^{-7}	4.176×10^{-6}	19.133	23.382	

Table 2.2: Dual-site Langmuir parameters for adsorbents considered in this study. Henry selectivity was calculated at 303.15K

Calculations using dual-site Langmuir model along with the experimental data, at 303.15K, are shown in Figure 2.3. Figure 2.3 show that carbons in general have higher saturation capacity than the titanosilicates (ETS). Also, at 303.15K the isotherms for ETS family are sharp which indicates that low vacuum pressures are required to desorb the gas. The results also suggest that titanosilicates might require higher operation temperature in order to make the isotherm less rectangular and avoid very low desorption pressures.

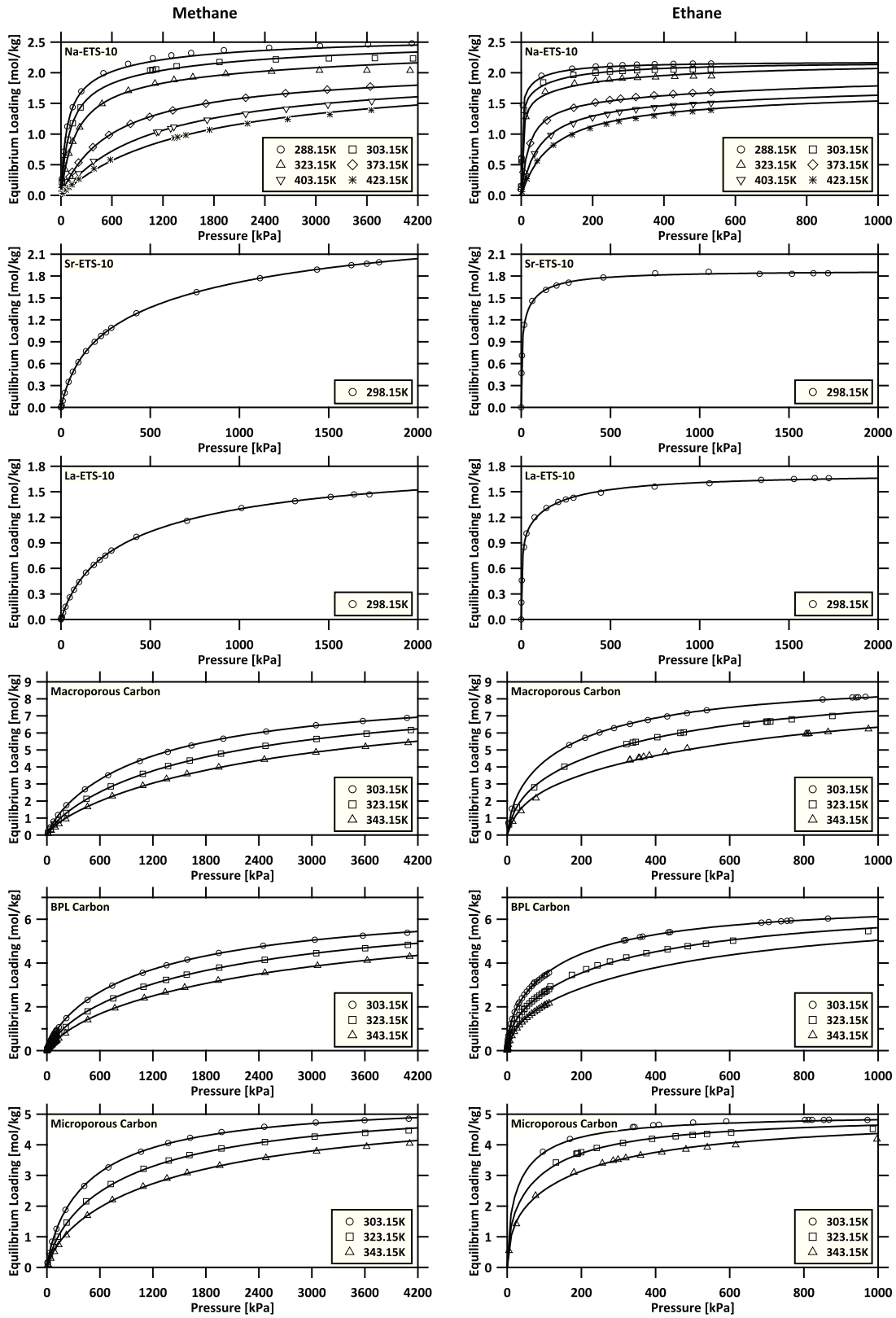


Figure 2.3: Adsorption Isotherms. Symbols and lines represent experimental and fitted values, respectively.

2.3.4 Heat of adsorption

Heat of adsorption is a measure of the strength of interactions between adsorbate molecules and adsorbent sites. From process engineering point of view, heat of adsorption is a measure of the energy required for adsorbent regeneration and provides an indication of temperature variations that can be expected on the bed during adsorption and desorption steps assuming adiabatic conditions in the process.

The $-\Delta U_i$ for all the components and the two sites are shown in Table 2.2. This values were obtained using the fitting process depicted in Figure 2.2. When energetic heterogeneity occurs in an adsorbent the higher energy sites will be occupied first by the adsorbate. Therefore, the internal energy calculated at Henry's region and compared with the change of internal energy obtained from the fitting process will provide a useful indication about the adsorbent heterogeneity and which component is the more strongly adsorbed. The Henry's constant for dual-site Langmuir model is defined as the summation of the product between the affinity parameter and the saturation capacity as shown below:

$$K_i = q_{sb,i}b_i + q_{sd,i}d_i \quad (2.9)$$

The temperature dependency of the Henry's constant is:

$$K_i = q_{sb,i}b_{0,i}e^{-\Delta U_{b,i}/RT} + q_{sd,i}d_{0,i}e^{-\Delta U_{d,i}/RT} \quad (2.10)$$

After the calculation of the Henry's constant from Equation 2.10, the change in internal energy can be obtained using the linearized form of the Henry's equation for the single-site Langmuir model:

$$\ln(K_i) = \frac{1}{T} \left(\frac{-\Delta U_i}{R} \right) + \ln(b_{0,i}) \quad (2.11)$$

The heat of adsorption is determined by plotting $\ln(K_i)$ versus $(1/T)$ using the experimental data at different temperatures. The points are fitted with a straight line whose slope gives the value of the $-\Delta U_i/R$. The Henry's constant is calculated, assuming linear behavior at low pressure, as the slope of the plot of experimental loading versus experimental pressure. Further, the heat of adsorption was also calculated by using the Henry's equation for the dual site Langmuir model as shown in Equation 2.10.

For a heterogeneous adsorbent, the internal energy obtained from the fitting of adsorption equilibrium data over a wide range gives the average value. Hence, it is expected to be lower than the value obtained from the linear range data. The plots of $\ln(K_i)$ versus $1/T$ for C1 and C2 on the four adsorbents measured in the lab are depicted in Figures 2.4 and 2.5. For La-ETS-10

and Sr-ETS-10, it was not possible to calculate the heat of adsorption because experimental measurements at different temperatures were not available.

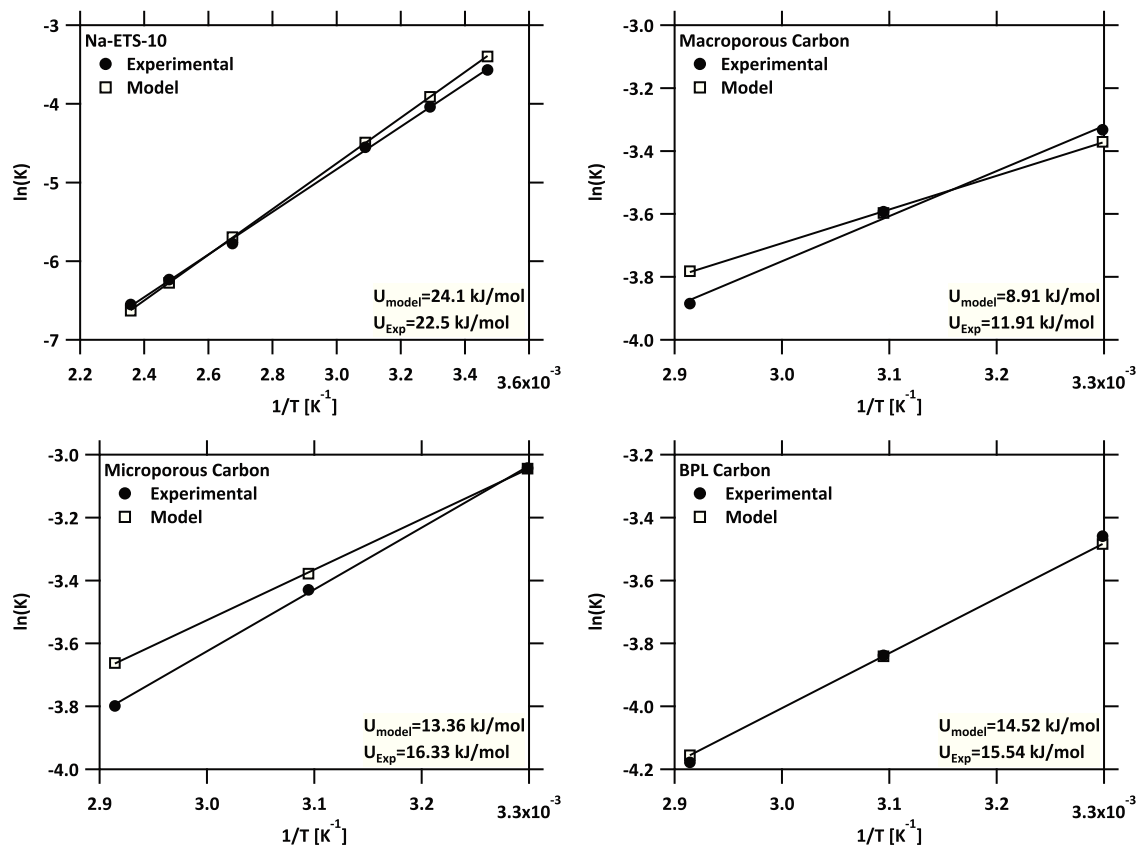


Figure 2.4: C1 heat of adsorption.

The results shown on Figures 2.4 and 2.5 point out the heterogeneous feature of the adsorbents used in this work. As was expected for this type of adsorbents, the heat of adsorption in the linear range was higher than obtained using the fitted parameters. Heat of adsorption calculated from the dual-site Langmuir model corresponds to the average value in the complete range the experiments were carried out. On the other hand, it was possible to verify that the heat of adsorption for C2 is higher than C1 for all the adsorbents, which points out C2 is the more strongly adsorbed component. Furthermore, C1 and C2 on Na-ETS-10 present the highest heat of adsorption when compared to the other materials. High heat of adsorption means that significant temperature variations during the adsorption process can be expected and hence, its overall performance will be affected.

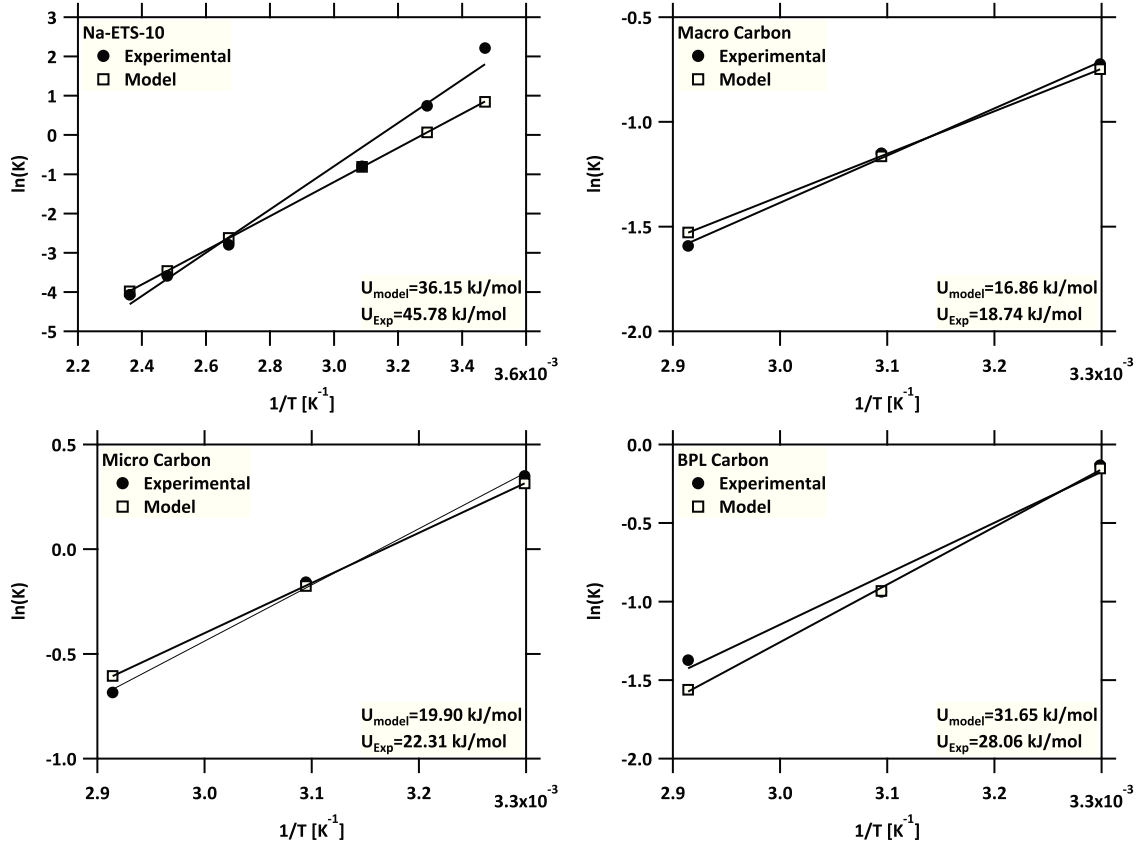


Figure 2.5: C2 heat of adsorption.

2.4 Conclusion

In this chapter, the description of the experimental procedure to measure adsorption equilibrium on solid adsorbents was presented. Three titanosilicates and 5 activated carbons (2 from literature) were selected to evaluate their performance on the separation of C1-C2 mixtures. Single component isotherms of methane and ethane on Na-ETS-10, Microporous, Macroporous and BPL activated carbons were measured at three different temperatures. As for Sr-ETS-10 and La-ETS-10, isotherms at a single temperature were measured.

Dual-site Langmuir model was selected because it was able to predict accurately the experimental data in the wide range of pressures. Therefore, a complete set of parameters for methane and ethane on the adsorbents selected was generated by minimization of the errors. Furthermore, heat of adsorption calculated from the experimental data points and the model were compared. For all the adsorbents, Ethane has higher heat of adsorption when compared to methane. Finally, by comparing the heats of adsorption obtained from the experiments and the model was possible to conclude that the adsorbents selected are energetically heterogeneous.

Chapter 3

Modeling and simulation

3.1 Introduction

In this chapter, a detailed simulation model is described for a generic adsorption process. The chapter starts with the description of the model assumptions and the constitutive transport equations. Further, boundary conditions for each step of the PVSA process are detailed. Subsequently, a discussion about the numerical techniques used to solve the model equations and the presentation of the finite volume method implemented in this work is presented. Finally, a validation of the model, based on the mass balances, and a detailed analysis about different process configuration is carried out.

3.2 Model equations

In order to develop a mathematical model for a one-dimensional dynamic column, the following assumptions were made:

- The bulk fluid flow is represented using an axially dispersed plug flow model.
- The gas phase obeys the ideal gas law.
- Mass transfer kinetics within the solid phase can be described by the linear driving force (LDF) model.
- Darcy's law is used to describe the pressure drop in the axial direction.
- Bed voidage and particle size are uniform across the column.
- The dual-site Langmuir model with single component isotherm parameters applies for binary equilibrium.
- The fluid and adsorbent are in thermal equilibrium.

- Temperature, pressure, and concentration gradients in the radial direction are neglected.
- Outer column wall is in equilibrium with ambient temperature.

Under these assumptions, mass, energy, and transport equations can be derived and are shown in Table 3.1 [19].

Model equations	
overall	
mass balance	$\frac{1}{P} \frac{\partial P}{\partial t} - \frac{1}{T} \frac{\partial T}{\partial t} = -\frac{T}{P} \frac{\partial}{\partial z} \left(\frac{P}{T} v \right) - \frac{1-\epsilon}{\epsilon} \frac{RT}{P} \sum_{i=1}^{n_{comp}} \frac{\partial q_i}{\partial t} \quad (3.1)$
Component	
mass balance	$\frac{\partial y_i}{\partial t} + \frac{y_i}{P} \frac{\partial P}{\partial t} - \frac{y_i}{T} \frac{\partial T}{\partial t} = \frac{T}{P} D_L \frac{\partial}{\partial z} \left(\frac{P}{T} \frac{\partial y_i}{\partial z} \right) - \frac{T}{P} \frac{\partial}{\partial z} \left(\frac{y_i P}{T} v \right) - \frac{RT}{P} \frac{1-\epsilon}{\epsilon} \frac{\partial q_i}{\partial t} \quad (3.2)$
Mass transfer rate	$\frac{\partial q_i}{\partial t} = k_i (q_i^* - q_i) \quad (3.3)$
Isotherm model	$q_i^* = \frac{q_{sb,i} b_i c_i}{1 + \sum_{i=1}^{n_{comp}} b_i c_i} + \frac{q_{sd,i} d_i c_i}{1 + \sum_{i=1}^{n_{comp}} d_i c_i} \quad (3.4)$
Pressure drop	$-\frac{\partial P}{\partial z} = \frac{150}{4} \frac{1}{r_p^2} \left(\frac{1-\epsilon}{\epsilon} \right)^2 \mu v \quad (3.5)$
Column energy balance	$\left[\frac{1-\epsilon}{\epsilon} \left(\rho_s C_{ps} + C_{pa} \sum_{i=1}^{n_{comp}} q_i \right) \right] \frac{\partial T}{\partial t} = \frac{K_z}{\epsilon} \frac{\partial^2 T}{\partial z^2} - \frac{C_{pg}}{R} \frac{\partial}{\partial z} (vp) - \frac{C_{pg}}{R} \frac{\partial P}{\partial t} - \frac{1-\epsilon}{\epsilon} C_{pa} T \sum_{i=1}^{n_{comp}} \frac{\partial q_i}{\partial t} + \frac{1-\epsilon}{\epsilon} \sum_{i=1}^{n_{comp}} \left((-\Delta H_i) \frac{\partial q_i}{\partial t} \right) - \frac{2h_{in}}{\epsilon r_{in}} (T - T_w) \quad (3.6)$
Wall energy balance	$\rho_w C_{pw} \frac{\partial T_w}{\partial t} = K_w \frac{\partial^2 T_w}{\partial z^2} + \frac{2r_{in} h_{in}}{r_{out}^2 - r_{in}^2} (T - T_w) - \frac{2r_{out} h_{out}}{r_{out}^2 - r_{in}^2} (T_w - T_a) \quad (3.7)$

Table 3.1: Model equations for modeling adsorption column dynamics.

3.3 Solution technique

Through the years and with the evolution of numerical methods to solve systems of coupled non-linear differential equations, different techniques have been proposed to solve the mathematical model for an adsorption process. Apart from models based on the equilibrium theory [40], the solution of the dynamic model for a PSA simulation requires numerical solutions. Different techniques such as orthogonal collocation [41], finite differences [42], method of characteristics [5], finite elements [43], and finite volume [19, 44, 45] have been proposed in literature. Among all these methods, finite volume has received special attention because it provides stability, robustness, and computational efficiency for different types of systems. Robustness implies that the

method provides accurate and meaningful results especially when the problem deals with difficult equations, such as nonlinear systems of hyperbolic equations which model realistic problems as the case of the cyclic adsorption. Apart from linear isotherms, where most of the numerical methods work well, for systems with curved, sharp isotherms, a fine discretization scheme is necessary in order to capture and describe the phenomena within the adsorption column.

A fine discretization increases the number of differential equations, resulting in longer computational time. Finite volume method is able to deal with sharp discontinuities and also reduce the nonphysical oscillations around them using fewer volume elements when compared with other methods [19]. An additional feature of this method is the local conservation of the numerical fluxes, i.e., the numerical flux is conserved from one discretization cell to its neighbor. Finite volume methods are based on a discretization of the integral forms of the conservation equations. The basic idea is to divide the work domain into a set of discrete control volumes. Figure 3.1 shows the discretization of one-dimensional domain into computational cells of width Δz . The cell centers are indicated by filled circles and cell edges by vertical lines; the cell number is shown above the filled circles while the numbers outside the column indicate cell edges and j represents the cell index.

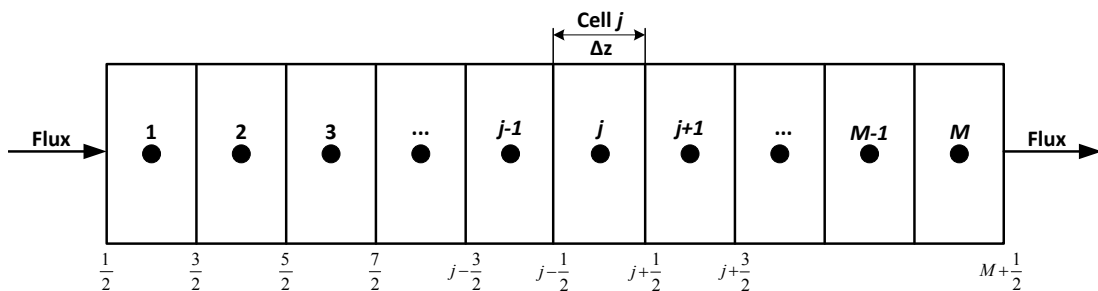


Figure 3.1: Schematic of a column discretized in finite volume.

In the finite volume method conserved quantities are approximated by a cell average given by [19]:

$$f(t) = \frac{1}{\Delta V} \int V_j f(t) dt \quad (3.8)$$

Using this approach, the equations were discretized in distance and a set of coupled differential equations in time was obtained. Prior to discretization, the system of equations was converted to a dimensionless form. The detailed information about the dimensionless equations and its discretization can be found elsewhere [19]. The implementation of the equations was carried out in Matlab using ode23s to solve the system of coupled differential equations. In all the simulations 30 volume elements, a balance between efficiency and speed, was used.

For hyperbolic problems such as the PVSA process, it is required that the estimation of the

values at the edge of the cell be accurate. The use of a simple scheme, i.e., finite difference approximation, will cause oscillations and low-order accuracy solution. Therefore, a high-order and robust methods such as high resolution total diminishing (TVD) or weighted essentially non-oscillatory (WENO) method are used [46]. In this work, a TVD method using Van Leer scheme was used [47]. The edge fluxes of the j^{th} cell can be obtained using this approximation. The equations for this scheme are shown as follow:

$$f_{j+0.5} = f_j + \frac{1}{2}\phi(r_{j+0.5})(f_{j+1} - f_j) \quad (3.9)$$

$$r_{j+0.5} = \frac{f_j - f_{j-1} + \delta}{f_{j+1} - f_j + \delta} \quad (3.10)$$

The successive slope ratio ($r_{j+0.5}$) is a measure of the smoothness of the solution whereas δ is constant with a very small value (10×10^{-10}) [19]. Further, flux limiters functions ($\phi(r_{j+0.5})$) are used to eliminate the effect of non-physical oscillations and limit the solution gradient near shocks or discontinuities.

$$\phi(r_{j+0.5}) = \frac{r_{j+0.5} + |r_{j+0.5}|}{1 + |r_{j+0.5}|} \quad (3.11)$$

3.4 The 4-step PVSA process

In order to demonstrate the model capabilities, a simple pressure vacuum swing adsorption process (PVSA) is considered. The process consists of 4 steps: adsorption, forward blowdown, reverse evacuation, and pressurization. As shown in Figure 3.2. Each step has unique features that are described below:

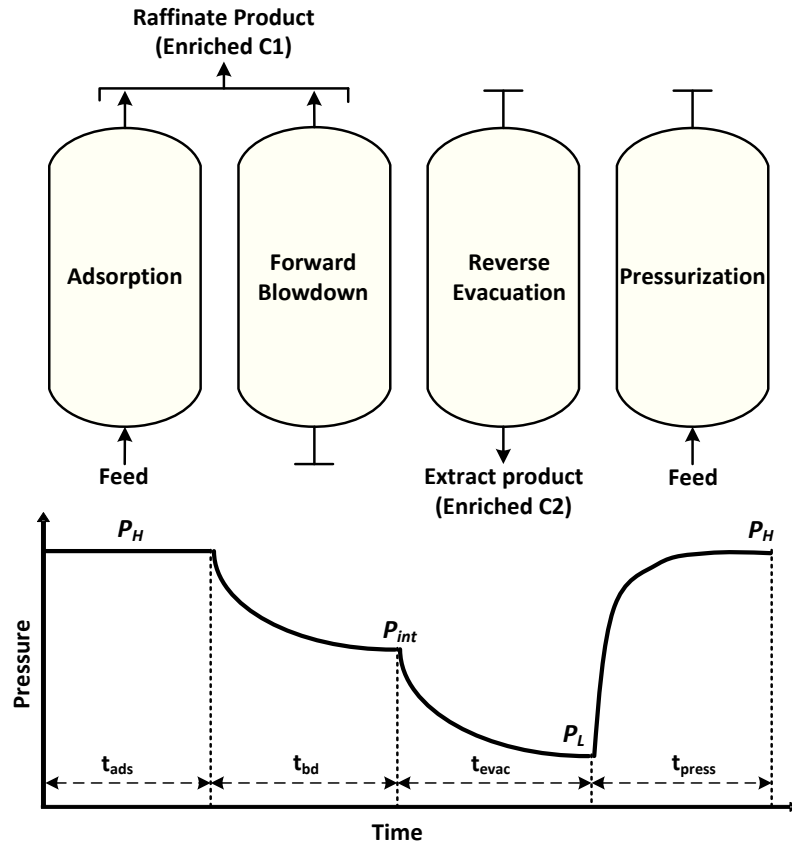


Figure 3.2: Basic 4-step PVSA process and corresponding pressure profile.

3.4.1 Adsorption

During the adsorption step the column is kept at constant high pressure ($P_H = 24$ bar) through time. A typical residue gas mixture, 2.4 mol% C2, rest C1, coming from the cryogenic distillation process at a pressure of 24 bar is fed into the column at $z=0$ while the end at $z=L$ is open to allow the weakly adsorbed component, C1, leave the column and be collected. Ethane, which is the heavy component, is preferentially adsorbed compared to C1. The time interval for this step must be less than the breakthrough time for Ethane to avoid losing this component. The pressure drop across the column is calculated from the overall mass balance shown in Table 3.1 and velocity (v) profile is calculated from Darcy's law. Since the inlet velocity (v_{feed}) is known for the duration of the adsorption step, inlet pressure is calculated from the Darcy's law.

3.4.2 Forward blowdown

At this step the feed end of the column is closed ($z=0$) and vacuum is applied using the product end ($z=L$) to reduce from high pressure (P_H) to an intermediate pressure (P_{int}) of 0.5 bar. It is expected to remove most of the C1 in both the gas and solid phases; thereby C2 is concentrated

in the column especially at the feed end zone. Because of the vacuum pressure, a small fraction of the preferentially adsorbed component will be lost, but most of it will remain inside the column. The desorption profile is assumed to obey an exponential change in pressure (Table 3.2) at $z=L$. In addition, velocity at $z=0$ is assumed to be zero.

3.4.3 Reverse evacuation

Ethane is the target product that is obtained from the feed end of the column ($z=0$). The evacuation step is carried out using this end while the product end is closed. A deeper vacuum is applied and the pressure is reduced from intermediate pressure ($P_{int} = 0.5$ bar) to low pressure ($P_L = 0.1$ bar). At this pressure, C2 along with the remaining C1 is released from the adsorbent and collected outside the column. At the end of this step the adsorbent is completely regenerated and ready to start over the process. In this step velocity is assumed to be zero at $z=L$. The desorption profile follows the same functional form as forward blowdown but at $z=0$.

3.4.4 Pressurization

The column at low pressure ($P_L = 0.1$ bar) requires to be pressurized up to the adsorption step pressure (24 bar). Feed stream, as described in adsorption step, is introduced into the column through the feed end ($z=0$) whereas the product end ($z=L$) is kept closed. The velocity is assumed to be zero at $z=L$ and the desorption profile is same as in reverse evacuation.

Danckwerts's boundary conditions for a dispersed plug flow system were used for the component mass balance in all the steps of the process. Regarding the column energy balance, analogous boundary conditions as in component mass balance were implemented for all the steps. The definitions and assumptions specified above define the necessary boundary conditions for each step of the process in order to solve the system of differential equations are described in Table 3.1. Although the equations showed in Table 3.1 are general, the boundary conditions define physical and mathematical specifications for each end of the column. A summary with the boundary conditions for the four steps is presented in Table 3.2.

Step	$z = 0$	$z = L$
Pressurization	$P _{z=0} = P_H + (P_L - P_H)e^{(-\alpha_p t)}$	$\frac{\partial y_i}{\partial z} _{z=L} = 0$
	$D_L \frac{\partial y_i}{\partial z} _{z=0} = -v _{z=0} (y_{i,feed} - y_i _{z=0})$	$\frac{\partial P}{\partial z} _{z=L} = 0$
	$\frac{\partial T}{\partial z} _{z=0} = -\epsilon v _{z=0} \rho_g C_{pg} (T_{feed} - T _{z=0})$	$\frac{\partial T}{\partial z} _{z=L} = 0$
	$T_w _{z=0} = T_a$	$T_w _{z=L} = T_a$
Adsorption	$v _{z=0} = v_{feed}$	$P _{z=L} = P_H$
	$D_L \frac{\partial y_i}{\partial z} _{z=0} = -v _{z=0} (y_{i,feed} - y_i _{z=0})$	$\frac{\partial y_i}{\partial z} _{z=L} = 0$
	$\frac{\partial T}{\partial z} _{z=0} = -\epsilon v _{z=0} \rho_g C_{p,g} (T_{feed} - T _{z=0})$	$\frac{\partial T}{\partial z} _{z=L} = 0$
	$T_w _{z=0} = T_a$	$T_w _{z=L} = T_a$
Blowdown	$v _{z=0} = 0$	$P _{z=L} = P_{int} + (P_H - P_{int})e^{(-\alpha_p t)}$
	$\frac{\partial y_i}{\partial z} _{z=0} = 0$	$\frac{\partial y_i}{\partial z} _{z=L} = 0$
	$\frac{\partial T}{\partial z} _{z=0} = 0$	$\frac{\partial T}{\partial z} _{z=L} = 0$
	$\frac{\partial P}{\partial z} _{z=0} = 0$	$T_w _{z=L} = T_a$
Evacuation	$P _{z=0} = P_L + (P_{int} - P_L)e^{(-\alpha_p t)}$	$v _{z=L} = 0$
	$\frac{\partial y_i}{\partial z} _{z=0} = 0$	$\frac{\partial y_i}{\partial z} _{z=L} = 0$
	$\frac{\partial T}{\partial z} _{z=0} = 0$	$\frac{\partial T}{\partial z} _{z=L} = 0$
	$T_w _{z=0} = T_a$	$\frac{\partial P}{\partial z} _{z=L} = 0$

Table 3.2: Boundary conditions for a 4-step PVSA process.

3.5 Model validation

Validation of the model requires the simulation of the entire PVSA process until the process reaches cycled steady state. At the beginning of the simulation, it is considered the column is saturated with 100% C1. A cycle implies the simulation of every step of the PVSA once in a specific sequence. The state of the column at the end of a step is taken as the initial condition for the subsequent step. The parameters for the model simulation can be found in Table 3.3.

Parameter		Value	
Column Length	L	1	[m]
Inner column radius	r_{in}	0.1445	[m]
Outer column radius	r_{out}	0.1620	[m]
Column void fraction	ε	0.39	[-]
Particle voidage	ε_p	0.35	[-]
Particle radius	ε_p	7.50×10^{-04}	[m]
Tortuosity	τ'	3	[-]
Column wall density	ρ_s	7800	[kg/m ³]
Specific heat capacity of gas phase	$C_{p,g}$	41.66	[J mol ⁻¹ K ⁻¹]
Specific heat capacity of adsorbed phase	$C_{p,a}$	40.02	[J mol ⁻¹ K ⁻¹]
Specific heat capacity of adsorbent phase	$C_{p,s}$	1070	[J kg ⁻¹ K ⁻¹]
Specific heat capacity of column wall	$C_{p,w}$	502	[J kg ⁻¹ K ⁻¹]
Fluid viscosity	μ	1.317×10^{-05}	[kg m ⁻¹ s ⁻¹]
Molecular diffusivity	D_m	1.53×10^{-05}	[m ² s ⁻¹]
Adiabatic constant	γ	1.4	[-]
Effective gas thermal conductivity	K_z	4.38×10^{-02}	[J m ⁻¹ K ⁻¹ s ⁻¹]
Thermal conductivity of column wall	K_w	16	[J m ⁻¹ K ⁻¹ s ⁻¹]
Inside heat transfer coefficient	h_{in}	8.6	[J m ⁻² K ⁻¹ s ⁻¹]
Outside heat transfer coefficient	h_{out}	2.5	[J m ⁻² K ⁻¹ s ⁻¹]
Universal gas constant	R	8.314	[m ³ Pa mol ⁻¹ K ⁻¹]
Interstitial feed velocity	η	1	[m s ⁻¹]
High Pressure	P_H	24	[bar]
Low Pressure	P_L	0.1	[bar]
Intermediate Pressure	P_{int}	0.5	[bar]
Ambient Temperature	T_a	298.15	[K]

Table 3.3: Parameters used in the process simulation.

Since adsorption is a dynamic process, PVSA requires the simulation of as many cycles as necessary in order to reach cyclic steady state condition and meet mass balance constraints. Considering the adsorption step, a general mass balance of the column is obtained:

$$\text{moles in} - \text{moles out} = \text{accumulation} \quad (3.12)$$

$$\text{moles in} = \frac{A\varepsilon}{RT_{feed}} \int_0^{t_{ads}} P_0 y_{feed} v_0 dt \quad (3.13)$$

$$\text{moles out} = \frac{A\varepsilon}{R} \int_0^{t_{ads}} \frac{P_0 y_{(t),out} v(t)}{T(t)} dt \quad (3.14)$$

$$\text{accumulation} = \text{accumulation in fluid phase} + \text{accumulation in solid phase} \quad (3.15)$$

$$\text{accumulation in fluid phase} = \frac{LA}{R} \int_0^z \frac{P_0 y(z) \epsilon}{T(z)} \Big|_{final} dz - \frac{LA}{R} \int_0^L \frac{P_0 y(z) \epsilon}{T(z)} \Big|_{initial} dz \quad (3.16)$$

$$\text{accumulation solid phase} = LA \int_0^z (1 - \epsilon) q_f \Big|_{final} dz - LA \int_0^z (1 - \epsilon) (q_i) \Big|_{initial} dz \quad (3.17)$$

In the previous equations A , L and ϵ are column cross sectional area, column length, and bed voidage, respectively. q_f and q_i are the equilibrium loadings at initial and final states of the process. As for the mass balance for the complete 4-step cycle, at cyclic steady state (CSS) conditions the accumulation after the evacuation step is close to zero and the moles coming into the process at the beginning of the cycle are equal to the moles withdrawn from the column at the end of the cycle. At every cycle, a mass balance error is evaluated in order to verify if the process has reached CSS:

$$\text{mass balance error} = \frac{|mass_{in} - mass_{out}|}{mass_{in}} * 100 \quad (3.18)$$

If the mass balance error is below 0.6% and there is no change in the column profiles of all state variables after each step for 5 consecutive cycles, it is assumed that the process has reached cyclic steady state and the simulation is stopped. In order to verify the model implemented, a simulation of a 4-step PVSA, using the dual-site Langmuir parameters for Na-ETS-10 described in Table 2.2, was performed using non-optimized operating conditions. Before the feed starts coming into the column, it is assumed that the bed is saturated with 100% C1. The process conditions used in this simulation are described in Table 3.4.

$y_{feed,C1}$	t_{ads}	t_{bd}	t_{evac}	P_H	P_I	P_L	v
[-]	[s]	[s]	[s]	[bar]	[bar]	[bar]	[m/s]
0.967	30	37	95	24	0.5	0.1	0.25

Table 3.4: Process conditions for the 4-step PVSA process.

A simulation was carried out using the conditions given above. Figure 3.3 depicts the mass balance error as a function of the number of cycles. After CSS the profile is totally flat and below 0.6% error.

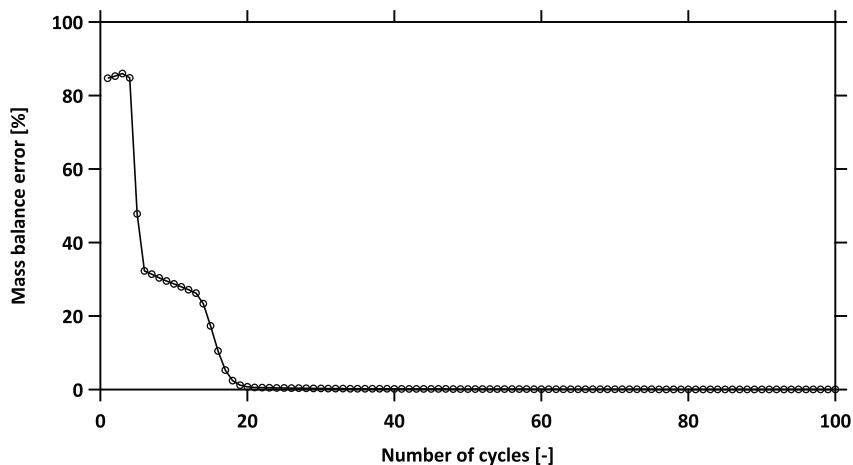


Figure 3.3: Decrease of the mass balance error with the number of cycles.

It is also worth showing the evolution of the column dynamics with the number of cycles until the process reaches cyclic steady state (CSS). Figure 3.4 shows the transient profiles for pressurization, adsorption, blowdown, and evacuation from the beginning of the cyclic operation up to steady state. Each profile in Figure 3.4 depicts the C2 gas phase composition throughout the column at the end of each step. Over the cycles, profiles start overlapping each other until CSS is reached, the profiles have a fast evolution and CSS condition is reached in the range of 60-80 cycles, which is fast compared to another separations systems whose range varies in the magnitude of hundreds [19]. As mentioned above, the criterion for cyclic steady step is based on the global mass balance error and the constant column profiles of all state variables. If during 5 consecutive cycles the mass balance error is less than 0.6% and there is no change in the column profiles, it is considered that CSS is reached.

Once the model was validated, simulations for the different adsorbents at different conditions can be performed. Also, different cycle configurations and optimization can be carried out in order to improve specified performance parameters. The development of this topics will be discussed in next chapters.

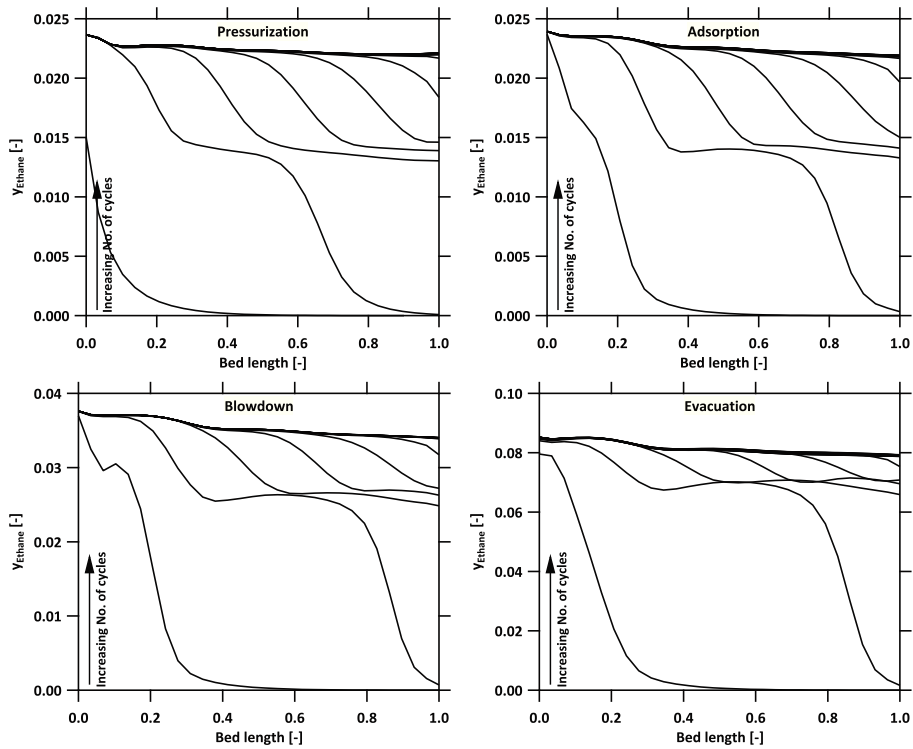


Figure 3.4: Transient profiles for each step of the PVSA cycle. Starting from the first cycle, profiles for every fifth cycle are shown

3.6 Conclusion

A complete and robust model to simulate a 4-step pressure vacuum swing adsorption (PVSA) process was presented. The model takes into account most of the transport phenomena present in an adsorption process. Finite volume method using Van Leer scheme [47] was chosen to discretize in distance the set of coupled differential equations. The method provides a good equilibrium between accuracy and efficiency requiring just 30 volume cell in order to capture with accuracy the evolution in the dynamic process for each state variable. The simulation performed showed the capability of the model to accomplish the cyclic steady state constraints assigned.

Chapter 4

Ethane recovery from residue gas

4.1 Introduction

In this chapter, the separation of C2 from residue gas using three different configurations of PVSA processes are presented. Apart from the basic 4-step cycle presented in Chapter 3, two new configurations are added to find the best configuration in terms of C2 purity and recovery. Simulations of the three cycles proposed are carried out using the adsorbents described in Chapter 2. Comparisons between the cycles are made in terms of purity and recovery and taking into account the effect of feed temperature. Also, the importance of a model which includes heat effects is described by performing isothermal and non-isothermal simulations. It was observed that isothermal simulations produced results that delivered significant deviation compared to non-isothermal simulations.

4.2 Process design and configuration

PVSA process design is a complex task due to the extensive number of possible process configurations and conditions that can be changed and improved; for example, intermediate and lower pressures, feed velocity and temperature, time span for each step and so on. Additionally, each adsorbent selected will have its own set of operating conditions, where the process produces better results in terms of defined performance metrics compared with a different adsorbent plus process configurations.

Process conditions such as adsorption pressure (P_H) and evacuation pressure (P_L) were selected based on industrial constraints. The adsorption pressure fixed at 24 bar is because the feed stream is a residue gas which comes from the cryogenic distillation process operated at this pressure. As for the evacuation pressure, 0.1 bar of vacuum pressure was chosen for the simulations described in this chapter because it represents a feasible industrial operating value. Deeper vacuum pressures could be achieved but operating costs would convert the PVSA process eco-

nominally unfeasible. The duration of the adsorption step (t_{ads}) was selected to avoid loss of C2 in the product stream. Blowdown and evacuation times were chosen long enough in order to remove completely the material that can be withdrawn at the pressures defined for these steps. Blowdown pressure (P_{int}) value should be chosen in order to remove most of the C1 in the column, but avoiding C2 removal.

It has been shown in literature that the basic 4-step cycle described in Chapter 3 presents some disadvantages such as loss of the strongly adsorbed component during the adsorption and blowdown steps, resulting in a decrease of purity and recovery of the heavy component [34]. Since the composition of C2 in the feed is extremely low (2.4%), it is necessary to avoid loss of C2 in the steps mentioned above. To overcome this issue, two cycle configurations, found in literature to separate CO₂, were implemented in this work [34]. Basic 4-step cycle with light product pressurization (LPP) instead of feed pressurization and 5-step cycle with light product pressurization and heavy reflux (LPP+HR) were chosen and are depicted in Figure 4.1 along with the Basic 4-step cycle and the operating conditions used in the simulations.

Purity (Pu) and Recovery (Re) are the indicators to evaluate the performance of the cycle configuration and the adsorbent. Purity and recovery were also performance targets requested from the industrial partner as the PVSA unit will be tightly integrated to the cryogenic distillation unit and the overall process economics can be calculated using these metrics. Besides, purity is calculated based on the ratio between the number of moles of ethane (C2) obtained and the total number of moles both measured at the end of evacuation step for one cycle. Equation 4.1 allows calculating purity for the Basic 4-step and LPP cycles.

$$\text{Purity (Pu)} = \frac{\text{moles of C2 in extract stream collected in 1 cycle}}{\text{total moles of C1 + C2 in extract stream collected in 1 cycle}} * 100 \quad (4.1)$$

Recovery for both basic 4-step and LPP cycles is defined as the ratio between the moles of C2 obtained in the evacuation step and the moles of C2 fed in the adsorption step:

$$\text{Recovery (Re)} = \frac{\text{moles of C2 in extract stream collected in 1 cycle}}{\text{total moles of C2 fed in 1 cycle}} * 100 \quad (4.2)$$

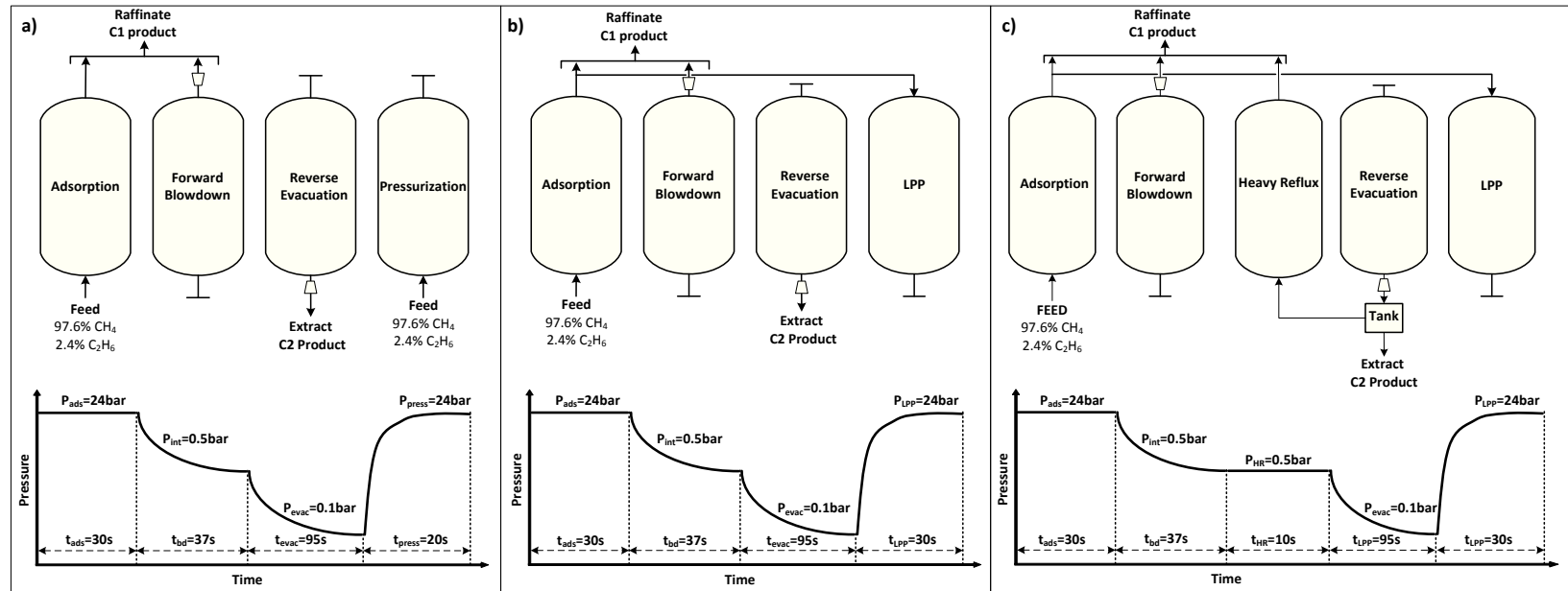


Figure 4.1: Cycle configuration and process conditions. a) Basic 4-step; b) Basic 4-step with light product pressurization (LPP); c) 5-step with LPP and heavy reflux (LPP+HR).

4.2.1 4-step cycle with light product pressurization (LPP)

In this cycle, the stream used for pressurization step is changed from feed stream to the product stream obtained at the end of adsorption step which is concentrated C1 (the light product). Besides, the stream coming into the column to pressurize it is fed using the product end of the column ($z = L$) which is counter-current to the original 4-step cycle. The use of C1 to pressurize in the reverse direction changes the dynamics of the column mainly in two ways:

- The light product, C1, will push the C2 present in the raffinate product end towards the feed end, thereby avoiding the loss during the adsorption step resulting in improved recovery.
- Since C2 is mainly concentrated at the feed end of the column ($z = 0$), the intermediate pressure for the blowdown step can be lower when compared to the basic 4-step cycle. It will increase the amount of C1 removed from the bed during blowdown step and thus, the purity of C2 during evacuation step.

As was mentioned above, the LPP uses adsorption product to pressurize the column, so this effluent should be stored in a tank until the PVSA cycle reaches the pressurization step in order to reflux it into the column. To implement this step in the simulation, it is necessary to calculate both, total and component mass balances of the adsorption product stream during the entire time span of the adsorption step. Although component mole fractions change through time, it was assumed that at the end of the step, the product is perfectly mixed within the tank and a final mole fraction is calculated using the mass balance shown in Equation 4.3

$$\text{moles out} = \frac{A\epsilon}{R} \int_0^{t_{ads}} \frac{P_0 y_{(t),out} v(t)}{T(t)} dt \quad (4.3)$$

The Ethane mole fraction in the tank is calculated from:

$$y_{Ethane|ads} = \frac{\text{moles out } C_2|_{ads}}{\text{total moles out}|_{ads}} \quad (4.4)$$

It is worth noting that this methodology is routinely applied in PSA modeling with minor loss in accuracy [34, 48, 49]. Using this stream as feed, the LPP step is carried out in the same way as the pressurization step. Two extra events should be taken into account. First, the mass in the tank is limited, so a constraint must be written in the simulation code to avoid violations of the mass balance, i.e., the number of moles used for pressurization cannot be greater than what was collected. If the mass in the tank is not enough to pressurize the column, an external feed is used to accomplish the adsorption pressure (24 bar). All of these possibilities were considered in the code and in the overall mass balance equation for the process. Second, the stream in LPP step is fed into the column at $z = L$ instead of $z = 0$ in the normal pressurization step. This change is translated in the simulation code by changing the direction of the feed. Another rare

but possible situation is when the number of moles collected in the tank is more than what is required for the pressurization. In this case, the contents of the tank are added to the raffinate product.

4.2.2 5-step cycle with light product pressurization and heavy reflux (LPP+HR)

In this process configuration, a LPP step, explained in the previous section, and a Heavy Reflux (HR) step were implemented. The use of a Heavy Reflux at the blowdown pressure (P_{int}) increases C2 purity while the LPP step increases its recovery. As shown in Figure 4.1, a fraction (θ) of the evacuation product is taken, stored in a tank, and refluxed into the column using the feed end ($z = 0$). The tank for this step was modeled in the same way as the LPP step explained in Section 4.2.1. In addition to the tank, in HR step a pump is necessary to feed the product at the blowdown pressure. Note that the vacuum pump used to remove the extract stream will delivered the product at atmospheric pressure and hence, there will be no need for an additional fluid mover to introduce the reflux.

The HR step will cause enriching of the heavy component at the feed end of the column. Methane present either in the gas phase or solid phase will be moved toward the product end of the column and a product stream rich in this component will be obtained during HR step. Furthermore, C2 purity in the evacuation step will increase because of both removal of C1 in HR step and C2 enriching at the product end of the column. The performance of this cycle is also measured in terms of purity and recovery described as follows:

$$\text{Purity (Pu)} = \frac{\text{mole}_{\text{out C2}}|_{\text{evac}}}{\text{mole}_{\text{out Total}}|_{\text{evac}}} * 100 \quad (4.5)$$

$$\text{Recovery (Re)} = \frac{(1 - \theta)\text{mole}_{\text{out C2}}|_{\text{evac}}}{\text{mole}_{\text{in C2}}|_{\text{Ads}}} * 100 \quad (4.6)$$

The number of moles which come into the column at the HR step are calculated as:

$$\text{mole in total}|_{\text{HR}} = \text{mole out total}|_{\text{evac}}(\theta) \quad (4.7)$$

Ethane mole fraction inside the tank at the end of evacuation step is obtained from:

$$y_{\text{C2}}|_{\text{evac}} = \frac{\text{moles out Ethane}|_{\text{evac}}}{\text{moles out total}|_{\text{evac}}} \quad (4.8)$$

In terms of the simulation, HR step can be simulated as an adsorption step, but at low pressure. It implies that boundary conditions for adsorption step are used in HR step with the exception of the feed velocity boundary condition that is obtained in a different way. The mass fed to the

column in this step is a known value and is the mass within the tank, so by fixing the time span the feed velocity can be calculated from the following mass balance equation [34].

$$v_{HR} = \frac{\text{mole in } C2|_{HR}}{t_{HR} A \epsilon \frac{P|_{z=0}}{RT_{feed}|_{HR}}} \quad (4.9)$$

4.3 Column dynamics of the PVSA cycles

To observe the dynamics within the adsorption column at each step and for the three cycles chosen, simulations were performed at the same conditions using Na-ETS-10 as adsorbent. The main purpose of this simulations is to show the behavior of both gas phase and solid phase profiles throughout the column when the cycle reaches cyclic steady state. It is also important to analyze what is the effect across the column when LPP and HR steps are implemented. Operating conditions for this simulations are described in Figure 4.1 and the feed temperature was assumed to be 298.15K.

Figure 4.2 depicts the C2 gas phase and composition profiles at the end of each step for the basic 4-step, 4-step cycle with LPP, and 5-step cycle with LPP and HR. The gas phase profile for the basic 4-step cycle shows that during the adsorption step the column is completely saturated with feed which means the adsorption time is exceeding the breakthrough time and Ethane is being lost in the product stream. The analysis of the solid phase for the same cycle shows a long tail of ethane up to the product end of the column, confirming Ethane is being lost. To avoid loss of C2 during the adsorption step in this cycle, it would be necessary either to reduce the time span of the adsorption step or the feed velocity.

Furthermore, a slight variation (<0.2 mol/kg) in the solid loading between the adsorption and evacuation steps means that most of the C2 is still present in the adsorbent. The reason for this can be found in the isotherms showed in Figure 2.3. At 298.15K the isotherm of C2 on Na-ETS-10 is sharp and rectangular; hence, deeper evacuation pressure should be used in order to release C2 from the adsorbent. As was mentioned above, the use of deeper vacuum pressure increases the operational cost of the process, thereby making unfeasible the process. However, an alternative solution can be posed. Instead of lower evacuation pressure, increasing the feed temperature will cause that the C2 isotherm be less rectangular; as a result, more C2 can be recover during the evacuation step. The basic 4-step process yielded a C2 purity and recovery of 6% and 11%, respectively.

As for the 4-step cycle with LPP, the profiles depicted in Figure 4.2 show the effect of adding LPP step. The solid phase composition profile shows how the light component fed during the LPP step moves the C2 concentration front towards the feed end thereby, the loss of this component during the adsorption step and increasing the recovery from 11% in the basic 4-step process to 14% in the cycle with LPP

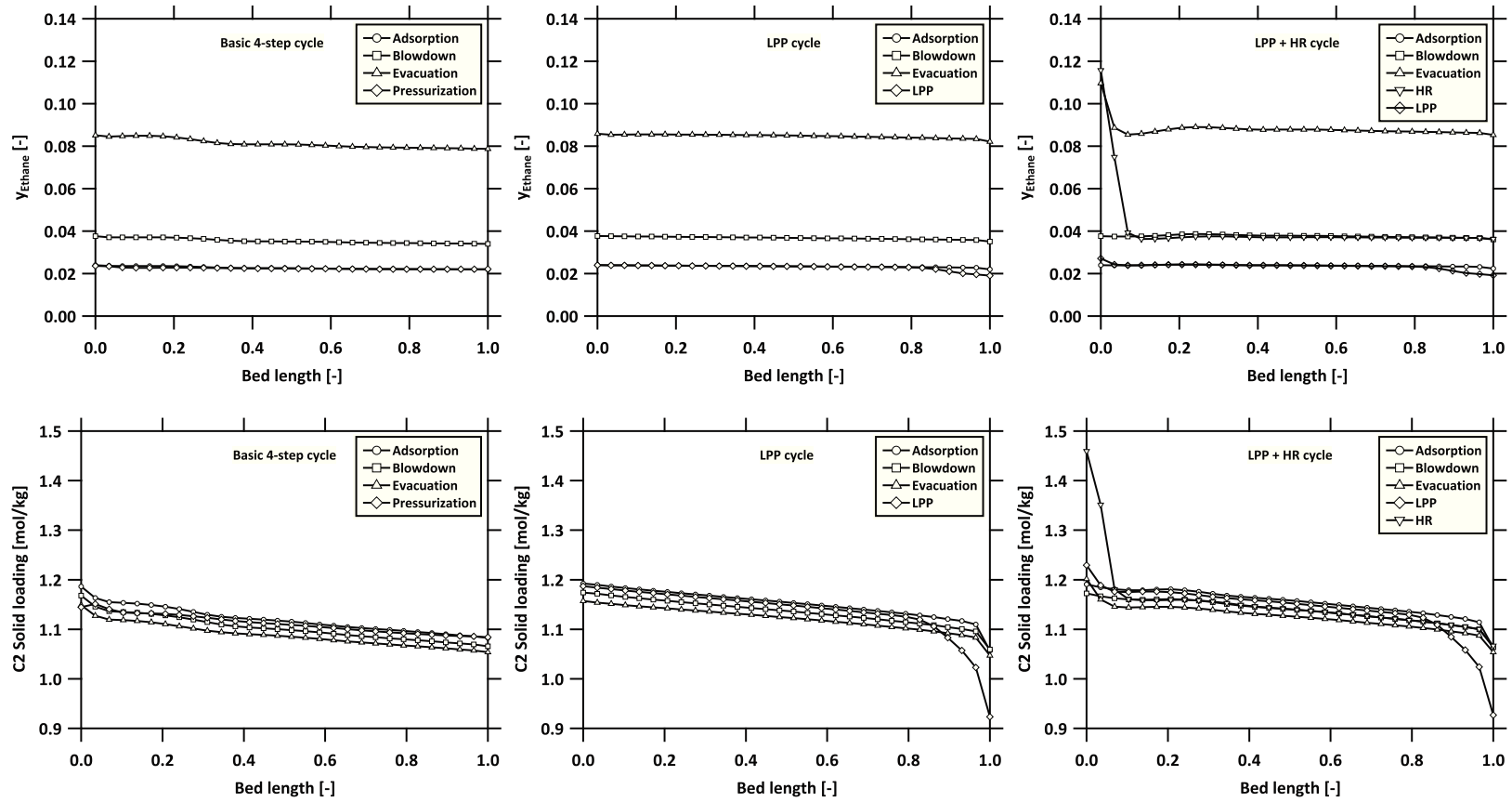


Figure 4.2: C2 gas and solid phase column profiles for the cycles chosen using Na-ETS-10.

The feed end section of the column ($z = 0$) has now a higher concentration of C2 in the solid phase which will increase slightly the C2 purity, but due to the sharpness of the isotherm at the given temperature most of the gas stays on the solid phase. The 5-step cycle with LPP and HR provides a significant advantage in terms of purity with respect to the previous cycles, from 6% to 10%, as can be seen in Figure 4.2. The use of HR step increases considerably the C2 concentration at the feed end of the column while the LPP step moves the C2 front from the product end ($z = L$) to the feed end ($z = 0$) of the column. As a result, the stream collected in the evacuation step will have a higher concentration of C2 when compared with the Basic and LPP cycle. The increase in C2 purity brings also a decrease in its recovery due to the amount of C2 which has to be refluxed into the column.

4.3.1 Effect of light product pressurization and heavy reflux (LPP+HR) on process performance

Now that the column dynamics for each step and cycle has been explained, it is possible to move forward and perform simulations for all the adsorbents described in Chapter 2. To compare the adsorbents, it is necessary to establish a common set of operating conditions. Those conditions are given in Figure 4.1. Using this conditions, simulations of the three proposed cycles were performed for the eight adsorbents described in Chapter 2. A feed temperature of 298.15K was chosen because at this temperature it is possible to evaluate La-ETS-10 and Sr-ETS-10. It is important to remember that for these two adsorbents the experimental measurements were performed at only one temperature; therefore, isothermal simulations at the experimental temperature must be considered for these pair of adsorbents. Figure 4.3 shows the performance in terms of purity and recovery for all the adsorbents.

It is clear from Figure 4.3 that the best performance, at the conditions specified, is for La-ETS-10, Sr-ETS-10, and one of the activated carbons from literature, i.e. A. Carbon 1 [17]. The rest of the adsorbents have similar performance which is inferior at least by a factor of 2 when compared with the best performing adsorbents. Looking at the isotherms of A. Carbon for both components, it was noticed that the isotherm for C2 on this carbon is less rectangular than the rest of the adsorbents. Therefore, at the evacuation pressure this adsorbent is able to provide higher C2 working capacity increasing both purity and recovery. As for La-ETS-10 and Sr-ETS-10, although the shape of the isotherms and the adsorption capacity of these two is similar to that shown by Na-ETS-10, the performance of Na-ETS-10 is inferior. This behavior might be attributed to the difference in the simulation conditions, while for Na-ETS-10 a non-isothermal simulation was considered, for La-ETS-10 and Sr-ETS-10 isothermal simulations were considered. This will be the focus of the next section.

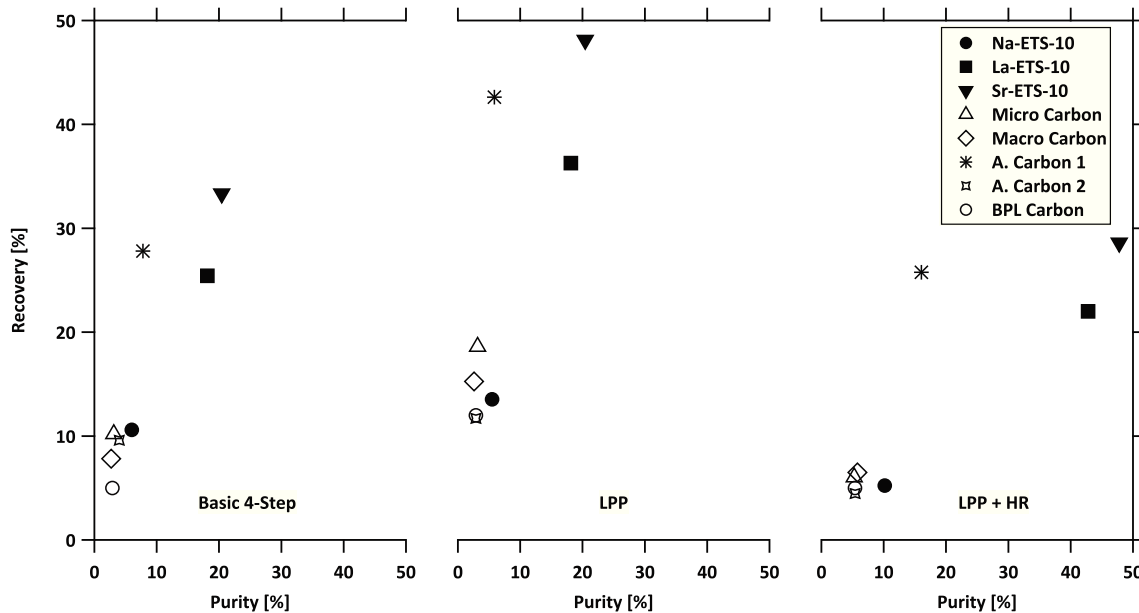


Figure 4.3: Comparison of Basic, LPP and LPP+HR cycles at 298.15K. Operating conditions shown in Figure 4.1.

4.3.2 Effect of isothermal assumption in the simulation

Isothermal and non-isothermal simulations were performed in order to see the difference in performance using these two conditions. It is worth noting that industrial columns, owing to their dimensions, i.e., large diameters, typically operate under adiabatic conditions. However, many simulations are usually performed under isothermal conditions, either because isotherm data is not available at multiple temperatures or because of the difficulties in simultaneously solving the mass and heat balances. Hence, it is important to illustrate the differences between these two operating conditions. In addition, LPP+HR cycle was selected to make the comparison. Results in terms of purity and recovery are shown in Figure 4.4. It can be inferred that isothermal simulations over-predict the performance of the adsorbents. It is clear that heat effects play a key role in the process and neglect them can produce misleading results.

In order to understand how the PSA process is affected when heat effects are taken into account, temperature profiles for the basic 4-step cycle at two different feed temperatures are depicted in Figure 4.5. From the Figure it can be seen that there is a significant change in temperature during the pressurization step in part due to the big increase of pressure within the column (from 0.1 bar to 24 bar) and also, because of the exothermic nature of the adsorption phenomenon. Increasing the feed temperature from 298.15K to 423.15K, increases the temperature within the column. Furthermore, during the evacuation and blowdown steps the decrease in pressure, up to vacuum levels, causes a strong reduction in temperature within the column.

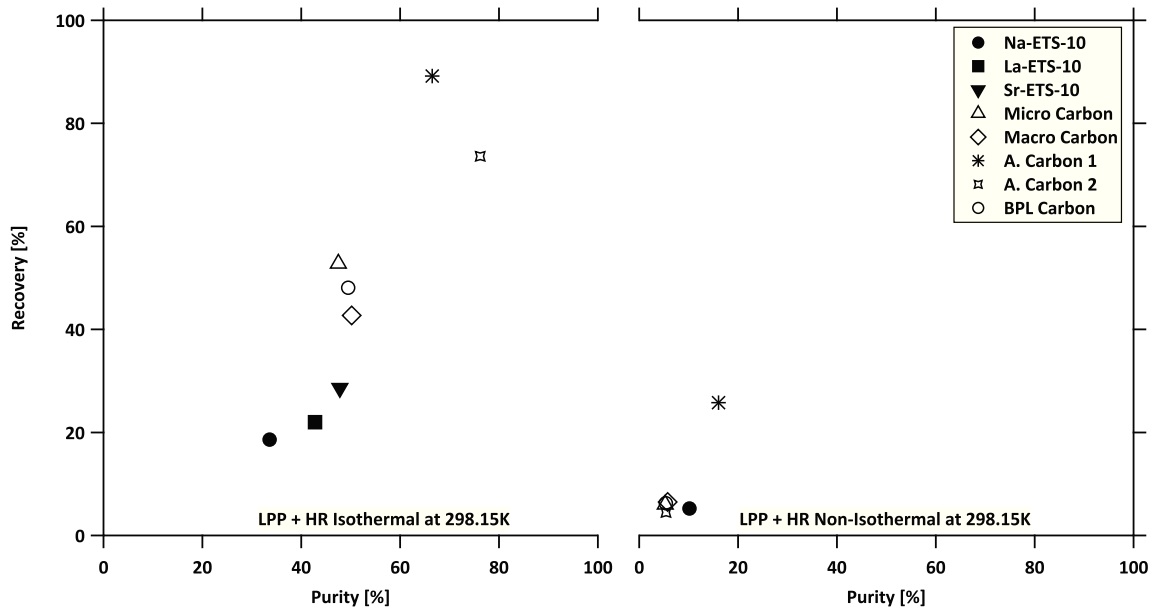


Figure 4.4: Comparison between isothermal and nonisothermal simulations. Note that for the case of La-ETS-10 and Sr-ETS-10, only isothermal simulations were performed due to lack of experimental data at multiple temperatures.

The temperature gradient within the column due to the pressure changes affects the performance of the process. The decrease in temperature during evacuation and blowdown reduce the amount of C2 that can be desorb because at lower temperatures gas molecules are more attached to the adsorbent and additionally it has more adsorption capacity. On the other hand, if the process is considered completely isothermal and equal to the feed temperature, the desorption steps will occur at this temperature and more C2 can be desorbed. It explains why at isothermal conditions C2 purity and recovery is much higher than those using non-isothermal conditions. Therefore, isothermal simulations provide results that are very different from the real dynamics of the PSA process that can derive in misleading conclusions. Heat effects play a key role in the process dynamics.

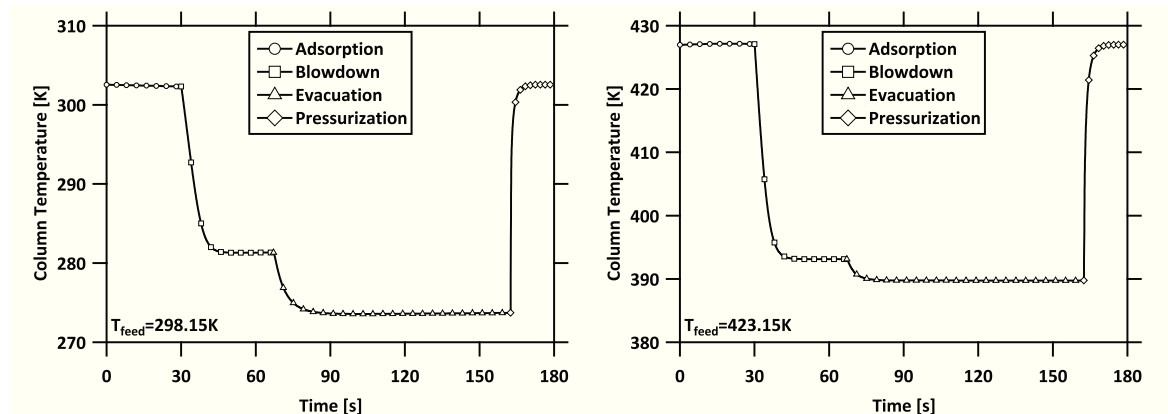


Figure 4.5: Temperature profiles in the 0.5 non-dimensional length of the column for the basic 4-step cycle using two different feed temperatures. Operating conditions depicted in Figure 4.1.

4.3.3 Effect of temperature on process performance

As was discussed in Section 4.3, feed temperature can be increased in order to reduce the sharpness of the isotherms resulting in a significant decrease of the adsorbent capacity at the evacuation pressure limit, thereby more C2 is desorbed during the evacuation step. Accordingly, it is expected that increasing feed temperature will enhance purity and recovery of the process. The change in the isotherms shape with the increase of the temperature can be seen in Figure 4.6. Three different temperatures, namely, 298.15K, 343.15K, and 373.15K were used. Higher temperatures make the isotherms less rectangular. It is also interesting the effect of temperature on isotherms on Na-ETS-10, at 373.15 the adsorption capacity for C1 has decreased considerable while the adsorption capacity for C2 had a small reduction, which means that at higher temperatures the concentration of C2 in the adsorbed phase is higher than at low temperatures and hence, C2 purity and recovery will increase.

To verify this, simulations of the 5-step cycle with LPP+HR were performed for 6 adsorbents using the same temperatures of Figure 4.6. La-ETS-10 and Sr-ETS-10 were excluded due to the inconclusive results showed by the isothermal simulations. LPP + HR was chosen because it is the cycle which has shown better results when compared with the basic 4-step and the 4-step cycle with LPP. The results of the simulations are depicted in Figure 4.7.

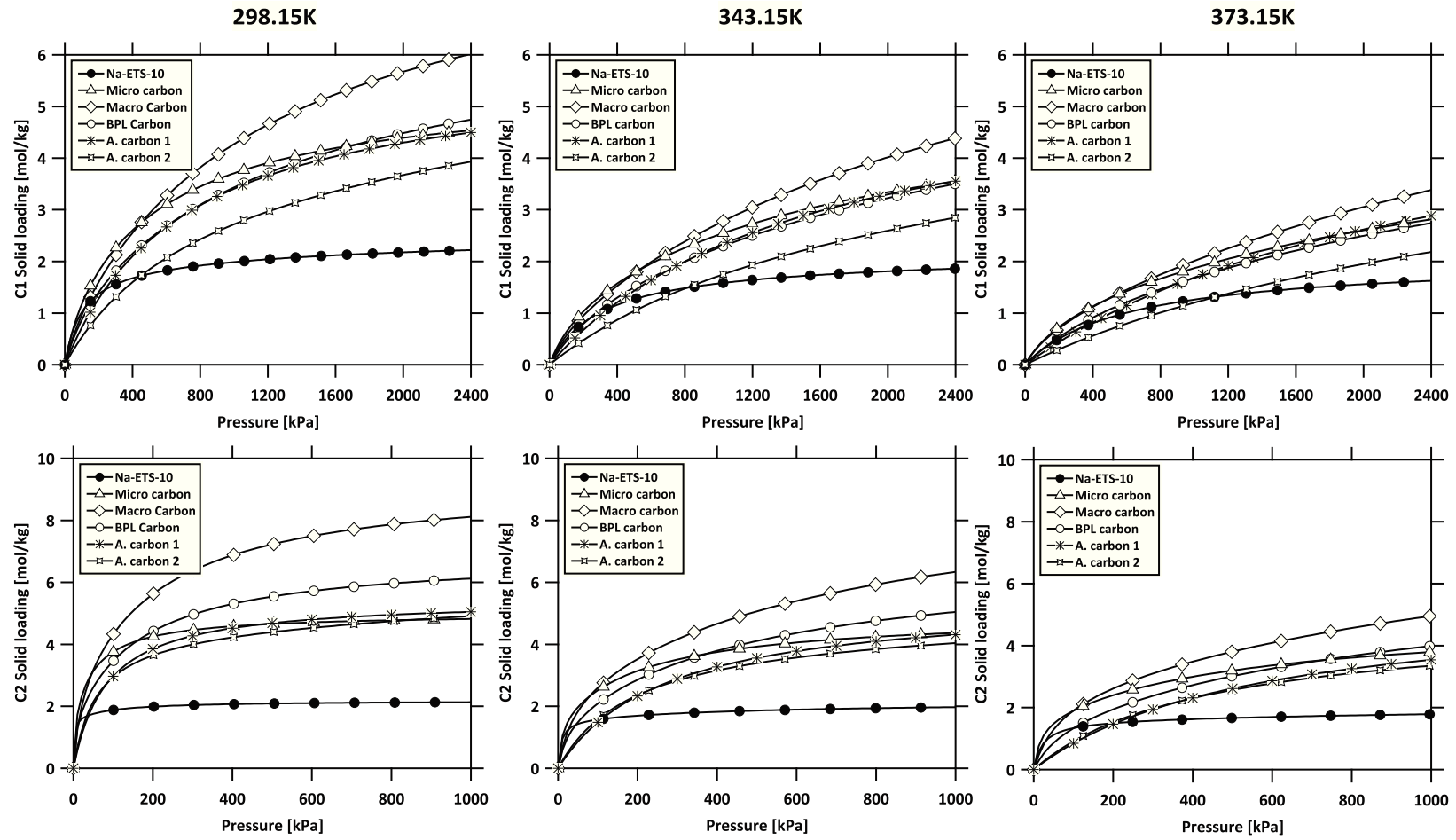


Figure 4.6: Adsorption isotherms of C1 and C2 on all the adsorbent at different temperatures.

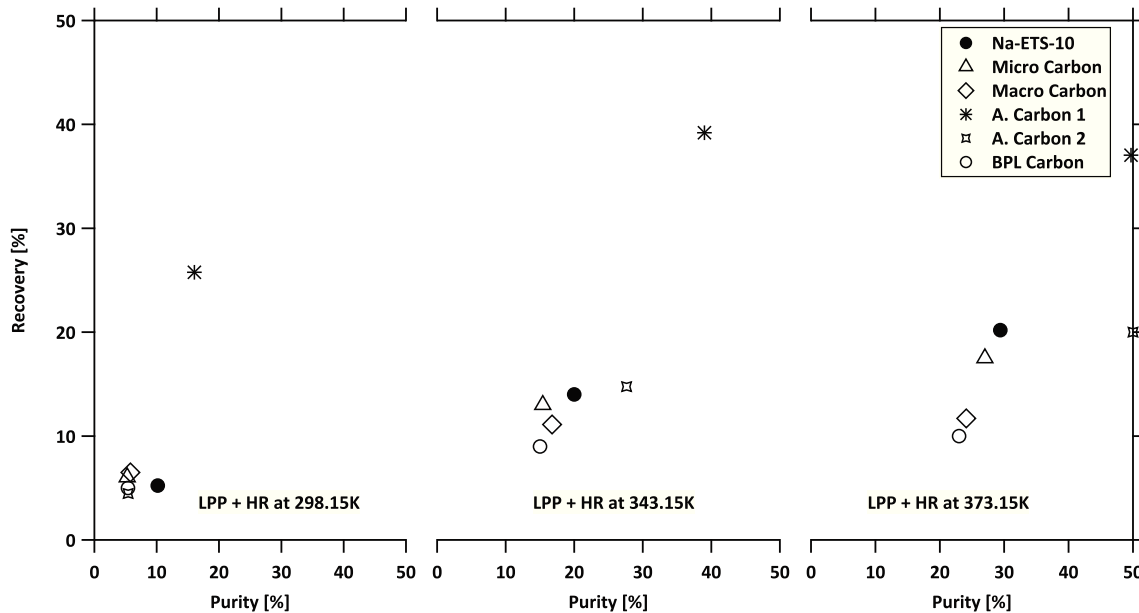


Figure 4.7: LPP+HR Cycle at different temperatures.

From the figure, it can be seen that effectively the increase of feed temperature enhances the performance of the cycle. All the adsorbents show better results at high temperatures especially Na-ETS-10. It is because at higher temperatures, namely, 343.15K and 373.15K Ethane isotherms are less rectangular and more C2 can be desorbed during the evacuation step. It is possible to conclude from this results that adsorption capacity is not an indicator to choose adsorbents or to evaluate the performance. Activated carbons tested in-house have higher adsorption capacity than Na-ETS-10, both classes of adsorbent have similar performance at 298.15K, but at higher temperature Na-ETS-10 exhibits a better performance.

It is also important to analyze how the gas and solid phase profiles within the column change with the increase of feed temperature. With this purpose, gas and solid phase profiles of C2 using Na-ETS-10 as adsorbent are depicted in Figure 4.8. The same cycle and feed temperatures illustrated in Figure 4.7 were considered. At 298.15K the solid phase profile shows that the adsorbent has a higher capacity when compared to the other two temperatures. However, the amount of C2 desorbed during the evacuation step is small due to the sharpness of the isotherm at this temperature which leads to a poor working capacity. It can be verified looking at the gas phase profile at the same temperature. The area between blowdown and evacuation profile is narrow, which means that a small amount of C2 was desorbed during this step.

With the increase of feed temperature the adsorbent capacity decreases, as can be seen in the solid phase profiles at 343.15K and 373.15K from Figure 4.8. Nevertheless, increasing temperature enhance the working capacity of the adsorbent since the sharpness of the isotherm is significantly reduced and hence, more C2 can be desorbed at the evacuation step.

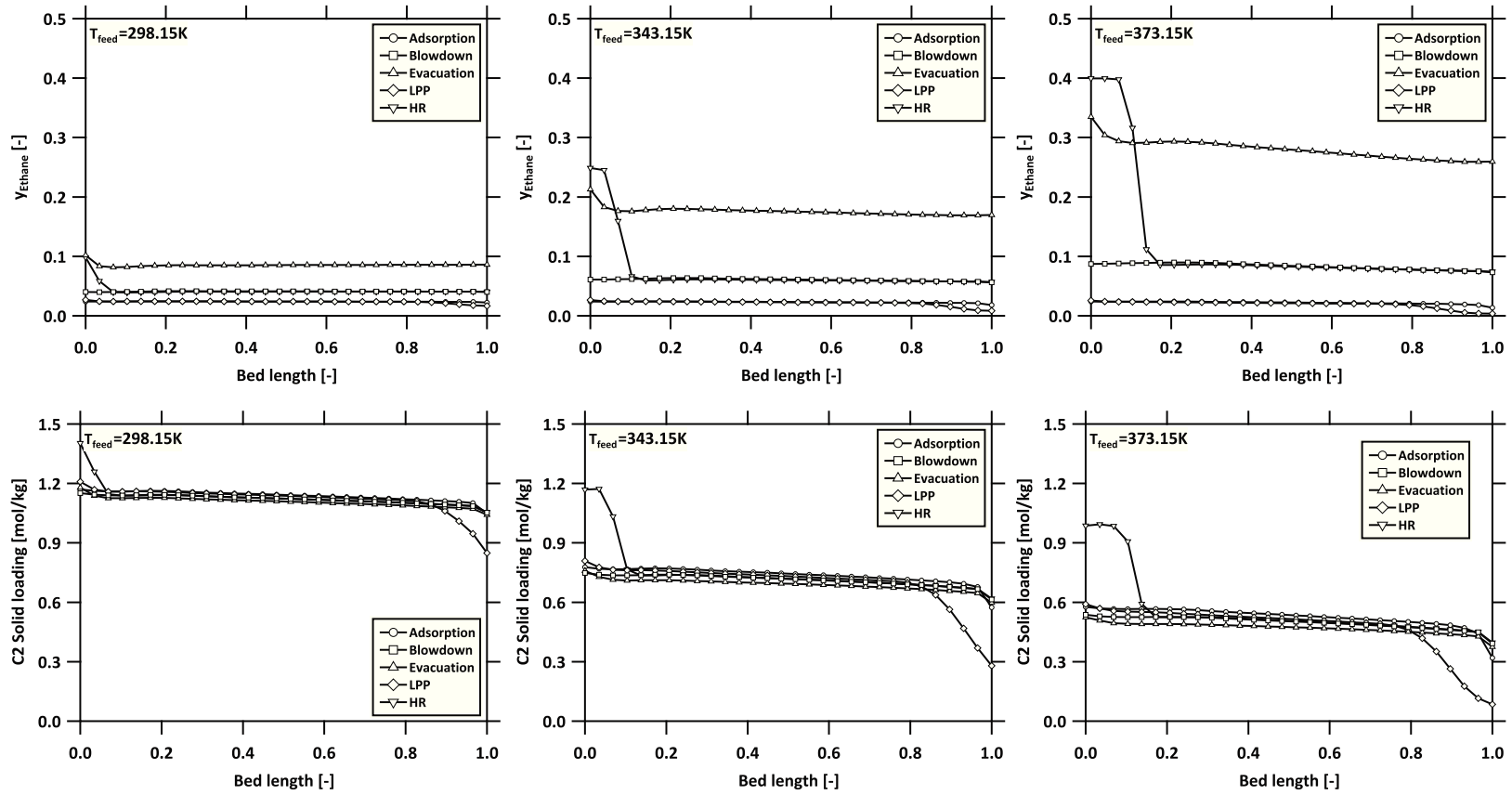


Figure 4.8: C2 gas and solid phase column profiles for 5-step cycle with LPP+HR at different feed temperatures using Na-ETS-10.

Further, the area between the gas phase profiles for blowdown and evacuation is broader with the increase of temperature, causing a higher concentration of C2 in the gas phase, thereby improving purity and recovery. It is also noteworthy the change in the HR profile with the increase in feed temperature. At higher temperatures the C2 concentration front during the HR step moves further inside the column resulting in a larger region within the column enriched with C2.

Globally, the adsorbents which perform better at the specified operations conditions are the Activated carbons taken from literature, i.e. A. Carbon 1 [17] and A. Carbon 2 [39]. Follow them, Na-ETS-10 shows the best results among ETS family of adsorbents. If higher feed temperatures are used, it is possible that the performance of Na-ETS-10 may be better than the other adsorbents. To find the optimal temperature and operating conditions requires a multi-objective optimization process which will be discussed in next chapter.

4.4 Conclusion

In this chapter, the 4-step cycle with LPP and the 5-step cycle with LPP+HR were presented. A performance comparison with the basic 4-step cycle was made by running simulations with the same non-optimized operating conditions for all the three cycles. It was found that the cycle with LPP and LPP+HR present an outstanding performance when compared to the basic 4-step. The LPP step increases the recovery of C2 due to the use of adsorption product to pressurize the column from the product end, thereby moving the C2 concentration front to the feed end of the column. The HR increases the purity of C2 by taking a fraction of the evacuation product and refluxing it into the column after the blowdown step. It causes an increase of the C2 concentration at the feed end of the column and also, the displacement of the C1 concentration front to the product end of the column. The heat effects within the column were also addressed. Simulations were carried out neglecting and taking into account heat effects. When heat effects are neglected, the performance of the process is higher since the significant temperature gradient during the evacuation and pressurization, which affect the process performance, do not occur. Therefore, to make conclusions about the process performance based on isothermal simulations, for processes with a considerable drop in pressure, will lead to misleading interpretations. Finally, the effect of increasing the feed temperature was shown. At higher feed temperature, the performance of the process is improved due to the change in the shape of the isotherms, thereby increasing the working capacity of the adsorbent.

Chapter 5

Material selection through optimization

5.1 Introduction

In this chapter, a rigorous multi-objective optimization study was performed to simultaneously maximize (C2) purity and recovery. The aim of the optimization is to find the optimal process conditions which maximize purity and recovery. Furthermore, the optimization is an affective adsorbent screening method to evaluate the performance of each material in terms of the objective functions. Both the 4 step cycle with light product pressurization (LPP) and 5 step cycle with heavy reflux (LPP+HR) were optimized for all the adsorbents described in Chapter 2. As a result, Pareto solution along with the process conditions for each adsorbent in both cycles were obtained. A full comparison of the performance for all the adsorbents in terms of the objective function is also obtained.

5.2 Issues with current methods to select materials

Different methods to screen adsorbents can be found in literature [9, 50–52]. Methods found vary in complexity and metrics used to evaluate and compare the performance. Sorbent selection parameter (S) takes into account the thermodynamics of the system through selectivity and the adsorption-desorption pressures through the working capacity; thereby the product of these two metrics gives the parameter S [50, 51]. The adsorbent with the highest S is expected to be the best adsorbent. Adsorbent Performance Indicator (API) takes into account three metrics, working capacity, selectivity and heat of adsorption along with three adjustable exponents which vary depending on the type of separation (bulk or trace component) [52]. There is no clarity as to how the exponents can be adjusted or fitted for each case. Webley and coworkers developed a simplified 3-step PVSA cycle in order to evaluate the adsorbent performance for a specific gas mixture [9]. The method uses a simple adsorption-desorption-pressurization cycle taking

into account heat effects for each step along with the specific work needed to pressurize and depressurize the column. This method can be considered one step forward of the methods based only on metrics [50–52] and one step behind of the methods based on full and rigorous adsorption simulation and optimization [19, 34].

The methods described above are not general, i.e., they were applied to specific separation systems with a reduced number of adsorbents. However, they were applied with success in those cases and their simplicity in the calculations make them a good first approach in the adsorbent screening task. On the other hand, a full model optimization provides a clearer answer about the best adsorbent for a specific separation problem but it has some drawbacks such as the computational time and machine power are significantly higher. Nowadays with the increase of computational power, it is feasible to perform a multi-objective optimization of a rigorous PVSA model in the order of 8-10 hours. Depending on the scope of the problem, the objective of the problem can be focused on maximizing purity and recovery without taking into account energy and productivity constraints or a problem where the objective is to minimize energy and maximize productivity taking into account the purity/recovery constraints. In this work, the PSA is highly integrated to the cryogenic distillation process and the industrial partner was interested in evaluating the purity-recovery trade-off. Hence, the first approach was adopted and the optimization problem focused on the search of an adsorbent which maximizes these two variables.

5.3 Formulation of the optimization problem

In order to identify the optimal process conditions of the 4-step with LPP and the 5-step with LPP+HR, both optimization variables and process constraints should be defined before performing the multi-objective optimization. As for process constraints, adsorption and evacuation pressures are fixed due to the plant requirements and limitations. Adsorption pressure (P_H) and lowest vacuum pressure (P_L) are fixed at 24 bar and 0.1 bar respectively. The duration of the adsorption, blowdown and evacuation steps are considered decision variables as well as feed velocity (v_{feed}), feed temperature (T_{feed}), and intermediate or blowdown pressure (P_{int}). The duration of pressurization and LPP is determined by the time needed to reach the adsorption pressure.

To perform the optimization, a nondominated sorting genetic algorithm II (NSGA-II) available in Matlab was used [33]. Advantages such as parallel computing, its implementation simplicity, its global search in a broad range of conditions which allow to understand how the operating conditions affect the process, make the NSGA-II an appropriate algorithm for the optimization of the PVSA process. All computations reported were carried out on a desktop workstation with two quad-core Intel Xeon 3.1 GHz processors and 128 GB RAM.

The number of the population was equal to 10 times the number of decision variables ($10n_{DV}$),

a number considered adequately large enough to perform a full search of the process conditions. With the passing of generations the algorithm chooses the points where the objective functions are maximized. In this optimization problem the NSGA-II usually goes up to ~ 100 generations. A distinct characteristic of genetic algorithm is its ability to consider points that are not essentially close to the optimum value. This adds diversity and hence, provides an opportunity to find solutions in the entire range of search. A complete optimization is a full two-objective Pareto solution and it is obtained for each adsorbent tested. As mentioned earlier, the two objectives are ethane (C2) purity and recovery.

5.3.1 Optimization of the 4-step cycle with LPP

For the optimization of the 4-step cycle with LPP, seven decision variables with their respective upper and lower bounds were established and are summarized in Table 5.1.

	t_{ads} [s]	t_{bd} [s]	t_{evac} [s]	P_{int} [bar]	P_{low} [bar]	V_{feed} [m/s]	T_{feed} [K]
Lower bound	5	20	20	0.5	0.1	0.05	303.15
Upper bound	100	200	200	24	0.4	2	423.15

Table 5.1: Optimization bounds for the 4-step LPP process.

As shown in Table 5.1, upper and lower bounds were defined in order to allow the optimizer to search in a broad range of process conditions. All the optimization variables chosen are considered critical for the process performance. Optimized time steps, feed velocity and intermediate pressure affect the column dynamics and minimize the loss of C2 during the adsorption and blowdown steps. As for feed temperature, an optimal value will maximize the adsorbent performance which means there will be a trade-off between the adsorption and desorption capacities in order to release the highest quantity of C2 during the evacuation. The study carried out in Chapter 4 showed that for all the adsorbents chosen, higher temperatures are favorable for the adsorbent performance due to the sharpness of the isotherms at low temperatures.

The vacuum pressure (P_L) has a minimum allowable value of 0.1 as reflected by the lower bound. One of the largest energy consuming components in a PVSA is the vacuum pump that is required to reach sub-atmospheric pressures. Therefore, it is worth including P_L as an optimization variable to see if the best performance of the cycle can be reached at a P_L higher than 0.1 bar reducing the operational costs. For all the six adsorbents the same optimization bounds were used and the optimization routine was performed for each of them. As a result, Pareto fronts for all of them were obtained and are shown in Figure 5.1.

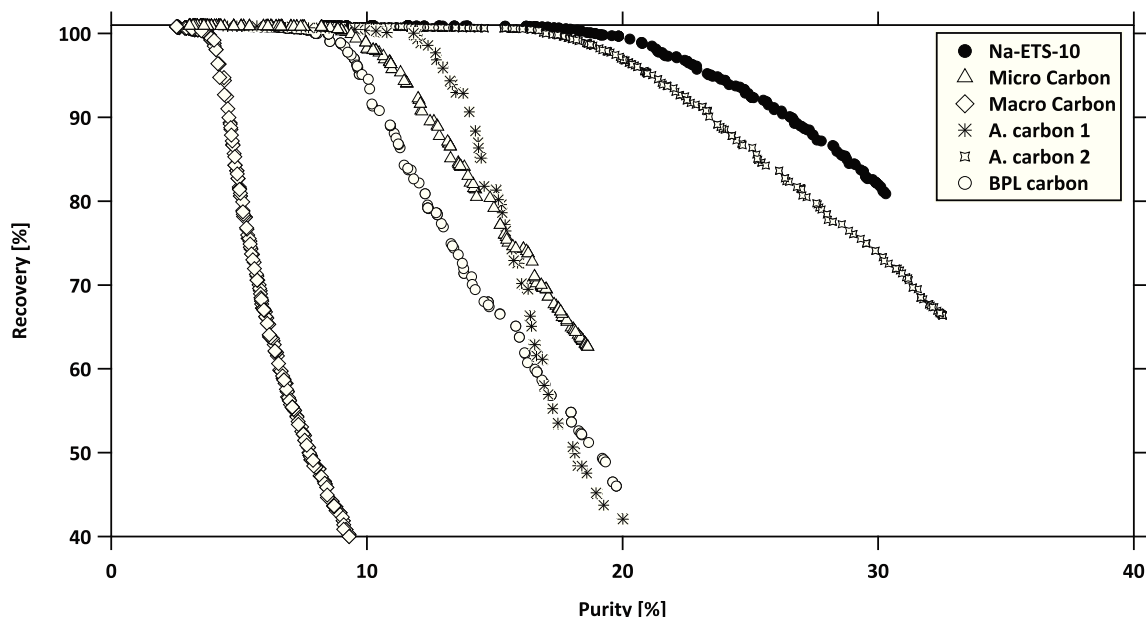


Figure 5.1: Pareto fronts for the LPP process.

Before comparing the performance of the different adsorbents, it is worth considering the Pareto curve. The optimization problem considers simultaneously maximizing both purity and recovery of the heavy component (C2). They cannot be simultaneously improved. In other words, there is always a trade-off between the purity and recovery and the Pareto curve represents the best possible trade-off. The region towards the top right of the curve is infeasible while that towards the bottom left is sub-optimal. Hence, it is always desirable to operate the adsorption unit on the Pareto curve. The exact operating point is decided by the operator. A key attraction of the optimization technique is that each point on the Pareto curve corresponds to a unique set of operating conditions, which will aid the operator to implement the process in practice.

Figure 5.1 shows the comparison of the Pareto curves for the different adsorbents. Na-ETS-10 globally performs better than the other adsorbents in terms of C2 purity and recovery. The 2 carbons taken from literature follow Na-ETS-10 in performance, whereas the carbons measured in-house show the least desirable performance. It is noteworthy that 100% recovery is achievable with all the sorbents making purity the decisive metric. The 100% C2 recovery is directly related with the optimization of the time of adsorption and blowdown pressure, if the blowdown pressure is high then it is possible to prevent the loss of C2 in the raffinate stream and collect it in the extract stream.

Nevertheless, the multi-objective optimization should find a trade-off between C2 purity and recovery and according to Figure 5.1 an increase in purity will cause a decrease in recovery. It can be explained by the blowdown or intermediate pressure (P_{int}) value. When recovery has a value of 100% the optimizer has chosen P_{int} values where C2 is not removed from the column but at the same time, part of the C1 remains within the column, this results in low value of C2

purity due to the significant amount of C1 present during the evacuation step. In order to reach higher purities, the P_{int} value must decrease to remove most of the C1 during the blowdown step. Unfortunately, a reduction in the P_{int} will also cause that C2 starts desorbing resulting in a decrease of C2 recovery.

To understand how the variation of the optimization variables affect the global performance of the process, it is necessary to analyze their variations with respect to one of the decision variables, either purity or recovery. To illustrate this, the material with the best performance was chosen, i.e., Na-ETS-10. C2 purity was selected as the decision variable for the analysis. Figure 5.2 depicts the behavior of the optimization variables against purity. It is important to mention that Figure 5.2 was built using only the points belonging to the Pareto front. For the rest of the adsorbents, the plots of the decision variables against purity can be found in Appendix A.

Analyzing each plot in Figure 5.2, it can be seen that for the adsorption time (t_{ads}) the optimizer converged to one specific value (~ 20 s); this points out that above this value C2 will start breaking through. Blowdown and evacuation times are long enough to allow the gas within the column to be released and collected at the end of each step. A further increase in the evacuation and blowdown time will not change the values of purity and recovery because at the end of these steps the molar flow tends to zero. Feed velocity is hitting the lower bound fixed for the optimization, it produces a very slow movement of the C2 concentration front across the column, thereby avoiding losses of C2 during the adsorption step. As expected for both intermediate and low pressure (P_{int} , P_L), a decrease of their values will increase C2 purity substantially. Both variables are close to the lower bound fixed for the optimization, so decreasing P_{int} and P_L increases purity but decreases recovery. The feed temperature shows an interesting trend. To maximize recovery a lower value of temperature is suggested whereas purity maximization is attained at higher temperatures. This trend directly relates to the change in the isotherms shape, making them less rectangular and increasing the amount of gas that can be desorbed at the specified pressures.

In order to verify purity and recovery values obtained and achieve a better comprehension of the column dynamics a point from the Pareto front for Na-ETS-10 was taken. Using the optimized values from that point a single 4-step simulation with LPP was carried out. The optimized values extracted from the Pareto front and subsequently used in the simulation are described in Table 5.2

	t_{ads} [s]	t_{bd} [s]	t_{evac} [s]	P_{int} [bar]	P_{low} [bar]	V_{feed} [m/s]	T_{feed} [K]	Purity [%]	Recovery [%]
Value of decision variable	21.82	52.62	138.39	0.50	0.12	0.13	422.58	30.30	80.89

Table 5.2: Optimized conditions for LPP process using Na-ETS-10.

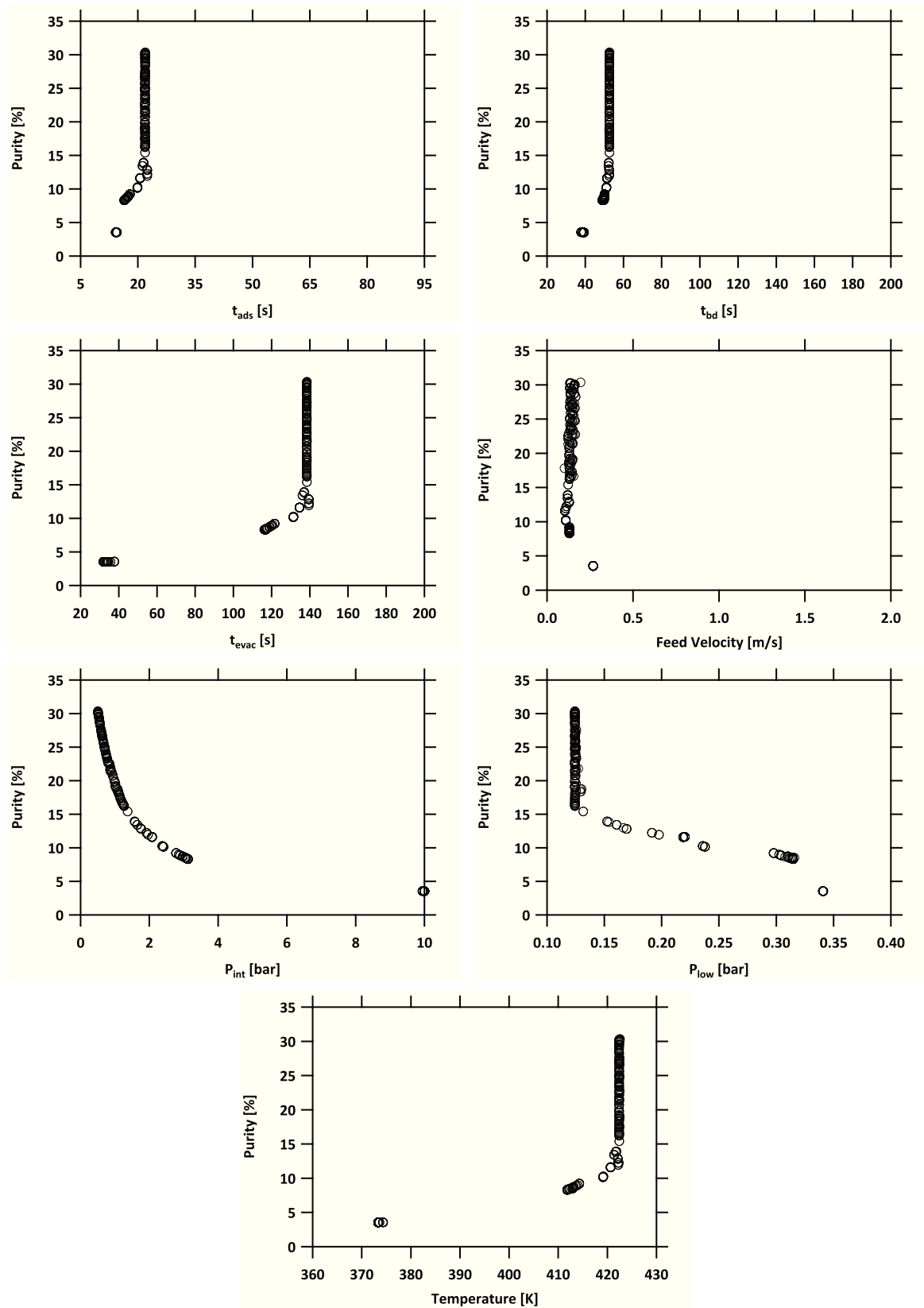


Figure 5.2: The decision variables corresponding to the Pareto front of the 4-step PVSA cycle with LPP. The lower and upper bound of the x axis refer to the bounds used for the optimization.

The 4-step cycle with LPP simulation was performed and the gas and solid phase axial profiles for C2 are plotted in Figure 5.3. The axial profiles clearly show the effect of using optimized conditions; for instance, adsorption profile of C2 gas phase composition tends to zero at the product end of the column ($z = 1$), which points out that C2 is not being lost at this step. Also, gas phase composition at the end of the LPP step shows how the C2 front is pushed towards the feed end of the column ($z = 0$) and the tail at the end of the evacuation step is completely removed with this step. As for evacuation and blowdown, the effect of operating the process at high temperature (423.15K) is clearly observed in the axial profiles. The gas phase concentration of C2 increases as the process moves from P_{int} to P_L since the working capacity of C2 between P_{int} and P_L is larger than the working capacity of C2 between P_H and P_{int} , which makes C2 desorption at P_L more favorable. Profiles presented in Chapter 3 for the same cycle but using 303.15K as feed temperature showed a minimal change in solid and gas phase profiles for blowdown and evacuation pressure. The less rectangular isotherm at 423.15K allow the process to desorb more C2 during the evacuation step.

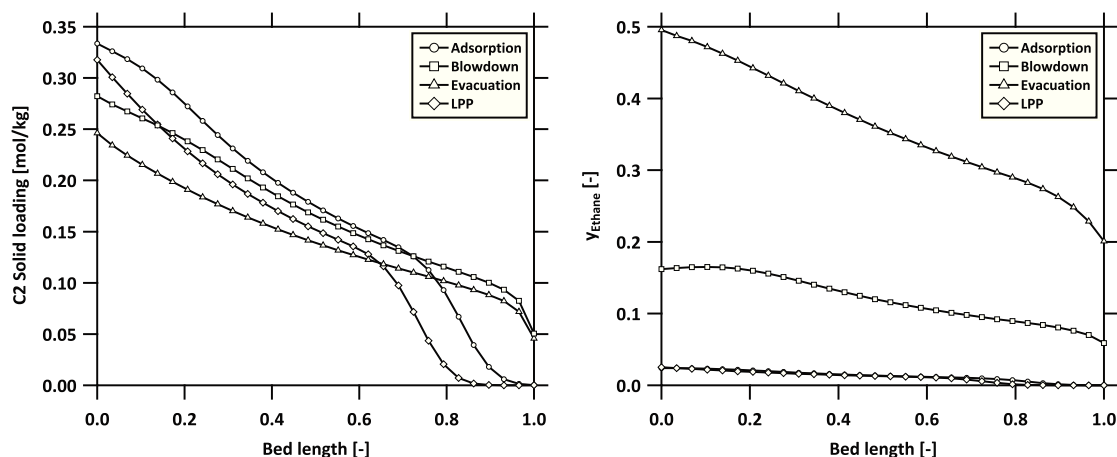


Figure 5.3: Gas and solid phase profiles for C2 on Na-ETS-10 using optimized conditions from Table 5.2.

An interesting behavior is also depicted in the Pareto fronts (Figure 5.1) for A. carbon 1 and Micro carbon. The Pareto for these two adsorbents shows a crossing point around 75% recovery, it means that above 75% recovery A. carbon 1 has a better performance in terms of purity than the Micro carbon. Nevertheless, below 75% recovery, the trend is reversed. However, the absolute differences are small enough that the two adsorbents, for practical purposes, be consider to offer similar performance.

5.3.2 Optimization of the 5-step cycle with LPP and heavy reflux

For this cycle optimization, one optimization variable was fixed and two were added to the set of decision variables. Based on the results obtained in the optimization of the 4-step cycle with

LPP, low pressure P_{low} was removed from the optimization variables because the results showed that the best performance is reached at the lowest value of P_{low} . Therefore, P_{low} was fixed at 0.1 bar. Furthermore, for the 5-step cycle with LPP and HR two new decision variables should be considered, the reflux fraction (θ) and the time of the heavy reflux step (t_{HR}). Hence, a set of eight decision variables are taken into account for the optimization and their lower and upper bounds are described in Table 5.3.

	t_{ads} [s]	t_{bd} [s]	t_{evac} [s]	t_{HR} [s]	P_{int} [bar]	θ_{HR} [-]	V_{feed} [m/s]	T_{feed} [K]
Lower bound	5	20	20	5	0.5	0.1	0.05	303.15
Upper bound	100	200	200	20	24	0.9	2	423.15

Table 5.3: Optimization bounds for the 5-step LPP+HR process.

The upper and lower bounds described in Table 5.3 give to the optimizer a broad range of conditions to search for the set of decision variables which maximizes C2 purity and recovery. For this optimization, three adsorbents were selected based on the results obtained in Section 5.3.1. The best two adsorbents from the Pareto curve were chosen, namely, Na-ETS-10 and A. carbon 2. The third adsorbent chosen was one of the carbons measured in-house, i.e., Microporous carbon. Thereby, one adsorbent from the titanosilicates family, one activated carbon from literature [39], and one activated carbon measured in the laboratory are the materials chosen for the optimization.

Optimizations were carried out for the three adsorbents mentioned above and their respective Pareto fronts are depicted in Figure 5.4. It is observed that the Pareto fronts for the 5-step cycle with LPP+HR have the same trend as those of the 4-step cycle with LPP, i.e., Na-ETS-10 has the best performance in terms of the objective functions, followed by the A. carbon 2 and the Micro carbon. This result seems to confirm observations from literature that if one adsorbent performs better than the other for a specific system using a simple cycle configuration, the same adsorbent will perform better in more complex cycle configurations [9]. Nonetheless, more rigorous work is needed to ascertain this general observations.

In order to illustrate the effect of the HR step, the Pareto front for Na-ETS-10 from the LPP process is shown in Figure 5.4. The addition of a HR step has a major impact on the process. For instance, at 80% recovery the C2 purity can be improved from $\sim 30\%$ to $\sim 72\%$ by the addition of HR step. The increase in C2 purity using the 5-step cycle with LPP+HR is due to the HR step. This step is analogous to the reflux in a distillation column; thereby if the reflux fraction is increased, the purity of the heavy product during the evacuation step also increases [34]. Refluxing heavy product before the evacuation step increases the concentration of it in the feed end of the column. Additionally, the reflux will cause the moving of the light component from the feed end to the product end of the adsorption column. Because the HR step is carried out at intermediate pressure, it is easier to push the light component to the other end of the column.

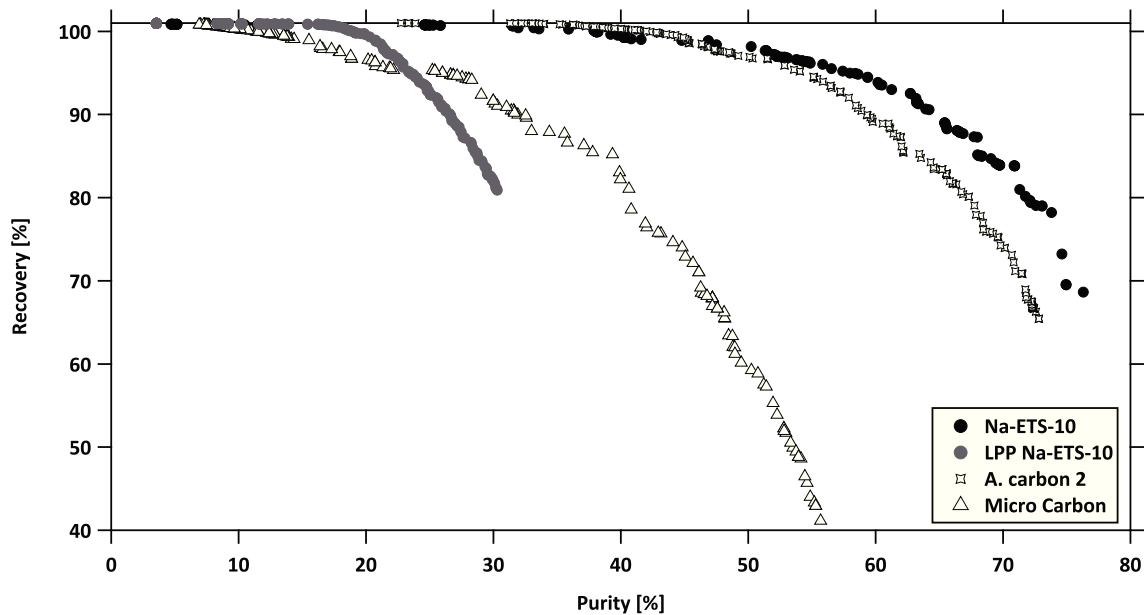


Figure 5.4: Pareto fronts for the 5-step cycle with LPP and HR.

Using the Pareto front of Na-ETS-10, the decision variables against C2 purity were plotted in Figure 5.5. For the rest of the adsorbents, the plots of the decision variables against purity can be found in Appendix B. It can be seen from the figure, that the time of adsorption (t_{ads}) converges to one specific value (~ 20 s). This value corresponds to the time just before the breakthrough time for C2; hence, the loss of the heavy component during this step is avoided. Blowdown and evacuation times provide a suitable time range for the process in order to collect product in both steps. Time of heavy reflux step varies between 6 and 7 s, this short time is due to the value of the intermediate pressure. Because P_{int} is hitting the lower bound (0.5 bar) the heavy reflux step should be short since the capacity of the adsorbent at this condition is low and C2 loss during HR step may occur if longer times are chosen.

The intermediate pressure approaches the lower bound while C2 purity increases. This means there is presence of C1 at this condition. Unfortunately, decreasing P_{int} will cause not only the withdrawal of C1 from the column but also a removal of C2 during blowdown step causing a decrease in recovery at expense of an increase in purity. As for the feed velocity, it is directly related with the adsorption time. The plot in Figure 5.5 for feed velocity shows that this is approaching the lower bound, thereby the concentration front of C2 will move slowly throughout the column and hence, avoiding C2 breakthrough.

As for feed temperature, Figure 5.5 shows that high temperatures are beneficial for the process performance. High temperature reduces the sharpness of the isotherm; hence, more C2 can be released during the evacuation step. The reflux fraction (θ) follows the expected trend, as the reflux fraction increases purity also increases up to the value reaches the upper bound.

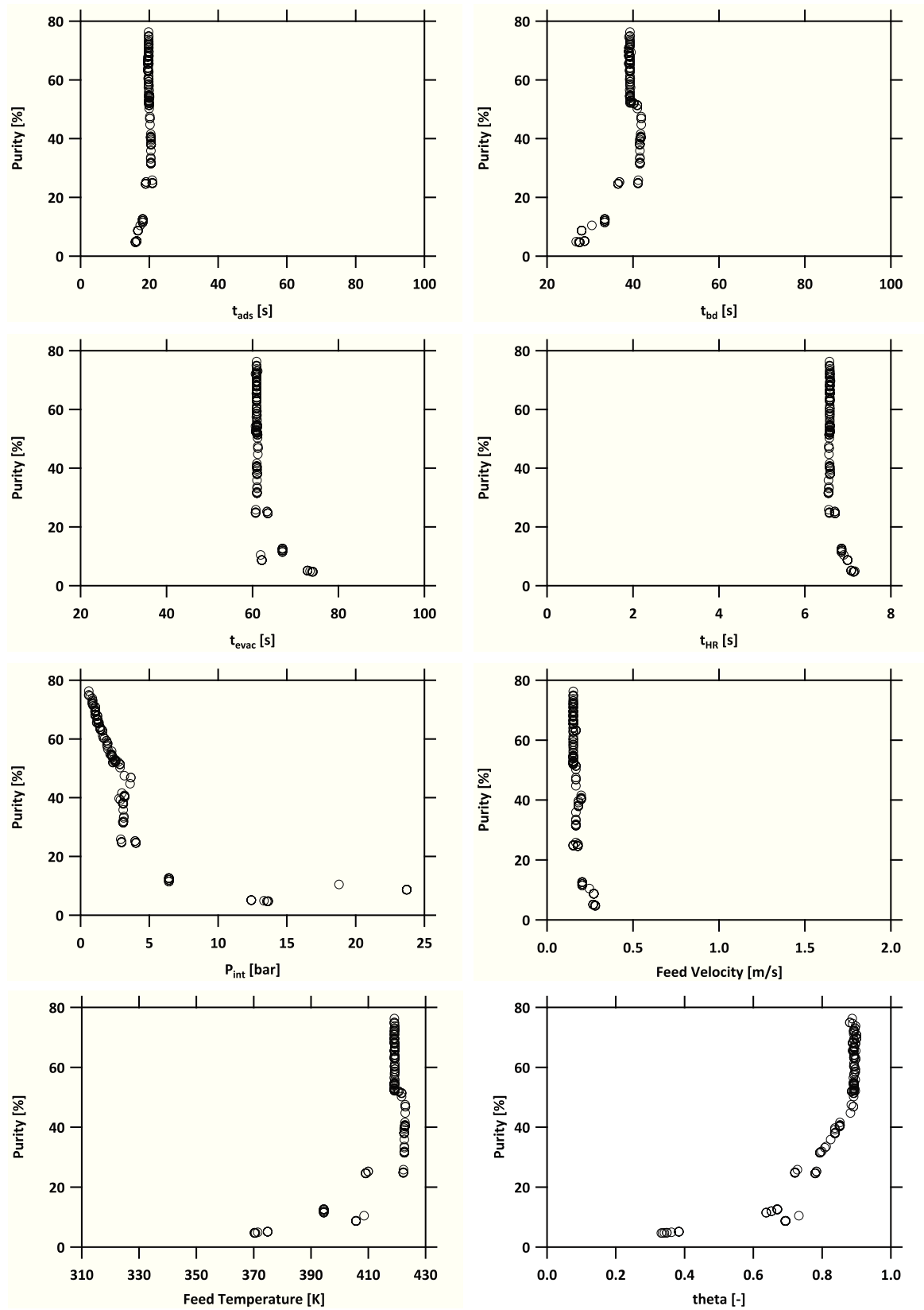


Figure 5.5: The decision variables corresponding to the Pareto front of the 5-step PVSA cycle with LPP+HR.

Although high reflux fraction increases purity, it also brings a decrease in recovery. To compare the performance of the three adsorbents, a point for each adsorbent at same recovery value from the Pareto fronts was taken. The operating conditions, at same recovery value, for each point chosen are described in Table 5.4. Simulations of the 5-step cycle with LPP+HR were carried out for the two carbons shown in 5.4 because they have similar operating conditions but their C2 purity value is completely different. Therefore, it is necessary to compare their gas and solid phases column profiles and their isotherms at the optimized operating conditions. Figure 5.6 shows the isotherms and column profiles for Micro carbon and A. carbon 1.

Adsorbent	t_{ads} [s]	t_{bd} [s]	t_{evac} [s]	t_{HR} [s]	P_{int} [bar]	P_{low} [bar]	V_{feed} [m/s]	T_{feed} [K]	θ [-]	Purity [%]	Recovery [%]
Na-ETS-10	19.76	39.29	60.93	6.57	0.59	0.1	0.15	419.09	0.88	76.29	68.6
A. Carbon 2	34.17	40.26	131.47	10.15	1.67	0.1	0.12	405.33	0.89	71.80	68.5
Micro Carbon	28.78	66.00	48.52	9.39	1.97	0.1	0.15	422.09	0.89	46.32	68.57

Table 5.4: Process conditions at same recovery from the Pareto fronts for Na-ETS-10, A. Carbon 2, and Micro Carbon.

The effect of the shape of the isotherms in the process performance can be seen in Figure 5.6. The isotherms of C1 and C2 on activated carbon are less rectangular than those on Micro Carbon. This means that using A. carbon 2 as adsorbent more C1 will be desorbed during the blowdown step while more C2 will be desorbed during the evacuation step. For Micro carbon, both C1 and C2 have a sharp isotherm, it avoids C1 to be released during the blowdown step and hence, the stream from the evacuation step will have a higher concentration of C1 causing a decrease in C2 purity. The gas and solid profiles also confirm this. C1 concentration in the gas phase at the end of evacuation step using Micro carbon is significantly higher than this using A. carbon 2 and hence, during the evacuation step these higher amount of C1 will be withdrawn from the column along with C2. The solid phase profile for blowdown also shows a higher loading of C1 on the Micro carbon (~ 0.55 mol/kg) while on the A. carbon 2 the C1 loading is ~ 0.25 mol/kg. In addition, the long evacuation time for A. carbon 2 can be also explained using the C1 solid phase profile. The plot shows that during the HR step the concentration front of the HR stream is saturating half of the bed and C1 is being moved to the product end of the column ($z = 1$). Since half of the bed was saturated with a stream rich in C2, a longer evacuation time is needed to remove all of it.

Profiles shown in Figure 5.6 at same recovery value, described clearly the effect of heavy reflux (HR) step in the process. HR step increases the concentration of C2 at the feed end ($z = 0$) of the column and hence, increasing purity. Further, LPP step moves the C2 front to the feed end of the column, thereby the product end of the column will be saturated with light product whereas the feed end will be saturated with heavy product.

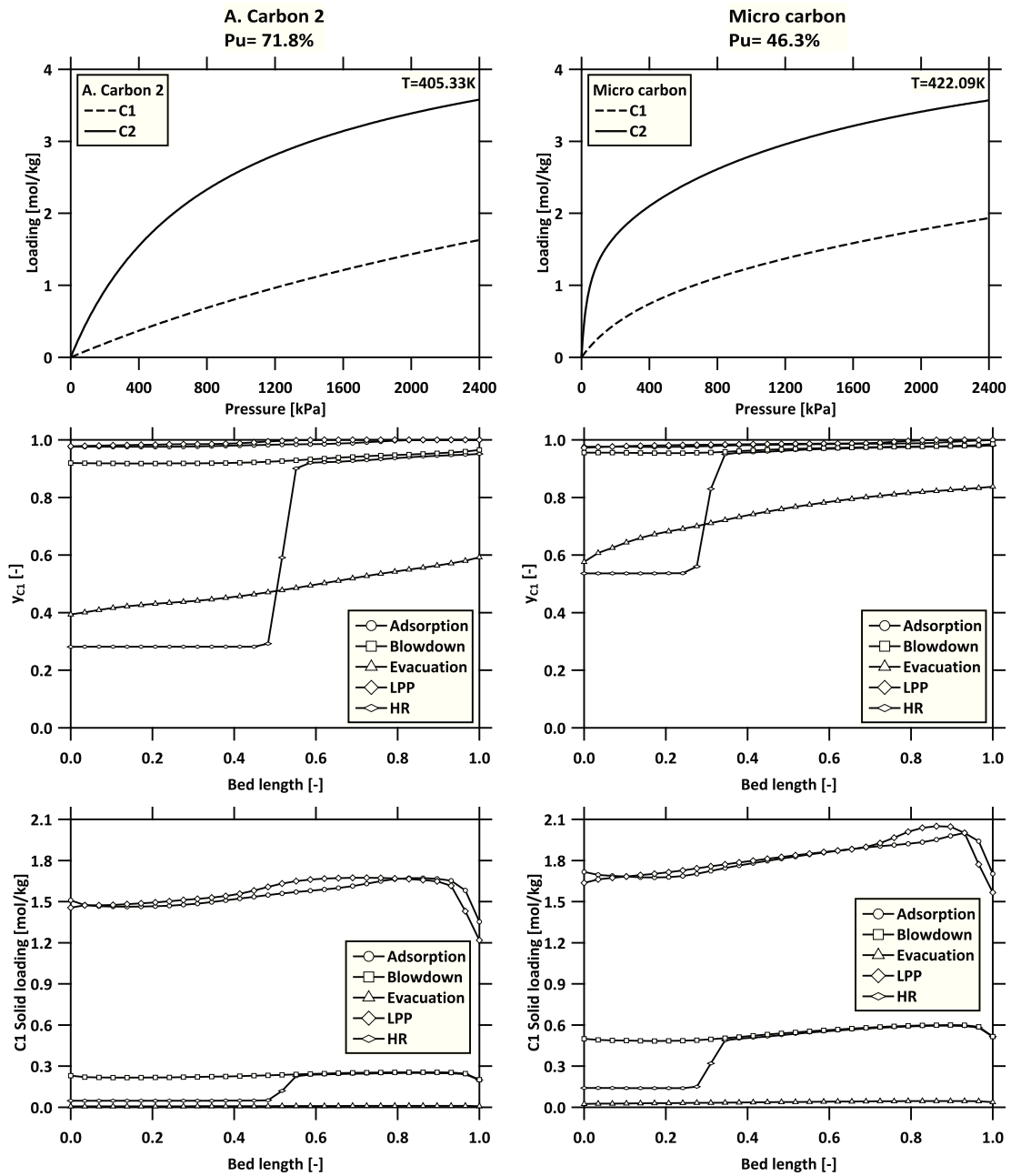


Figure 5.6: C1/C2 isotherms, gas and solid column profiles for C1 using Micro carbon and A. Carbon 1 and the optimal conditions from Table 5.4

5.4 Conclusion

In this chapter, multi-objective optimization for two PSA configurations selected, were carried out having C2 purity and recovery as objective functions. The Pareto sets for each configuration were depicted in purity-recovery plane. From the Pareto curves, three objectives are fulfilled. First, the determination of the optimal process conditions for each PSA cycle, second, the comparison between the PSA configurations chosen for the optimization, and third, the comparison of the adsorbents presented in this study. As for the first objective, optimized process conditions were obtained and verified through simulation of a single point from the Pareto curve. Also from the simulation of a single point, gas and solid phase profiles were plotted in order to analyze the behavior of the column profiles under optimized conditions and why such point belongs to the Pareto front. It is noteworthy the fact that the Pareto points which provide higher purity are featured by high feed temperature operation ($>400\text{K}$), it agrees with the statement formulated in Chapter 4 about the benefits to use higher temperatures. At this condition the sharpness of the isotherms decreases; hence, more C2 can be desorbed during the evacuation step. Regarding the second objective, Pareto curves pointed out that the 5-step cycle with LPP+HR performs better than the 4-step cycle with LPP. Purities of 70% are feasible for two specific adsorbents when the LPP+HR cycle is utilized. The heavy reflux has positive effect in the process since C2 is concentrated in the feed end of the column. However, for this configuration and extra-step and vacuum pump should be used making the process more expensive economically. Finally, the Pareto front provides a comparison of the adsorbents performance, this comparison is accurate as it was carried out using a full model optimization. The results showed that Na-ETS-10 has the best performance in terms of the objectives functions followed by A. carbon 2. The results from the Pareto curves also showed that the performance of the adsorbents is consistent no matter the cycle. For instance, Na-ETS-10 and A. carbon 2 were the best adsorbents in the two cycle configurations defined. The other adsorbents studied also showed the same consistency.

Chapter 6

Concluding remarks

6.1 Conclusions

In this thesis, modeling and optimization tools have been developed to evaluate both the potential of different adsorbents and the PSA cycle configurations proposed for the separation of ethane from residue gas. The experimental measurements of adsorption isotherms at different temperatures for the adsorbents selected in this study gave the necessary information to characterize them. This information was a key input parameter for the simulation and optimization for the process.

In Chapter 2, two major classes of adsorbents were chosen: titanosilicates (ETS) and activated carbons. Within the group of ETS, 3 different cations were used: Na-ETS-10, Sr-ETS-10, and La-ETS-10. As for the carbons, three activated carbons with different pore size distribution were chosen and whereas two activated carbon found in the literature were included for the purpose of comparing their performance in the process with the material measured in-house. The experimental determination of the single-component adsorption isotherms at different temperatures provided the needed information to characterize the adsorbents using the dual-site Langmuir model. The model showed a good correlation with the experimental data and heats of adsorption were also determined from both the experimental data and isotherm model to complete the characterization of the adsorbent. Based on evidence from literature and the difficulty to experimentally measure binary adsorption equilibria, the extended dual-site Langmuir model was used to predict competitive isotherms. The experimental measurements of adsorption isotherms determined that carbons have higher adsorption capacity when compared to titanosilicates. However, Henry's selectivity calculated at 298.15K gave higher values for ETS family than activated carbons.

In Chapter 3, a rigorous one-dimensional model consisting of mass and heat balances along with equations for adsorption isotherms, gas phase, and pressure drop throughout the column was presented. To implement the rigorous model a finite volume discretization in space using van Leer

scheme was developed and the resultant system of equations were integrated in time using an in-built ode solver from Matlab. The model developed was validated based on the accomplishment of mass balance closure and the verification of the gas and solid phases profiles. The model was able to capture accurately the dynamics of adsorption columns. This was verified through the simulation of the 4-step cycle where the characteristic profiles and transitions were observed. The method provides a good equilibrium between accuracy and computational efficiency requiring just 30 volume cell in order to capture with accuracy the evolution in the dynamic process for each state variable.

In Chapter 4, apart from the basic 4-step cycle, two cycle configurations with light product pressurization (LPP) and heavy reflux with light product pressurization (LPP+HR) were implemented using the model developed in Chapter 3. Simulations of the three PSA configurations using all the adsorbents showed that heat effects must be included when the pressure swing associated with the process is high, e.g., adsorption at 24 bar and evacuation at 0.1 bar. In this kind of processes, heat effects reduces the performance of the process because of significant drop in temperature during the evacuation step. Furthermore, it was determined that for all the adsorbents considered in this study high feed temperatures increased the working capacity of the adsorbent and hence, C2 purity.

In Chapter 5, a multi-objective optimization for the cycle configurations developed in chapter 4 was presented. Using C2 purity and recovery as objective functions and operating conditions as decision variables, the multi-objective optimization was carried out using a nondominated sorting genetic algorithm (NSGA-II). With a fair population the algorithm is capable to search in the entire range of the decision variables and to find the optimal pareto points and thereby, the optimal process conditions. Furthermore, the multi-objective optimization provides a rigorous criterion for the screening of adsorbents and the best cycle configuration. For the cases studied in this thesis, Na-ETS-10 showed the best performance in terms of performance objectives for the process and along with the 5-step cycle with heavy reflux (LPP+HR) they accomplished a C2 purity and recovery of 76% and 68%, respectively.

6.2 Outlook

This work has resulted in the development of tools to design, evaluate, and compared both adsorption processes and adsorbent materials. By a multi-objective optimization of a rigorous one-dimensional adsorption model, it is now possible to obtain a complete screening of the adsorbents considered for the process as well as the determination of the best process configuration along with its optimal operating conditions for the separation of ethane from residue gas using pressure swing adsorption. Although it was demonstrated that it is feasible, in terms of C2 purity and recovery, to separate and concentrate C2 by adsorption, there are different subjects that need further investigation.

In the area of the experimental measurements, it is necessary to complete the single-component adsorption isotherms at different temperatures for Sr-ETS-10 and La-ETS-10. Additionally, a collection of low-pressure data for all the adsorbents will allow a more accurate determination of the heat of adsorption. Furthermore, experiments of binary adsorption isotherms will provide a deeper insight about the behavior of the system and the accuracy of the extended dual-site Langmuir model. Breakthrough experiments will give the necessary information about the competitive isotherms, heat, and mass transfer effects within the column, which will be useful to accurately describe the process.

As for the PSA/PVSA process configuration, new cycle configurations may be considered in order to make a comparison to the cycles proposed in this thesis. Configurations that do not need deep vacuum pressures but with similar or better performance than the cycles proposed will make a big difference in terms of the process economics. It can also include the development of either new adsorbents that do not need evacuation pressures below atmospheric pressure to regenerate the bed or adsorbents for which adsorption capacity for methane is very low when compared to ethane. Besides, it is necessary to consider economical calculations for the process along with purity and recovery constraints.

Finally, multi-objective constrained optimization using energy and productivity for the process as objective functions is an aspect that would be interesting to investigate. Constraints in C2 purity and recovery will make the optimization more selective and just the adsorbents and processes which meet both can be considered. Furthermore, this type of optimization will provide a first approach to evaluate the capital and operational costs for this process.

Bibliography

- [1] U. EIA., *Annual Energy Outlook With Projections 2014*. Washington D.C.: U.S. Department of Energy, 2014.
- [2] Q. Wang, X. Chen, A. N. Jha, and H. Rogers, "Natural gas from shale formation - the evolution, evidences and challenges of shale gas revolution in united states," *Renew. Sustain. Energy. Rev.*, vol. 30, no. 0, pp. 1 – 28, 2014.
- [3] M. Melikoglu, "Shale gas: Analysis of its role in the global energy market," *Renew. Sustain. Energy. Rev.*, vol. 37, no. 0, pp. 460 – 468, 2014.
- [4] W. L. Luyben, "Control of a train of distillation columns for the separation of natural gas liquid," *Ind. Eng. Chem. Res.*, vol. 52, no. 31, pp. 10741–10753, 2013.
- [5] D. M. Ruthven, S. Farooq, and K. S. Knaebel, *Pressure swing adsorption*. New York, N.Y.: VCH Publishers, 1994.
- [6] D. M. Ruthven, *Principles of adsorption and adsorption processes*. New York: Wiley, 1984.
- [7] M. Tagliabue, D. Farrusseng, S. Valencia, S. Aguado, U. Ravon, C. Rizzo, A. Corma, and C. Mirodatos, "Natural gas treating by selective adsorption: Material science and chemical engineering interplay," *Chem. Eng. J.*, vol. 155, no. 3, pp. 553 – 566, 2009.
- [8] C. Skarstrom, "Method and apparatus for fractionating gaseous mixtures by adsorption," Jul. 1960. US Patent 2944627.
- [9] B. J. Maring and P. A. Webley, "A new simplified pressure/vacuum swing adsorption model for rapid adsorbent screening for CO₂ capture applications," *Int. J. Greenhouse Gas Control*, vol. 15, no. 0, pp. 16 – 31, 2013.
- [10] K. S. Robinson and W. J. Thomas, "The adsorption of methane/ethane mixtures on a molecular sieve," *Trans IChemE.*, vol. 58, no. 4, pp. 219 – 227, 1980.
- [11] M. W. Anderson, O. Terasaki, T. Ohsuna, A. Philippou, S. P. MacKay, A. Ferreira, J. Rocha, and S. Lidin, "Structure of the microporous titanosilicate ets-10," *Nature*, vol. 367, pp. 347–351, Jan. 1994.
- [12] N. Magnowski, A. Avila, C. Lin, M. Shi, and S. Kuznicki, "Extraction of ethane from natural gas by adsorption on modified ets-10," *Chem. Eng. Sci.*, vol. 66, no. 8, pp. 1697 – 1701, 2011.
- [13] S. Kuznicki, A. Avila, M. Shi, V. Strom, and P. Herrera, "Removal of ethane from natural gas at high pressure," Dec. 2011. U.S. Patent 20110315012 A1.
- [14] N. A. Al-Baghli and K. F. Loughlin, "Binary and ternary adsorption of methane, ethane, and ethylene on titanosilicate ets-10 zeolite," *J. Chem. Eng. Data*, vol. 51, no. 1, pp. 248–254, 2006.
- [15] A. Avila, F. Yang, M. Shi, and S. Kuznicki, "Extraction of ethane from natural gas at high pressure by adsorption on na-ets-10," *Chem. Eng. Sci.*, vol. 66, no. 13, pp. 2991 – 2996, 2011.

- [16] R. Reich, W. T. Ziegler, and K. A. Rogers, "Adsorption of methane, ethane, and ethylene gases and their binary and ternary mixtures and carbon dioxide on activated carbon at 212-301 k and pressures to 35 atmospheres," *Ind. Eng. Chem. Process Des. Dev.*, vol. 19, no. 3, pp. 336–344, 1980.
- [17] A. Malek and S. Farooq, "Comparison of isotherm models for hydrocarbon adsorption on activated carbon," *AIChE J.*, vol. 42, no. 11, pp. 3191–3201, 1996.
- [18] A. Malek and S. Farooq, "Kinetics of hydrocarbon adsorption on activated carbon and silica gel," *AIChE J.*, vol. 43, no. 3, pp. 761–776, 1997.
- [19] R. Haghpanah, A. Majumder, R. Nilam, A. Rajendran, S. Farooq, I. A. Karimi, and M. Amanullah, "Multiobjective optimization of a four-step adsorption process for post-combustion CO₂ capture via finite volume simulation," *Ind. Eng. Chem. Res.*, vol. 52, no. 11, pp. 4249–4265, 2013.
- [20] D. Diagne, M. Goto, and T. Hirose, "New psa process with intermediate feed inlet position operated with dual refluxes: Application to carbon dioxide removal and enrichment.," *J. Chem. Eng. Jpn.*, vol. 27, no. 1, pp. 85 – 89, 1994.
- [21] A. D. Ebner and J. A. Ritter, "Equilibrium theory analysis of rectifying psa for heavy component production," *AIChE J.*, vol. 48, no. 8, pp. 1679–1691, 2002.
- [22] D. Subramanian, J. A. Ritter, and Y. Liu, "Equilibrium theory for solvent vapor recovery by pressure swing adsorption: analytic solution with velocity variation and gas-phase capacity," *Chem. Eng. Sci.*, vol. 54, no. 4, pp. 475 – 481, 1999.
- [23] D. Diagne, M. Goto, and T. Hirose, "Parametric studies on CO₂ separation and recovery by a dual reflux psa process consisting of both rectifying and stripping sections," *Ind. Eng. Chem. Res.*, vol. 34, no. 9, pp. 3083–3089, 1995.
- [24] D. Diagne, M. Goto, and T. Hirose, "Numerical analysis of a dual refluxed psa process during simultaneous removal and concentration of carbon dioxide dilute gas from air.," *J. Chem. Technol. Biotechnol.*, vol. 65, no. 1, p. 29, 1996.
- [25] A. D. Ebner and J. A. Ritter, "Equilibrium theory analysis of dual reflux psa for separation of a binary mixture," *AIChE J.*, vol. 50, no. 10, pp. 2418–2429, 2004.
- [26] O. J. S. IV and A. W. Westerberg, "The optimal design of pressure swing adsorption systems," *Chem. Eng. Sci.*, vol. 46, no. 12, pp. 2967 – 2976, 1991.
- [27] S. Nilchan and C. Pantelides, "On the optimisation of periodic adsorption processes," *Adsorption*, vol. 4, no. 2, pp. 113–147, 1998.
- [28] D. Ko, R. Siriwardane, and L. T. Biegler, "Optimization of a pressure-swing adsorption process using zeolite 13x for CO₂ sequestration," *Ind. Eng. Chem. Res.*, vol. 42, no. 2, pp. 339–348, 2003.
- [29] D. Ko, R. Siriwardane, and L. T. Biegler, "Optimization of pressure swing adsorption and fractionated vacuum pressure swing adsorption processes for CO₂ capture," *Ind. Eng. Chem. Res.*, vol. 44, no. 21, pp. 8084–8094, 2005.
- [30] A. Agarwal, L. T. Biegler, and S. E. Zitney, "Superstructure-based optimal synthesis of pressure swing adsorption cycles for precombustion CO₂ capture," *Ind. Eng. Chem. Res.*, vol. 49, no. 11, pp. 5066–5079, 2010.
- [31] A. Agarwal, L. T. Biegler, and S. E. Zitney, "A superstructure-based optimal synthesis of psa cycles for post-combustion CO₂ capture," *AIChE J.*, vol. 56, no. 7, pp. 1813–1828, 2010.
- [32] M. M. F. Hasan, R. C. Baliban, J. A. Elia, and C. A. Floudas, "Modeling, simulation, and optimization of postcombustion CO₂ capture for variable feed concentration and flow rate. 2. pressure swing adsorption and vacuum swing adsorption processes," *Ind. Eng. Chem. Res.*, vol. 51, no. 48, pp. 15665–15682, 2012.

- [33] K. Deb, A. Pratap, S. Agarwal, and T. Meyarivan, “A fast and elitist multiobjective genetic algorithm: NSGA-II,” *IEEE Trans. Evol. Comput.*, vol. 6, pp. 182–197, Apr 2002.
- [34] R. Haghpanah, R. Nilam, A. Rajendran, S. Farooq, and I. A. Karimi, “Cycle synthesis and optimization of a vsa process for postcombustion CO₂ capture,” *AIChE J.*, vol. 59, no. 12, pp. 4735–4748, 2013.
- [35] S. M. Kuznicki, “Large-pored crystalline titanium molecular sieve zeolites,” Apr. 1991. U.S. Patent 5011591A.
- [36] N. institute of standars and technology, “Chemistry webbook,” November 2014.
- [37] D. Do, *Adsorption Analysis: Equilibria and Kinetics*. Chemical Engineer Series, Volume 2, Imperial College Press, 1998.
- [38] A. L. Myers and J. M. Prausnitz, “Thermodynamics of mixed-gas adsorption,” *AIChE J.*, vol. 11, no. 1, p. 121, 1965.
- [39] J. A. Ritter, S. J. Bhadra, and A. D. Ebner, “On the use of the dual-process langmuir model for correlating unary equilibria and predicting mixed-gas adsorption equilibria,” *Langmuir*, vol. 27, no. 8, pp. 4700–4712, 2011.
- [40] K. S. Knaebel and F. B. Hill, “Pressure swing adsorption: Development of an equilibrium theory for gas separations,” *Chem. Eng. Sci.*, vol. 40, no. 12, pp. 2351 – 2360, 1985.
- [41] N. S. Raghavan and D. M. Ruthven, “Numerical simulation of a fixed-bed adsorption column by the method of orthogonal collocation,” *AIChE J.*, vol. 29, no. 6, pp. 922–925, 1983.
- [42] J. Carter and M. Wyszynski, “The pressure swing adsorption drying of compressed air,” *Chem. Eng. Sci.*, vol. 38, no. 7, pp. 1093 – 1099, 1983.
- [43] E. S. Kikkinides and R. T. Yang, “Effects of bed pressure drop on isothermal and adiabatic adsorber dynamics,” *Chem. Eng. Sci.*, vol. 48, no. 9, pp. 1545 – 1555, 1993.
- [44] R. J. LeVeque, *Finite Volume Methods for Hyperbolic Problems*. Cambridge Texts in Applied Mathematics, New York: Cambridge University Press., 2002.
- [45] P. A. Webley and J. He, “Fast solution-adaptive finite volume method for psa/vsa cycle simulation; 1 single step simulation,” *Comput. Chem. Eng.*, vol. 23, no. 1112, pp. 1701 – 1712, 2000.
- [46] S.-J. Lin, W. C. Chao, Y. C. Sud, and G. K. Walker, “A class of the van leer-type transport schemes and its application to the moisture transport in a general circulation model,” *Mon. Wea. Rev.*, vol. 122, pp. 1575–1593, July 1994.
- [47] B. van Leer, “Towards the ultimate conservative difference scheme. v. a second-order sequel to godunov’s method,” *Journal of Computational Physics*, vol. 32, no. 1, pp. 101 – 136, 1979.
- [48] S. P. Reynolds, A. D. Ebner, and J. A. Ritter, “Stripping psa cycles for CO₂ recovery from flue gas at high temperature using a hydrotalcite-like adsorbent,” *Ind. Eng. Chem. Res.*, vol. 45, no. 12, pp. 4278–4294, 2006.
- [49] B.-K. Na, H. Lee, K.-K. Koo, and H. K. Song, “Effect of rinse and recycle methods on the pressure swing adsorption process to recover CO₂ from power plant flue gas using activated carbon,” *Ind. Eng. Chem. Res.*, vol. 41, no. 22, pp. 5498–5503, 2002.
- [50] S. U. Rege and R. T. Yang, “A simple parameter for selecting an adsorbent for gas separation by pressure swing adsorption,” *Sep. Sci. Technol.*, vol. 36, no. 15, pp. 3355–3365, 2001.
- [51] R. T. Yang, *Adsorbents: fundamentals and applications*. Hoboken, N.J.: Wiley-Interscience, 2003.
- [52] A. D. Wiersum, J.-S. Chang, C. Serre, and P. L. Llewellyn, “An adsorbent performance indicator as a first step evaluation of novel sorbents for gas separations: Application to metalorganic frameworks,” *Langmuir*, vol. 29, no. 10, pp. 3301–3309, 2013.

Appendix A

Decision variables for the 4-step cycle with LPP

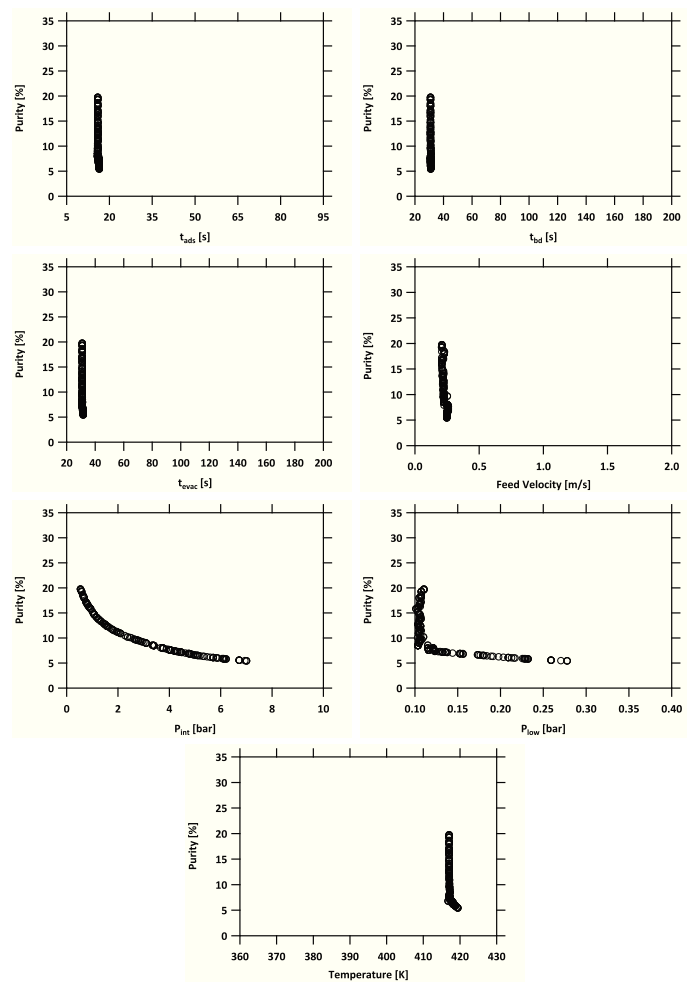


Figure A.1: The decision variables corresponding to the Pareto front for BPL carbon.

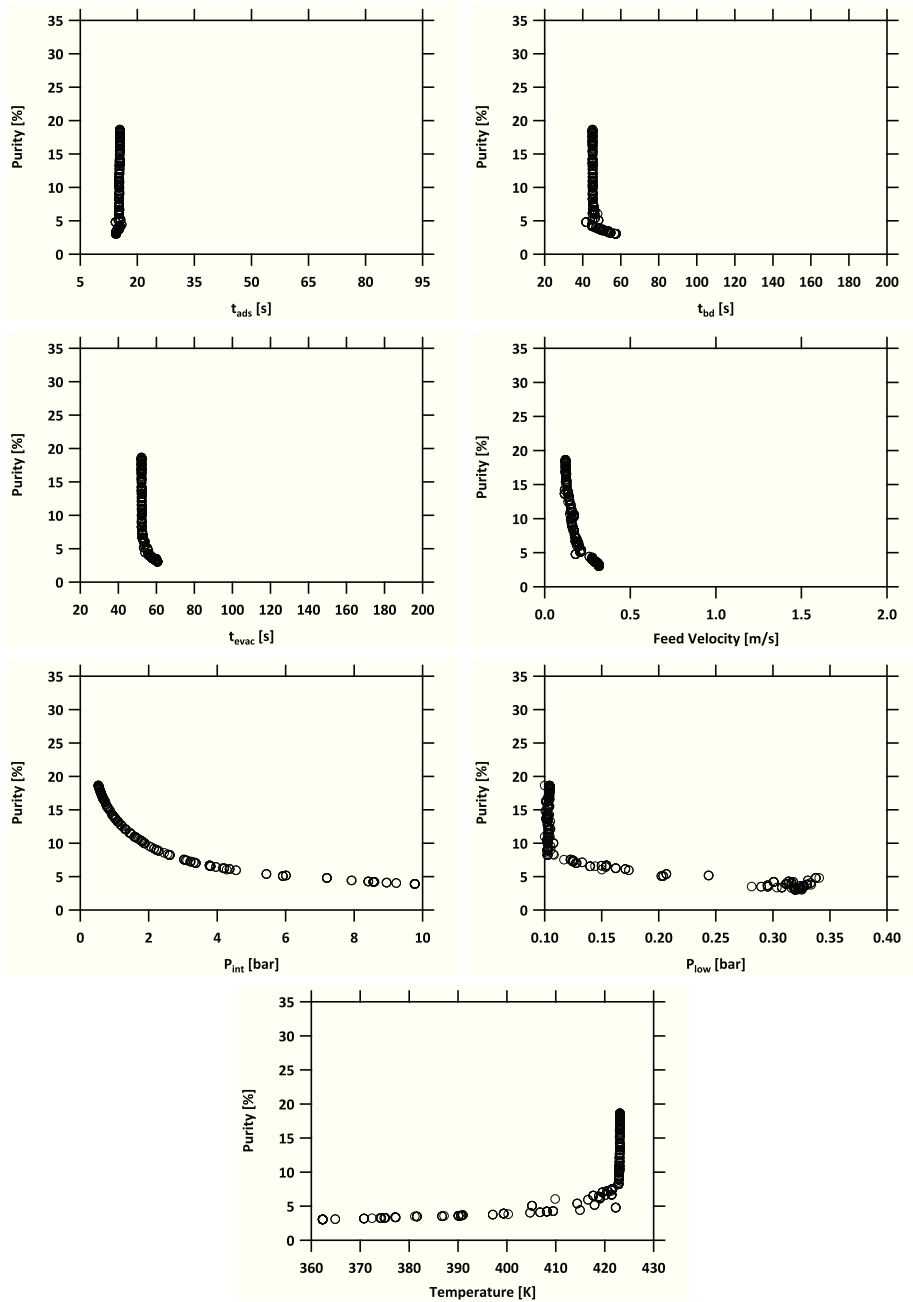


Figure A.2: The decision variables corresponding to the Pareto front for Micro carbon.

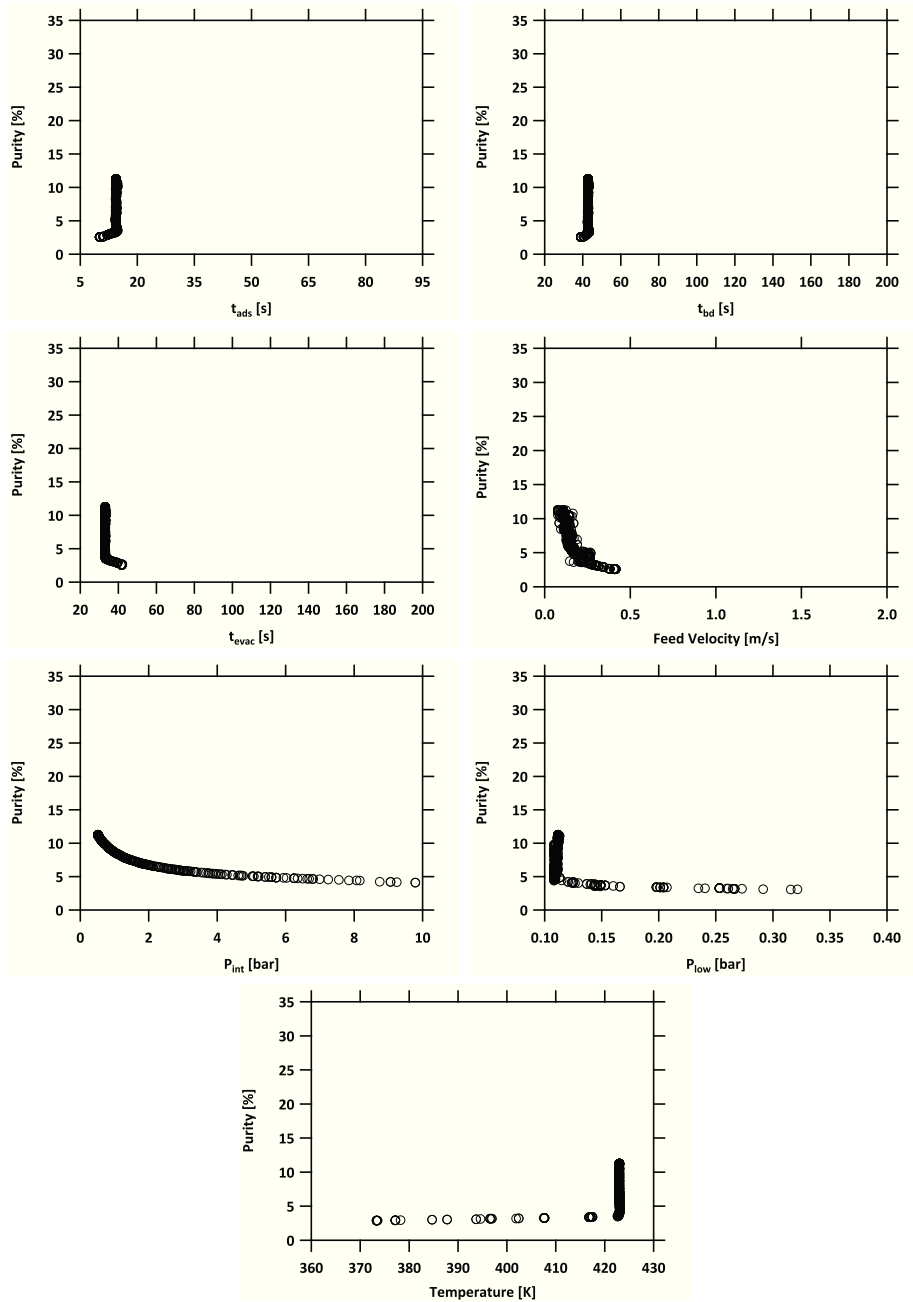


Figure A.3: The decision variables corresponding to the Pareto front for Macro carbon.

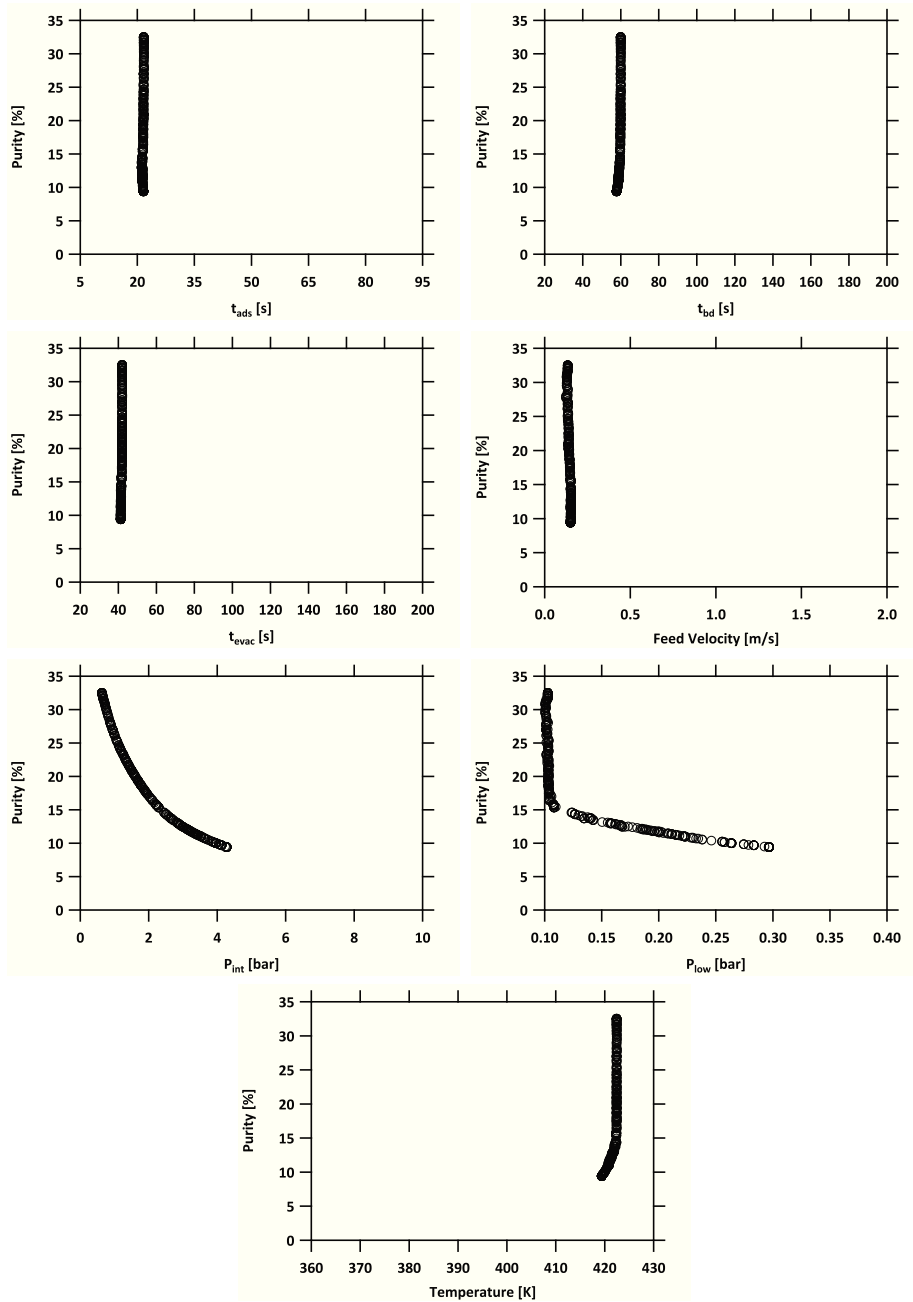


Figure A.4: The decision variables corresponding to the Pareto front for A. carbon 2.

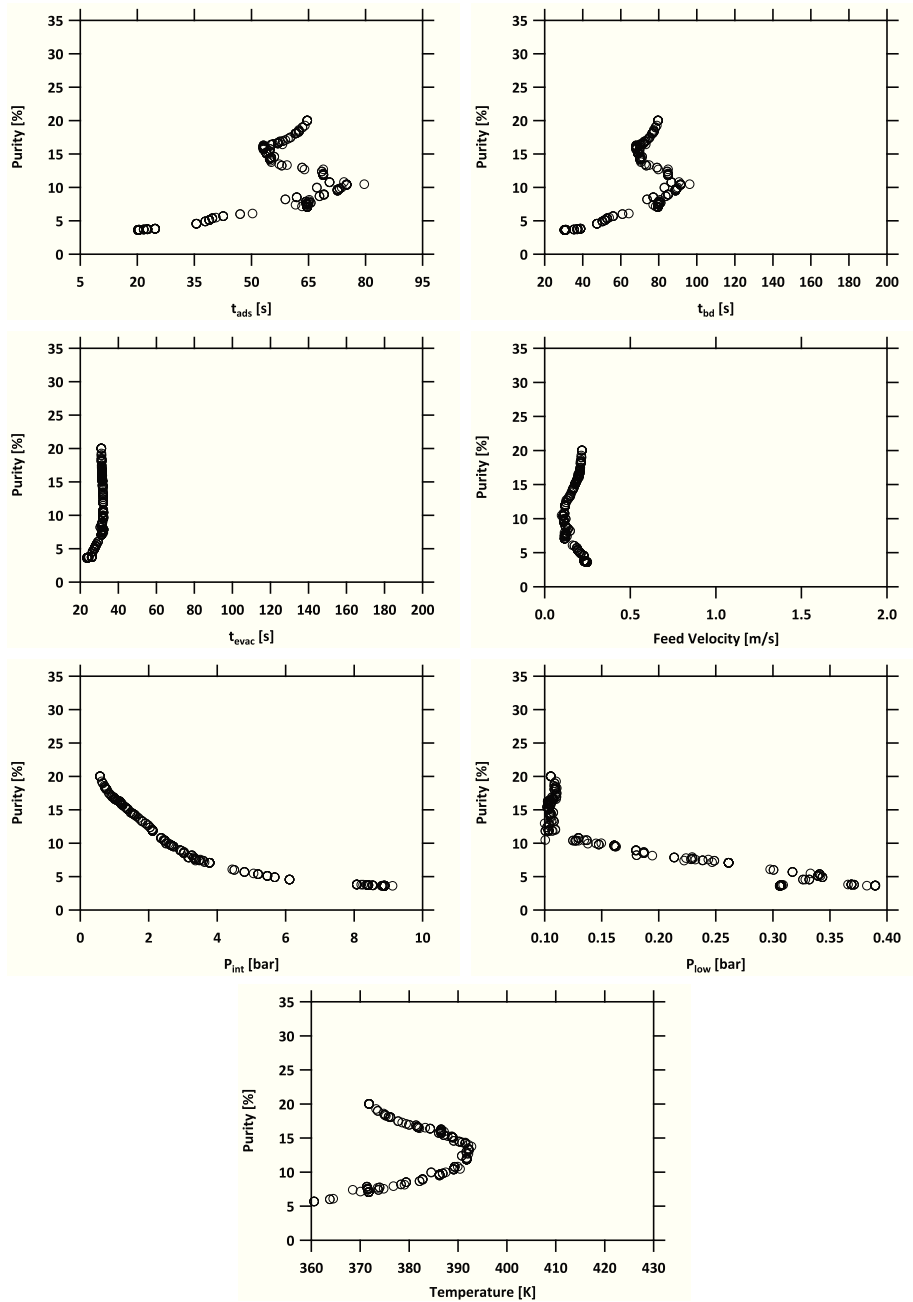


Figure A.5: The decision variables corresponding to the Pareto front for A. carbon 1.

Appendix B

Decision variables for the 5-step cycle with LPP+HR

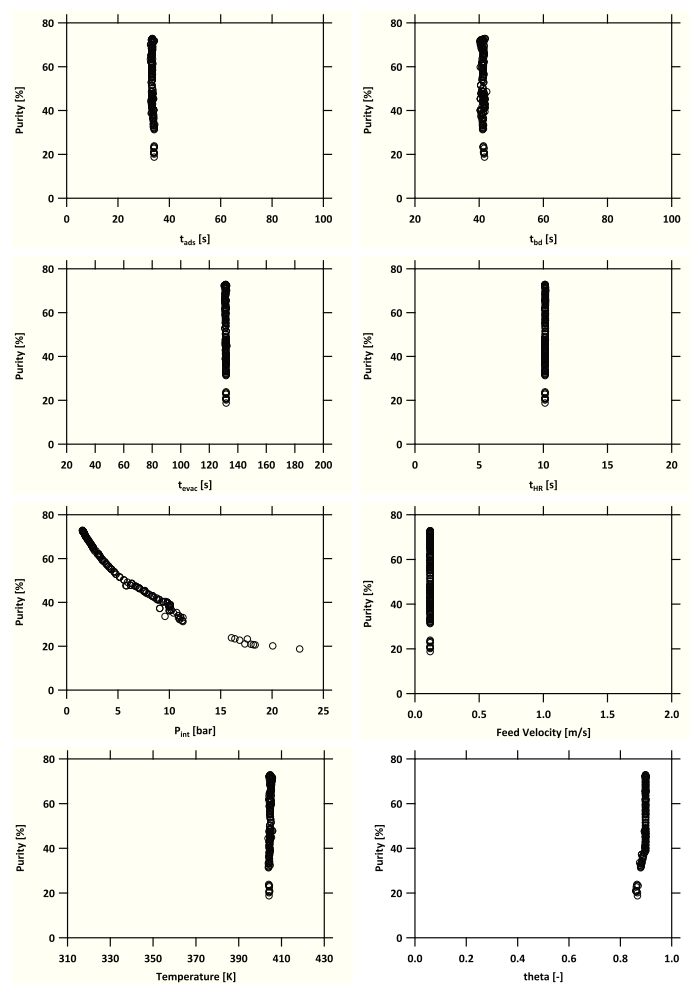


Figure B.1: The decision variables corresponding to the Pareto front for A. carbon 2.

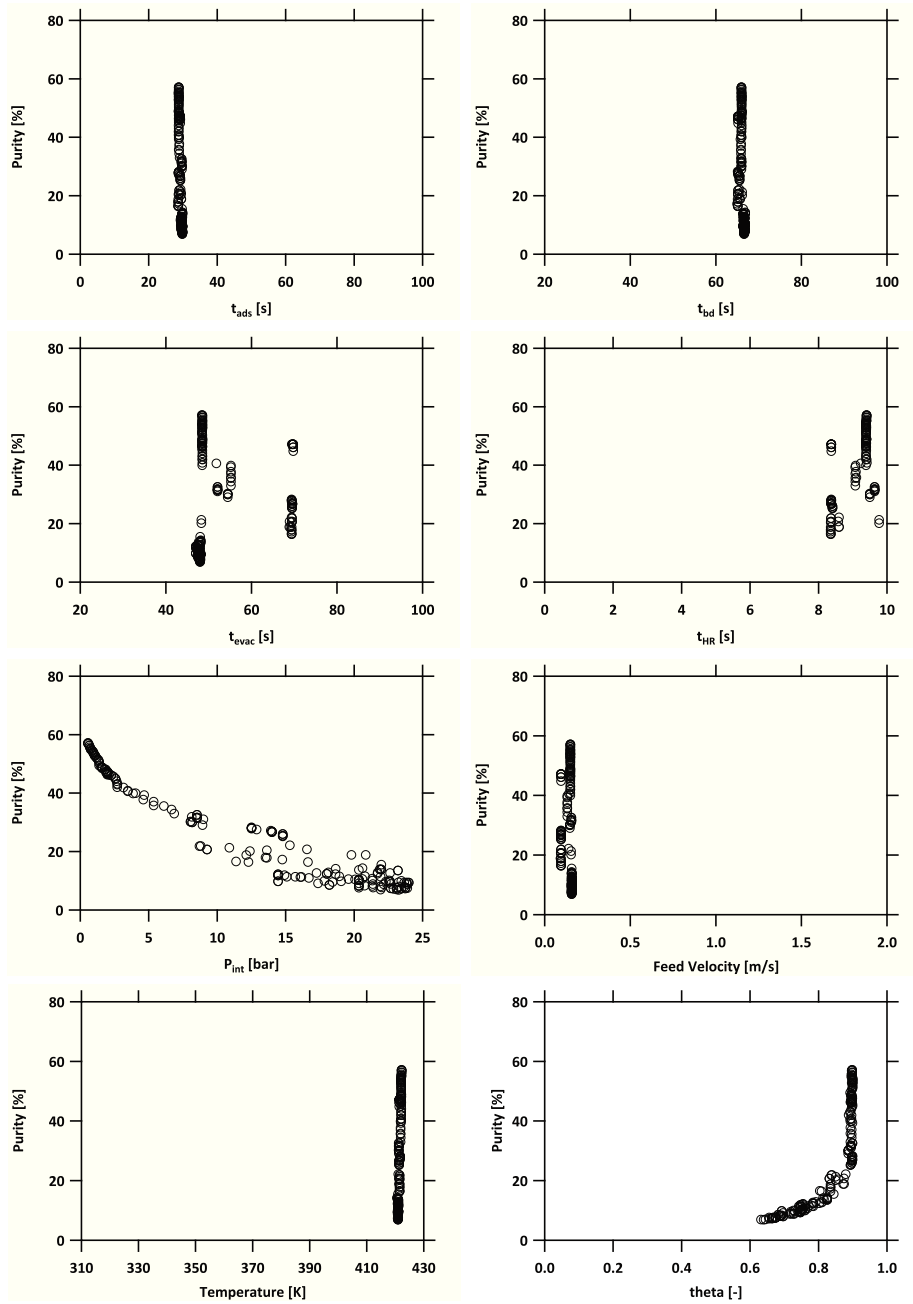


Figure B.2: The decision variables corresponding to the Pareto front for Micro carbon.